Received: 2023-03-27 | Accepted: 2024-01-09 | Published: 2024-02-20

New Archaeometallurgical Fingerprints of Copper and Slag from Early Iron Age Smelting Sites in Faynan and Timna

Michael Bode, Moritz Kiderlen, Giorgos Mastrotheodoros, Moritz Jansen, Erez Ben-Yosef, Omri Yagel, Martina Renzi, Eleni Filippaki, Yannis Bassiakos, Anno Hein and Andreas Hauptmann

Keywords
Faynan, Timna, Early Iron Age, copper, provenance studies

Abstract

The copper deposits of Faynan and Timna have been exploited in two major economic cycles: a Chalcolithic – Early Bronze Age cycle, and a Late Bronze Age – Early Iron Age cycle. The present study focuses on the Late Bronze Age - Early Iron Age cycle of the two districts and analyses a relatively large sample of smelting remains from their main smelting sites (slag, raw copper, archaeological ores). The analytical results from lead isotope analysis (LIA; n = 145), copper isotope analysis (CIA; n = 49), chemical analysis (n = 52) and microstructural analysis (n = 5) are compared with the current geological and mining archaeological knowledge and confirm earlier results according to which in Faynan only the ore type DLS was smelted in this phase and in Timna almost exclusively the ore type Amir/Avrona. Based on the analytical data, multidimensional models of these two copper types are developed, which presumably come relatively close to the copper types marketed in reality. Our models are intended to serve as a basis for comparison in future provenance studies.

Aims and approach

A growing list of archaeometric provenance studies has began to reveal the extent to which the Arabah export affected the Levantine and further Mediterranean copper markets of the Late Bronze (LBA) and Early Iron Ages (EIA). Indications for such exports have been published for Northern and Central Israel (Stos-Gale, 2006; Yahalom-Mack, et al., 2014; Yahalom-Mack and Segal, 2018; Yahalom-Mack and Segal, 2021; Yahalom-Mack, Finn and Erel, 2023), Jordan (Philip, et al., 2003), Lebanon (Vaelske and Bode, 2018-2019; Vaelske, et al., forthcoming), Syria (Degryse, et al., 2012), Lower Egypt (Stos-Gale, Gale and Houghton, 1995; Rademakers, Rehren and Pernicka, 2017; Vaelske, Bode and Loeben, 2019; Ben-Dor Evian, et al., 2021), the Arabian peninsula (Renzi and Rehren, 2016; Renzi, et al., 2016), Greece (Kiderlen, et al., 2016; Bode, et al., 2020), and Sardinia (Montero-Ruiz, 2018). About copper and trade in the South-Eastern Mediterranean see also Stos-Gale (2015).

Despite its importance, the comparative database for Arabah copper is still quite limited, being the result of heterogenous research interests and analytical strategies. This makes it difficult to address assignation problems in case of overlaps with other Ancient industrial regions (e.g. LI overlaps with Sardinian lead and copper, cf. Stos-Gale, 2023; Montero-Ruiz, 2023) and complicates internal distinctions between different potential sources within the Arabah (Timna vs. Faynan, but also vs. Wadi Amram and others). Recognising recycling and mixing processes is also made more difficult. Overall, these specific problems hinder our ability to map the distribution pathways of Arabah copper and understand its socio-economic functions.

In this study, we present an integrated dataset of new lead isotope analysis (LIA), copper isotope analysis (CIA), bulk chemical analysis, and microstructural analysis of industrial remains collected from well understood archaeological contexts at smelting (and mining) sites in Faynan and Timna. We aim to provide a comprehensive database that allows for a reliable and more precise modelling of the geochemical properties of the copper types that were marketed by including both new and previously published results. In turn, this database may serve as comparative material for future provenance studies on copper ingots, secondary copper metallurgy

DOI:10.46586/metalla.v27.2023.i2.167-219

debris, and finished copper-based objects. Moreover, the new data will also assist in shedding new light on changes in raw material selection during different chronological sub-phases on an intra-regional level, and on effects of modifications of smelting technology. Our samples represent different chronological sub-phases of the LBA-EIA industrial cycle from sites that are representative of the industrial output. They consist of a wide range of artefacts: copper prills, copper chunks, slags and archaeological ore relicts from smelting sites.

Background

Copper ore deposits of Faynan and Timna in the Wadi Arabah

The ore deposits of Faynan and Timna have a common geological history (Figure 1)(compact information in Beyth, Segev and Ginat, 2013). They are all sedimentary stratabound ore deposits with a long history beginning with the formation in Precambrian volcanic rocks, erosion in the lower Cambrian and epigenetic remobilization and subsequent deposition since the Miocene. Also, since the Oligocene/Miocene, the ore deposits of Faynan and Timna have been shifting apart along the Wadi Arabah fault to a present day distance of approximately 100 km. In both ore deposits, copper-based oxidic and, in traces, sulphidic ores as well as copper silicates are the predominant mineral assemblages (compact overview in Hauptmann, 2007).

Faynan

In Faynan, by far the richest mineralization occurs. It is embedded in Cambrian dolostones and sandstones and comprises secondary copper and manganese minerals, which occur within an area of roughly 20 x 25 km. Following along geologic-tectonic faults, a system of wadis have been formed with time. Here, large outcrops of copper mineralization are exposed at or near the surface (see illustration in Hauptmann, 2007, p.146). They are located in the north at Khirbet el-Jariye, Khirbet en-Nahas, El-Furn and Khirbet el-Ghuwebe, slightly smaller outcrops at Umm ez-Zuhur near Al-Qurayqira. In the east part, there is abundant ore mineralization at Ratiye, Wadi Khalid and Wadi Dana. The ore deposits on Jabal Mubarak and

Figure 1. Geological sections of Faynan and Timna (Hauptmann, 2007, Fig. 4.4). Simplified lithostratigraphy and copper mineralization in Faynan and Timna (the latter information from Bartura and Würzburger, 1974; Segev and Sass, 1989). Some geological and mineralogical characteristics, which play a role in differentiating between both deposits, are marked. The hammer and wedge symbol close to the Dolomite-Limestone-Shale Unit (cb2, called DLS in the following) in Faynan represents more than 100 mines (Hauptmann, et al., 1992).

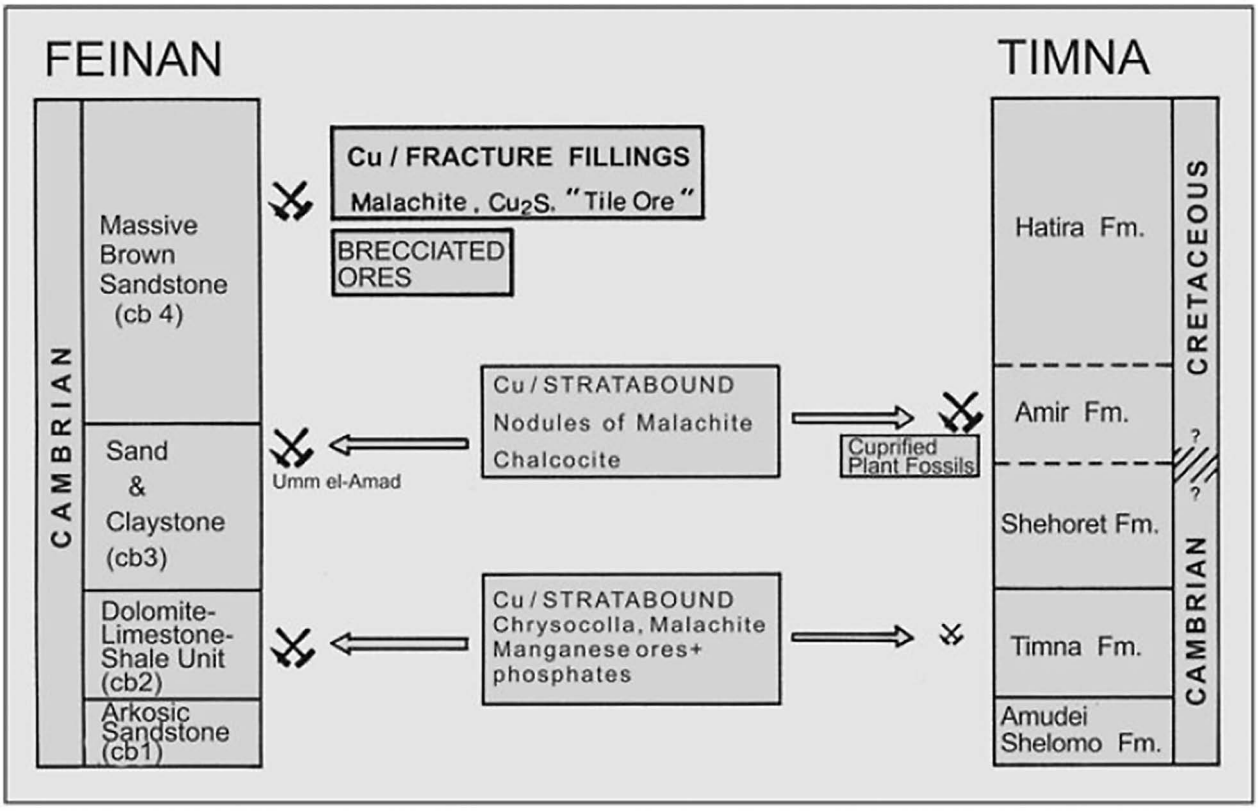

smaller occurrences at Salawwan mark the expansion into the south (see map in Hauptmann, 2007, p.86).

The Cambrian sediments, in which the predominant copper mineralizations are embedded, are divided in several units (Figure 1; see Hauptmann, 2007):

1. Arkosic Sandstones (cb1) (no mineralizations) of 60 m thickness mainly consisting of fluviatile, middle- to coarse-grained rocks:
2. Dolomitic-Limestone-Shale-Unit (cb2) (hereinafter: DLS) has been the main target during most exploitation periods in the past. It has a variable thickness of 20 to 40 m. There is a lateral development from sandy dolostones to coastal sandstones in the south, and from marine dolostones to open marine fossiliferous limestones in the north. Vertically, the geological sequence starts with sandstones (underlying bed), followed by sandy dolostones (middle unit) and silt and clay rocks and shales (top layer). Copper ores are deposited as pockets, matrix mineralizations and vein fillings in the dolostones, while, additionally there are strongly intergrown copper and manganese mineralizations of 1 to 1.5 m thickness with nodules and layers of phosphorite in the upper part of the dolostone layer and overlying shale unit. Locally, like at Qalb Ratiye, copper ores are associated with iron ores. Manganese as well as iron ores make the copper ores "self-fluxing".
3. Sand- and Claystones (cb3) with local copper and manganese ores of no commercial/historical importance, deposited with a thickness of about 50 m in a terrestrial environment. This formation is characterized by rapid lithologic changes. The basal part, which contains the ores, is dominated by conglomerates and coarse sandstones.
4. Massive Brown Sandstone (cb4) (hereinafter: MBS), which is the thickest unit, reaches up to 250 m. Formation of fine- to medium-grained sandstones took place under fluviatile conditions. Conglomerates and claystones are intercalated. Oxidic and sometimes sulphidic copper ores are partly coating these sandstones along a vertical system of fractures and were the focus of early mining activities.

Main copper minerals of DLS are (after Hauptmann, 2007):

1. Paratacamite ($Cu_2(OH)_3Cl$);
2. Chrysocolla ($CuSiO_3 \cdot 2H_2O$);
3. Malachite ($Cu_2[(OH)_2/CO_3]$);
4. Dioptase ($Cu_6[Si_6O_{18}] \cdot 6H_2O$);
5. Planchéite ($Cu_8[(OH)_2/Si_4O_{11}]_2$;
6. Pseudo-malachite ($Cu_5[(OH)_5/PO_4]_2$.

Main copper minerals of MBS are (after Hauptmann, 2007):

1. Malachite ($Cu_2[(OH)_2/CO_3]$);
2. Cuprite (Cu_2O);
3. Chalcocite ('Cu_2S') and covellite (CuS);
4. Paratacamite ($Cu_2(OH)_3Cl$).

Timna

Due to their common geological history, the lithostratigraphy of Faynan and Timna is similar (Figure 1). But in contrast to the ore assemblages in Faynan, the archaeological evidence suggests that only Lower Cretaceous ore were exploited in Timna during antiquity. Accordingly, dissimilar to Faynan, the ores used in Timna during the EIA are not rich in manganese, but only in iron (this chemistry led to the incidental iron smelting in Timna as described in Gale, et al., 1990). Nevertheless, outcrops of manganese rich rocks of the dolomitic phase of the Timna formation (which is parallel to the DLS in Faynan) do occur discretely within the valley, and these were used as flux in the final stages of the IA industry in Timna (see below).

1. The Amudei Shelomo formation is the counterpart of the Arcosic Sandstone Unit (cb1) in the Faynan mining district.
2. The subsequent Timna formation is almost identical with the DLS (cb2) of Faynan. Both bear the richest occurrences of copper ores. Nevertheless, the largest part of the Timna formation is not outcropping at the surface. Evidence for exploitation is only given in a few small pits at Har Timna at Givat Sasgon (site 250). If more exploitation of copper ores from the Timna formation took place further south remains open as modern open cast mining destroyed any archaeological information.
3. Above the Timna formation follow the Shehoret formation, which is the equivalent of the Faynan Sand- and Claystone (cb3). Like the Timna formation, it is only partly outcropping at the surface.
4. Ancient mining for ores in Timna took place at the border of the Amir and Avrona formations, both strata of the Lower Cretaceous (Segev and Sass, 1989; Segev, Beyth and Bar-Matthews, 1992). They are widely exposed at Timna. The Amir and Avrona formations belong to the Palaeozoic-Mesozoic Nubian sandstone, a sequence of predominantly terrestrial sediments. The Avrona formation is up to 60 m thick and basically consists of medium to coarse-grained sandstones. The transition to the Amir formation is irregular. This geological sequence varies in thickness between 10 and 30 m and is predominantly made of white friable, fine to medium grain quartz kaolinitic

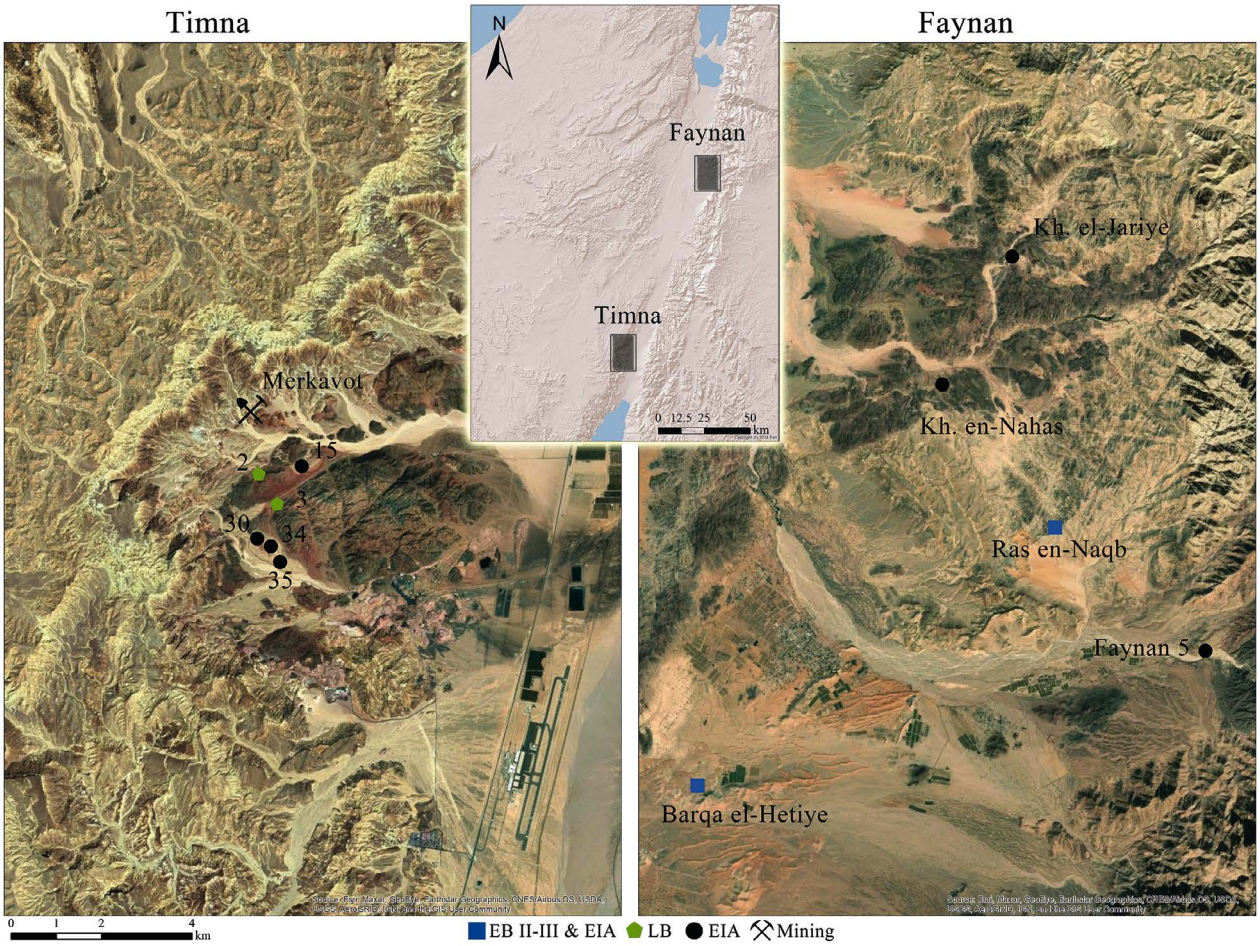

Figure 2. 'MAP'. Map of smelting sites from which samples were taken for this study. EB = Early Bronze Age, LB = Late Bronze Age, EIA = Early Iron Age. Source: Esn, Maxar, GeoEye, Earthstar Geographics, CNES/Airbus DS, USDA, USGS, AemGRID. IGN, and the GIS User Community, modified by E. Ben-Yosef and O. Yagel.

sandstones. Both formations are part of the Kurnub Group. The Amir and Avrona formations contain primary chalcocite and covellite and secondary malachite and (par-)atacamite embedded in sandstone. The ore assemblage is quite similar to those of the Sand- and Claystones unit (cb3) in Faynan. Also, occurrences of mixed Cu-Fe-ores are described for Timna, which give those ores, like the Cu-Mn-ores at Faynan, a self-fluxing property.

The Cambrian formations, Shehoret and to some extent Timna formation, contain chrysocolla, bisbeeite, malachite and minor amount of chalcocite. In addition, the dolomitic facies within the Timna formation include djurleite, paratacamite and malachite (Segal, et al., 2015).

The copper ores of Timna are complex and consist of (after Bartura, Hauptmann and Schöne-Warnefeld, 1980):

1. Malachite ($Cu_2[(OH)_2/CO_3]$);
2. Cuprite (Cu_2O);
3. various Fe-oxides/-hydroxides;
4. Chalcocite (Cu_2S) and covellite (CuS);
5. Azurite ($Cu_3[OH/CO_3]_2$);
6. Atacamite ($Cu_2(OH)_3Cl$) and Paratacamite ($Cu_2(OH)_3Cl$);
7. Chrysocolla ($CuSiO_3 \cdot 2H_2O$).

Technical and organisational development of mining and smelting in the Wadi Arabah

Faynan and Timna are the main districts of the LB-EIA Arabah copper mining region (map Figure 2**,** with sites mentioned in the text. For Faynan, see Hauptmann, 2007 (with site catalogue); Ben-Yosef, 2010; Levy, Najjar and Ben-Yosef, 2014; Liss, et al., 2020, for Timna, see Rothenberg, 1988; 1990; Rothenberg and Glass, 1992; Ben-Yosef, et al., 2012; Ben-Yosef, 2016; Ben-Yosef and Craddock, 2016; Ben-Yosef, Langgut and Sapir-Hen, 2017; Ben-Yosef and Sergi, 2018; Yagel). Copper ore exploitation in the Arabah dates back as early as the Chalcolithic (Chalc.) period. In the Chalcolithic and Early Bronze Age (EBA) I, activities focused mainly on

mining of ore (conveyed to distant settlements) and only discrete evidence testify to small scale smelting. In EBA II-IV periods, copper production at Faynan developed to an industrial scale in specialized settlements. Smelting is concentrated on hilltops using wind-powered furnaces. Also, during the EBA II, mining in Faynan shifted from the Fe rich MBS layers to the Mn rich DLS layers. This shift also caused a major change in LI ratios of the slags and metals from Faynan. After centuries of hiatus, in the 13th century BC, innovative copper extraction activities abruptly appeared in Timna (bellow-powered furnaces as attested by tuyères; but compare Löffler's (2017, p.160) suggestion that the tuyères might have functioned without bellows). Under Egyptian initiative, and using imported technology that probably originated in Sinai or the Hijazi desert, copper production in Timna during the LBA was characterized by production and technological and logistical arrays on an unprecedented industrial scale operated by a complex social organization. This industry is noticeable also in Faynan sometime in the 12th century and continued to operate and grow, not without technological and organizational changes, until the end of the 9th century BC. Within the EIA production period, both in Timna as in Faynan two major technological phases can be discerned, marked by the two slag types B and A. The transition from B to A was dated around 925 by ^{14}C of strata in slag heaps (Ben-Yosef, et al., 2012). Furthermore, the LBA-EIA timeframe was recently divided into four socio-technological production systems (see Figure 3) (Ben-Yosef, et al., 2019):

The initial phase, system 0, is characterized by small sized highly porous fayalite slag (note that this phase is not extensively attested to Faynan so far, but compare Hauptmann's observation about possibly LBA mining and smelting contexts of Wadi Dana (Hauptmann, 2007, p.122, with Figure 5.27 discussing thin plate slag and a tuyère fragment and comparing them to similar Timna specimens from site 30, stratum 2). Bulk chemical analysis of slag samples from this phase show relatively (to other LBA-EIA slag types from the Arabah) low standardization of the smelting charge. In the present study this phase is represented by samples from sites 2 and 3 in Timna. During the following phase, system 1, the Egyptian footprint in Timna disappears and evidence for smelting becomes clearer in Faynan. Archaeological excavations in both Timna and Faynan demonstrate a well-organized industry, yet spread over many unwalled small sites. Although the archaeological evidence shows similarities in tuyère shape and basic furnace design during system 1, a Mn-rich kneblite type of slag dominates in Faynan in opposite to a Fe-rich fayalite type of slag dominating in Timna. This phenomenon reflects the difference in raw materials selection between the regions. As mentioned above, in Faynan the DLS was the main geological layer exploited from the EBA II onwards. In Timna, however, mining activities focused on the Amir/Avrona formations. Slags of system 1 are nearly indistinguishable from slags of system 0 and do not suggest an inherent technological change. In the very late 11th century BC, system 2, the industry is converging and becoming more centralized. This system is evident in fewer, yet bigger in both architectural and production volume, fortified sites (e.g. Khirbet en-Nahas in Faynan and Sites 30 and 34 in Timna). Reduction in Cu content, Ca content and variation of other elements in slag samples from system 2 indicate a more energy efficient and highly standardized technology. Still, the basic charge materials in system 2 are similar to those of the systems 0 and 1. Towards the end of the 10th century BC the entire industry in the Arabah is experiencing a major turmoil as abrupt changes are introduced both in the social and industrial organization as well as technological ones. Innovations in furnace and tuyère size and design result in a new type of slag. Slags of system 3 (= slags of Type A) are much larger than previous ones, which helps to distinguish and map them in smelting archaeological surveys. System 3 is only operated in a few unwalled sites, where smelting is centralized (e.g. Khirbet en-Nahas and Faynan 5 in Faynan and Site 30 in Timna). At Faynan, the charge materials remain basically the same. At Timna, for the first (and only) time, knebelite becomes the main mineralogical phase and Mn the most dominant element in the slags (contra to high Fe content in previous systems) (for details see Ben-Yosef, et al., 2019).

Sample selection

Faynan samples

A total of 87 Faynan samples are taken from Hauptmann's archive of study material stored in the Deutsches Bergbau-Museum Bochum (DBM) in Bochum (Germany) that he compiled during his fieldwork in Faynan 1983-1993 (Hauptmann, 2000; 2007). Find spots and chronological assessment are taken from Hauptmann's labels on the archive boxes, with some modifications (e.g. chronology of Khirbet el-Jariye).

In order to achieve a statistically reliable representation of the overall output of the EIA Faynan mining industry, we concentrated on the three central smelting sites Faynan 5, Khirbet en-Nahas, and Khirbet el-Jariye. In addition, we selected samples from the minor smelt-

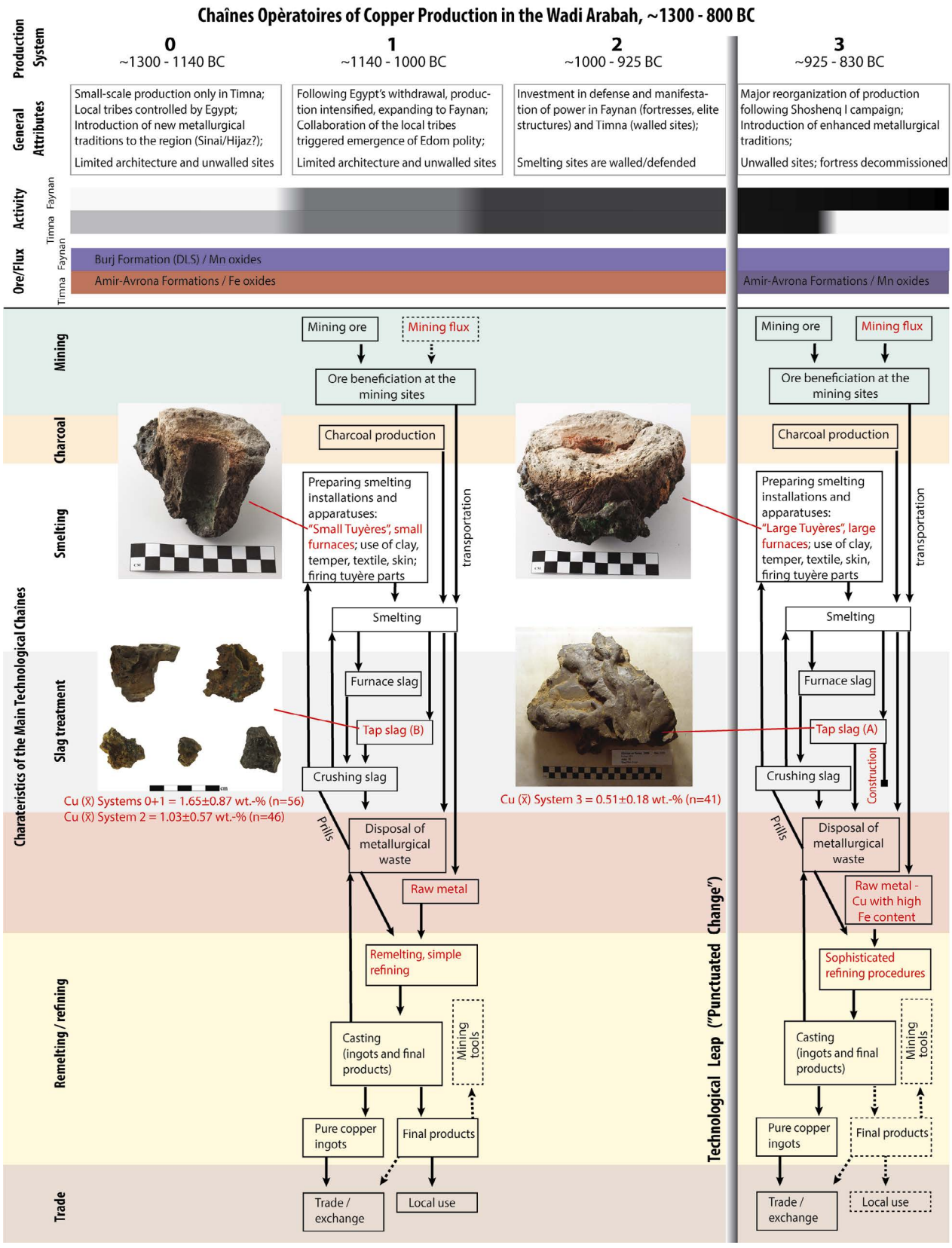

Figure 3. 'Production systems'. Main features of the organization of production and detailed chaîne opératoires for the copper industry in the Wadi Arabah during the Late Bronze and Early Iron Ages (dashed arrows and boxes indicate optional components with weak or no evidence) (after Ben-Yosef, et al., 2019, Fig. 5)

Table 1. Faynan samples listed according site and date, indicating the sort of analysis conducted on every sample.

Location/ site	Type/ description	Date	Inv.-no. archeol.	Lab.-no. DBM	LIA	CIA	Chemistry	Microstructure
Faynan 1	Copper	Roman-Byzantine	JD-1/30	5381-21	DBM	DBM	DBM	
Faynan 1	Copper	Roman-Byzantine	JD-1/33	5046-22		DBM		
Faynan 5	Slag	EIA	JD-1/52b	5224-20	FIERCE			
Faynan 5	Copper	EIA	JD-1/53a	3482-19	FIERCE	DBM	DBM	DEMOKRITOS
Faynan 5	Slag	EIA	JD-1/53b	3483-19	FIERCE			
Faynan 5	Slag	EIA	JD-1/53c	3484-19	FIERCE			
Faynan 5	Copper	EIA	JD-1/53d	3485-19	FIERCE		DBM	
Faynan 5	Copper	EIA	JD-1/53e	3486-19	FIERCE		DBM	
Faynan 5	Copper	EIA	JD-1/54a	3487-19a	FIERCE	DBM	DBM	
Faynan 5	Slag	EIA	JD-1/54b	3487-19b	FIERCE			
KeN	Slag	EIA	JD-2/20b	5222-20	FIERCE			
KeN	Slag	EIA	JD-2/20c	5227-20	FIERCE			
KeN	Slag	EIA	JD-2/20d	3470-19	FIERCE			
KeN	Slag	EIA	JD-2/22a	3464-19	FIERCE			
KeN	Slag	EIA	JD-2/22b	3465-19	FIERCE			
KeN	Slag	EIA	JD-2/22c	3466-19	FIERCE			
KeN	Slag	EIA	JD-2/22d	3467-19	FIERCE			
KeN	Slag	EIA	JD-2/22e	3468-19	FIERCE			
KeN	Copper	EIA	JD-2/22f	3469-19	FIERCE	DBM	DBM	
KeN	Copper	EIA	JD-2/23b	3471-19	FIERCE	DBM	DBM	
KeN	Slag	EIA	JD-2/23c	3472-19	FIERCE			
KeN	Slag	EIA	JD-2/23d	3473-19	FIERCE			
KeN	Copper	EIA	JD-2/23e	3474-19	FIERCE		DBM	
KeN	Copper	EIA	JD-2/23f	3475-19	FIERCE		DBM	
KeN	Slag	EIA	JD-2/23g	3476-19	FIERCE			
KeN	Copper	EIA	JD-2/23h	3477-19	FIERCE		DBM	
KeN	Copper	EIA	JD-2/27b | 4644	5220-20	FIERCE	DBM		
KeN	Copper	EIA	JD-2/27d	3480-19	FIERCE		DBM	DEMOKRITOS
KeN	Copper	EIA	JD-2/27d_II	5388-21	DBM	DBM	DBM	
KeN	Copper	EIA	JD-2/27e	5395-21	DBM	DBM	DBM	
KeN	Copper	EIA	JD-2/27f	3481-19	FIERCE	DBM	DBM	DEMOKRITOS
KeN	Slag	EIA	JD-2/27x	3479-19	FIERCE			
KeN	Slag	EIA	JD-2/37	5219-20	FIERCE			
KeN	Slag	EIA	JD-2/38a	5214-20	FIERCE			
KeN	Slag	EIA	JD-2/38b	5216-20	FIERCE			
KeN	Slag	EIA	JD-2/38c	5217-20	FIERCE			
KeN	Slag	EIA	JD-2/38d	5218-20	FIERCE			
KeN	Slag	EIA	JD-2/4	5223-20	FIERCE			
KeN	Slag	EIA	JD-2/41	5215-20	FIERCE			
KeJ	Slag	Iron I	JD-11/2	5225-20	FIERCE			
KeJ	Copper	Iron I	JD-11/3a	3462-19	FIERCE		DBM	
KeJ	Copper	Iron I	JD-11/3b	3463-19	FIERCE	DBM	DBM	
KeJ	Slag	Iron I	JD-11/3c	3460-19	FIERCE			
KeJ	Slag	Iron I	JD-11/3d	3461-19	FIERCE			
ReN	Copper	EBA II-III	JD-5/11e	5389-21	DBM	DBM	DBM	
ReN	Copper	EBA II-III	JD-5/11a	5392-21	DBM	DBM	DBM	
ReN	Copper	EBA II-III	JD-5/11b	5390-21	DBM	DBM	DBM	
ReN	Copper	EBA II-III	JD-5/11d	5393-21	DBM	DBM	DBM	
ReN	Copper	EBA II-III	JD-5/11f	5394-21	DBM	DBM	DBM	
ReN	Slag	Iron II	JD-5/3a	5221-20	FIERCE			
ReN	Slag	Iron II	JD-5/3c	5226-20	FIERCE			
Qualb Ratiye	Geol. copper ore (MBS)		JD-12/2	5049-22	DBM	DBM	Hauptmann, 2000; 2007	
Qualb Ratiye	Geol. copper ore (MBS)		JD-12/5b	5050-22	DBM	DBM		

Location/ site	Type/ description	Date	Inv.-no. archeol.	Lab.-no. DBM	LIA	CIA	Chemistry	Microstructure
Qualb Ratiye	Geol. copper ore (MBS)		JD-12/5c	5051-22	DBM	DBM		
Qualb Ratiye	Geol. copper ore (MBS)		JD-12/6a	5052-22	DBM	DBM		
Qualb Ratiye	Geol. copper ore (MBS)		GR-1	5047-22	DBM	DBM	Hauptmann, 2000; 2007	
Qualb Ratiye	Geol. copper ore (MBS)		GR-2	5048-22	DBM	DBM	Hauptmann, 2000; 2007	
Faynan 9	Copper	EBA II-III	JD-23/30a	5382-21	DBM	DBM	DBM	
Faynan 9	Copper	EBA II-III	JD-23/30b	5386-21	DBM	DBM	DBM	
Faynan 9	Copper	EBA II-III	JD-23/30d	5391-21	DBM	DBM	DBM	
Faynan 9	Copper	EBA II-III	JD-23/30f	5387-21	DBM	DBM	DBM	
Faynan 9	Copper	EBA II-III	JD-23/30h	5384-21	DBM	DBM	DBM	
Abu Kusheiba	Geol. copper ore (MBS)		JD-24/1b	5054-22	DBM	DBM	Hauptmann, 2000; 2007	
Wadi Abiad	Geol. copper ore (MBS)		WA-4	5053-22	DBM	DBM	Hauptmann, 2000; 2007	
BeH, Locus 9 (1993)	Copper chunk	EBA II-III or rather EIA I	JD-31/22e	5383-21	DBM	DBM	DBM	
BeH, Locus 9 (1993)	Copper chunk	EBA II-III or rather EIA I	JD-31/22f	5385-21	DBM	DBM	DBM	
BeH, Locus 9 (1993)	Copper chunk	EBA II-III or rather EIA I	JD-31/22n	5380-21	DBM	DBM	DBM	
BeH, Locus 9 (1993)	Copper chunk	EBA II-III or rather EIA I	JD-31/22p	5563-20	DBM		DBM	
BeH, Locus 9 (1993)	Copper chunk	EBA II-III or rather EIA I	JD-31/22q	5564-20	DBM		DBM	
BeH, Locus 9 (1993)	Copper chunk	EBA II-III or rather EIA I	JD-31/22r	5565-20	DBM		DBM	
BeH, Locus 9 (1993)	Copper chunk	EBA II-III or rather EIA I	JD-31/22s	5566-20	DBM		DBM	
BeH, Locus 9 (1993)	Copper chunk	EBA II-III or rather EIA I	JD-31/22t	5567-20	DBM		DBM	
BeH, Locus 9 (1993)	Copper chunk	EBA II-III or rather EIA I	JD-31/22u	5568-20	DBM		DBM	
BeH, Locus 9 (1993)	Copper chunk	EBA II-III or rather EIA I	JD-31/22v	5569-20	DBM	DBM	DBM	
BeH, Locus 9 (1993)	Copper chunk	EBA II-III or rather EIA I	JD-31/22w	5570-20	DBM	DBM	DBM	
BeH, Locus 9 (1993)	Copper chunk	EBA II-III or rather EIA I	JD-31/22x	5571-20	DBM	DBM	DBM	
BeH, Locus 9 (1993)	Copper chunk	EBA II-III or rather EIA I	JD-31/22y	5572-20	DBM		DBM	
BeH, Locus 9 (1993)	Copper chunk	EBA II-III or rather EIA I	JD-31/22z	5573-20	DBM		DBM	
BeH, Locus 9 (1993)	Copper chunk	EBA II-III or rather EIA I	JD-31/22aa	5574-20	DBM	DBM	DBM	
BeH, Locus 9 (1993)	Copper chunk	EBA II-III or rather EIA I	JD-31/22ab	5575-20	DBM		DBM	
BeH, Locus 9 (1993)	Copper chunk	EBA II-III or rather EIA I	JD-31/22ac	5576-20	DBM		DBM	
BeH, Locus 9 (1993)	Copper chunk	EBA II-III or rather EIA I	JD-31/22ad	5577-20	DBM		DBM	
BeH, Locus 9 (1993)	Copper chunk	EBA II-III or rather EIA I	JD-31/22ae	5578-20	DBM	DBM	DBM	
BeH, Locus 9 (1993)	Copper chunk	EBA II-III or rather EIA I	JD-31/22af	5579-20	DBM		DBM	
BeH, Locus 9 (1993)	Copper chunk	EBA II-III or rather EIA I	JD-31/22ag	5580-20	DBM	DBM	DBM	
BeH, Locus 9 (1993)	Copper chunk	EBA II-III or rather EIA I	JD-31/22ah	5581-20	DBM	DBM	DBM	
BeH, Locus 9 (1993)	Copper chunk	EBA II-III or rather EIA I	JD-31/22ai	5582-20	DBM		DBM	

Table 2. Timna samples listed according site and date, indicating the sort of analysis conducted on every sample.

Location/ site	Type/ description	Area	Locus/ context	Find type	Estimated date (BC)	Inv.-no. CTV	Lab.-no. DBM	LIA	CIA	Chemistry	Micro-structure
2	Slag		39/03	19	1300-1150	LIA012	3012-18	FIERCE			
2	Slag		30B/02	25	1300-1150	LIA013	3013-18	FIERCE			
2	Slag		35/2	18	1300-1150	LIA018	3018-18	FIERCE			
3	Copper chunk	Room 1	Layer 9	Box 5	1200-1100	LIA004	3004-18	FIERCE			
3	Slag	Surface	Group3	oyT3;06;Ut	1200-1100	LIA021	3021-18	FIERCE			
3	Slag	Survey			1300-1100	TIM3-G1-04.3-CP	4299-16	FIERCE			
3	Slag	Survey			1300-1100	TIM3-G2-05-UT	4293-16	FIERCE			
3	Slag	Survey			1300-1100	TIM3-G3-06.3-CP	4300-16	FIERCE			
3	Slag	Survey			1300-1100	TIM3-G3-06-UT	4294-16	FIERCE			
3	Arch. copper ore	Room 1	Layer 10	Box 8	1300-1100	TIM3-Lay10	4287-16	FIERCE	DBM		
15	Copper chunk	B1	308	IA I	1100-1000	LIA017	3017-18	FIERCE		DBM	
15	Slag	Surface	Group1	oyT15;20;Ut	1100-1000	LIA020	3020-18	FIERCE			
15	Copper	Surface	Band 010	IA I	1100-1000	LIA034	3034-18	FIERCE		DBM	DEMOKRITOS
15	Copper	C	901	IA I	1100-1000	LIA035	3035-18	FIERCE	DBM	DBM	
15	Copper	B	308	IA I	1100-1000	LIA036	3036-18	FIERCE	DBM	DBM	
15	Copper chunk	C	916	11215	1100-1000	LIA040	3040-18	FIERCE			
15	Arch. copper ore	B	307	1307	1100-1000	TIM15-307	4289-16	FIERCE	DBM		
15	Metal	B	308	1085	1100-1000	TIM15-308_1085	4279-16	FIERCE		DBM	
15	Metal	B	308	1105	1100-1000	TIM15-308_1105	4282-16	FIERCE		DBM	
15	Arch. copper ore	M	701	4003	1100-1000	TIM15-701	4288-16	FIERCE	DBM		
15	Metal	C	901	11011	1100-1000	TIM15-901_11011	4277-16	FIERCE		DBM	
30	Slag with visible prills	L	806	1002	1150-930	LIA023	3023-18	FIERCE			
30	Slag	L	811	1500	1150-930	LIA024	3024-18	FIERCE			
30	Slag	L	809	1800 (EDM 272)	930-800	LIA026	3026-18	FIERCE			
30	Slag	L	809	1800 (EDM 272)	930-800	LIA041	3041-18	FIERCE			
30	Slag	L	809	1800 (EDM 272)	930-800	LIA042	3042-18	FIERCE			
30	Slag	L	811	1512 (EDM 267)	930-800	LIA043	3043-18	FIERCE			
30	Slag	L	806	1000b	930-800	TIM30-806_1000B	4285-16	FIERCE			
30	Slag	S	901	552A	1150-930	TIM30-901_552A	4284-16	FIERCE			
34	Copper prill	GN	157	IA I-II	1030-930	LIA001	3001-18	FIERCE		DBM	
34	Slag with visible prills	13B	1113	1838	1030-930	LIA002	3002-18	FIERCE			
34	Slag with visible prills	G	462	5436	1030-930	LIA003	3003-18	DBM	DBM	DBM	DEMOKRITOS
34	Slag with visible prills	13A	525	6028	1030-930	LIA005	3005-18	FIERCE			
34	Slag with visible prills	13A	521	6014	1030-930	LIA006	3006-18	FIERCE			
34	Copper prill	GN	1154/ 1157	IA I-II	1030-930	LIA010	3010-18	FIERCE		DBM	
34	Tuyere with visible prills	GN	1154	17230	1030-930	LIA016	3016-18	FIERCE			
34	Slag	19A	130	102	1030-930	LIA019	3019-18	FIERCE			
34	Copper prill	GN	1154/ 1157	IA I-II	1030-930	LIA028	3028-18	FIERCE		DBM	

Location/ site	Type/ description	Area	Locus/ context	Find type	Estimated date (BC)	Inv.-no. CTV	Lab.-no. DBM	LIA	CIA	Chemistry	Micro-structure
34	Copper	G	410	IA I-II	1030-930	LIA033	3033-18	FIERCE		DBM	
34	Slag	19A	129	102	1030-930	TIM34-129	4295-16	FIERCE			
34	Slag	19A	132	101	1030-930	TIM34-132	4296-16	FIERCE			
34	Slag	Survey			1030-930	TIM34-17-1CP	4298-16	FIERCE			
34	Slag	Survey			1030-930	TIM34-18-1CP	4297-16	FIERCE			
34	Metal	GN	410	5342	1030-930	TIM34-410_5342	4280-16	FIERCE		DBM	
34	Arch. copper ore	13A	510	5825	1030-930	TIM34-510	4290-16	FIERCE	DBM		
34	Arch. copper ore	13A	517	8108	1030-930	TIM34-517	4291-16	FIERCE	DBM		
34	Arch. copper ore	13A	521	5898	1030-930	TIM34-521	4292-16	FIERCE	DBM		
35	Copper prill	A1	1246	IA I	1200-1000	LIA007	3007-18	FIERCE		DBM	
35	Copper prill	C1	1408	IA I	1200-1000	LIA008	3008-18	FIERCE	DBM	DBM	
35	Copper prill	B4	2233	18267	1200-1000	LIA011	3011-18	FIERCE			
35	Copper prill	C1	1409	IA I	1200-1000	LIA022	3022-18	FIERCE		DBM	
35	Copper prill	B4	2233	IA I	1200-1000	LIA027	3027-18	FIERCE		DBM	
35	Copper prill	C1	1409	IA I	1200-1000	LIA029	3029-18	FIERCE		DBM	
35	Copper prill	C1	1408	IA I	1200-1000	LIA030	3030-18	FIERCE		DBM	
35	Copper prill	A1	1246	IA I	1200-1000	LIA031	3031-18	FIERCE		DBM	
35	Copper	A1	1232	IA I	1200-1000	LIA037	3037-18	FIERCE		DBM	
35	Copper	C1	1402	IA I	1200-1000	LIA038	3038-18	FIERCE		DBM	
35	Copper prill	B1	1314	IA I	1200-1000	LIA039	3039-18	FIERCE		DBM	
35	Copper prill	A1	1241	13251	1200-1000	TIM35-1241_13251	4286-16	FIERCE			

ing site Ras en-Naqb. Our first choice always were copper prills and lumps, but since these are limited in number, we also sampled slags. For the relative importance and the time spans of smelting activities at these IA sites see the site catalogue in Hauptmann (2007), and recent research cited in the above chapter.

In addition to this Faynan material with secure IA date we sampled also a number of copper lumps, - possibly of miscast or chopped copper ingots -, that were collected by Hauptmann in Barqa el-Hetiye Locus 9. The date of this material is not clear. It may either stem from the EBA II-III phase of this smelting site, or rather from IA I, when the old slags were reworked. Some analytical data and comments on this material were already published by Hauptmann (2007, pp.203-204, Tab. A.18); for chronology of the site see also Ben-Yosef (2010, p.208).

Finally, we selected ten raw copper samples from the EBA II-III smelting sites Faynan 9 and Ras en-Naqap.

Timna samples

Samples from Timna (n = 64) include copper metal (prills and artefacts), slag and ore from archaeological contexts (see Table 2 for a complete list of samples from Timna). These samples stem from the fieldwork of the Central Timna Valley Project (CTV) (Ben-Yosef, 2018). The estimated dates of the samples are based upon analytical dating techniques, slag and ceramic typologies and historical considerations (for chronological clarifications see Ben-Yosef, et al., 2012; Ben-Yosef, 2018; Yagel, Ben-Yosef and Craddock, 2016).

Published comparative material related to Faynan

As part of the DBM Arabah project, a series of copper prills and lumps of the main phases of metallurgical activity in the Faynan (EBA II-IV; IA I-II) were analysed from 1983-1993 for their chemical composition (mostly using Atomic Absorption Spectroscopy/AAS) and in some cases also for their microstructure.

In addition, there is a more limited number of lead isotope analysis (LIA) of copper prills and lumps, slags, and ores (with Thermal Ionisation Mass Spectrometry/TIMS). These data are compiled and systematically discussed in Hauptmann (2007). Since then, Jansen (2011) and Jansen, et al. (2017) have published a number of LIA and for the first time copper isotope analysis (CIA) of ores conducted with multi-collector Inductively Coupled Plasma Mass

Table 3. Overview on published LIA of Faynan raw copper and slags (from Hauptmann, 2007).

Site	Copper	Slag	Total	Date
Wadi Fidan 4	5	1	6	EBA I
Wadi Fidan A	1	2	3	EBA I
Faynan 17	-	1	1	EBA I
Faynan 1	-	1	1	EBA II-III
Ras en-Naqab	2	-	2	EBA II-III
Wadi Dana	1	-	1	MBA-IA I
Faynan 5	1	-	1	IA IIA (probably also IA I and Persian)
Khirbet en-Nahas	3	-	3	IA I-IIA
Khirbet el-Jariye	1	-	1	IA I
Faynan 1	-	1	1	Roman
Faynan 1	1	-	1	Mameluk
Faynan 6	1	-	1	Mameluk
El Furn	1	-		Ayyubid

Spectrometry (ICP-MS). Below we are listing published LI analyses of copper prills, lumps, and slag, indicating their smelting sites and phases. Evidently, however, coverage of EIA with published LI data is quite low.

Furthermore, there are several collections of ingots that researchers linked to Faynan because of their geochemical properties and on circumstantial evidence. In this study we compare with our data:

- a cargo of loaf ingots from a LBA-EIA wreck site off Neve-Yam at the Carmel coast (Israel), analysed by Yahalom-Mack, et al. (2014). The authors conducted bulk chemical analysis with Inductively Coupled Plasma Atomic Emission Spectroscopy (ICP-AES), LIA with Multi-Collector Inductively Coupled Plasma Mass Spectrometer (MC-ICP-MS) (nine samples), and microstructural analysis;
- two find groups of Levantine bar ingots from EBA IV sites in the Negev: ʿEin Ziq and Beʾer Resisim (Segal, et al., 1996-1997; Segal, Halicz and Cohen, 1999). The authors conducted bulk chemical analysis with ICP-AES, LIA with low precision and accuracy Quadrupole-ICP-MS (Segal, Halicz and Cohen, 1999, p.180), and microstructure analysis;
- three find groups of Levantine bar ingots from EBA III-IV sites: Khirbet Hamra Ifdan in Faynan, Har Yehuram in the Negev, and Hebron Hills (Hauptmann, et al., 2015). The authors conducted bulk chemical analysis with Inductively Coupled Plasma - Optical Emission Spectrometry (ICP-OES), LIA with TIMS, and microstructural analysis. Jansen, et al. (2017) added CIA of the samples of the Khirbet Hamra Ifdan ingots conducted with MC-ICP-MS.

Analytical methods and results

Lead isotope analysis (LIA) of copper, slag, and archaeological ore (MC-ICP-MS)

LIA was conducted both at the FIERCE (Frankfurt Isotope & Element Research Center at Goethe Universität Frankfurt) (2014-2019) and at the DBM (Deutsches Bergbau-Museum Bochum, Research Department Forschungslabor) (since 2020).

Procedure at FIERCE: For the lead isotope determination with a multi-collector ICP-MS (Neptune Plus, Thermo Fisher Scientific), around 40 samples are usually analysed in a series of measurements. For this purpose, the dried lead eluate of the sample is diluted to about 125 ppb Pb with 2 % HNO_3. 10 ppb concentrated Tl solution standard solution (NIST SRM-997) is added to this sample solution for internal fractionation correction. Solutions of the lead standard with 125 ppb Pb (NIST SRM-981) are used as unknown samples to check the accuracy of the results and the stability of the instrument (mass drift) during the run after every 5 samples. For the samples presented, standard errors are shown in Table 4 and 5.

Procedure at DBM: An equivalent methodology was applied using a multi-collector ICP-MS (Neptune XT, Thermo Fisher Scientific) which was installed end of November 2020 at the DBM. Samples and NBS-981 were

Table 4. Lead isotope and copper isotope ratios of Faynan samples.

Location/ site	Type/ description	Date	Inv.-no. archeol.	Lab.-no. DBM	LIA	$^{206}Pb/^{204}Pb$	2SE	$^{207}Pb/^{204}Pb$	2SE	$^{208}Pb/^{204}Pb$	2SE	$^{207}Pb/^{206}Pb$	2SE	$^{208}Pb/^{206}Pb$	2SE	CIA	δ65Cu (NIST 976)	2SE
Faynan 1	Copper	Roman-Byzantine	JD-1/30	5381-21	DBM	17.947	<0.001	15.623	<0.001	38.058	0.001	0.87058	<0.00001	2.12050	0.00003	DBM	-0.03	±0.01
Faynan 1	Copper	Roman-Byzantine	JD-1/33	5046-22												DBM	-0.43	±0.01
Faynan 5	Slag	EIA	JD-1/52b	5224-20	FIERCE	17.938	0.002	15.631	0.002	38.058	0.005	0.87139	0.00002	2.12164	0.00007			
Faynan 5	Copper	EIA	JD-1/53a	3482-19	FIERCE	17.948	0.003	15.636	0.003	38.085	0.008	0.87121	0.00002	2.12198	0.00008	DBM	0.17	±0.01
Faynan 5	Slag	EIA	JD-1/53b	3483-19	FIERCE	17.946	0.003	15.632	0.003	38.071	0.008	0.87112	0.00002	2.12153	0.00007			
Faynan 5	Slag	EIA	JD-1/53c	3484-19	FIERCE	17.959	0.002	15.636	0.002	38.095	0.006	0.87069	0.00002	2.12125	0.00008			
Faynan 5	Copper	EIA	JD-1/53d	3485-19	FIERCE	17.948	0.003	15.639	0.003	38.091	0.007	0.87140	0.00002	2.12239	0.00007			
Faynan 5	Copper	EIA	JD-1/53e	3486-19	FIERCE	17.952	0.003	15.636	0.003	38.088	0.007	0.87100	0.00002	2.12172	0.00009			
Faynan 5	Copper	EIA	JD-1/54a	3487-19a	FIERCE	17.963	0.002	15.636	0.002	38.100	0.006	0.87042	0.00003	2.12085	0.00009	DBM	0.19	±0.01
Faynan 5	Slag	EIA	JD-1/54b	3487-19b	FIERCE	17.950	0.002	15.638	0.002	38.090	0.004	0.87116	0.00002	2.12195	0.00009			
KeN	Slag	EIA	JD-2/20b	5222-20	FIERCE	17.974	0.003	15.636	0.003	38.103	0.008	0.86995	0.00003	2.11993	0.00009			
KeN	Slag	EIA	JD-2/20c	5227-20	FIERCE	17.986	0.002	15.634	0.002	38.117	0.006	0.86919	0.00003	2.11919	0.00008			
KeN	Slag	EIA	JD-2/20d	3470-19	FIERCE	17.957	0.002	15.634	0.002	38.074	0.005	0.87064	0.00002	2.12029	0.00005			
KeN	Slag	EIA	JD-2/22a	3464-19	FIERCE	17.968	0.002	15.633	0.002	38.094	0.004	0.87003	0.00002	2.12005	0.00009			
KeN	Slag	EIA	JD-2/22b	3465-19	FIERCE	17.971	0.003	15.633	0.003	38.084	0.007	0.86990	0.00003	2.11912	0.00014			
KeN	Slag	EIA	JD-2/22c	3466-19	FIERCE	17.955	0.002	15.636	0.002	38.085	0.004	0.87085	0.00002	2.12118	0.00006			
KeN	Slag	EIA	JD-2/22d	3467-19	FIERCE	17.943	0.003	15.631	0.002	38.065	0.006	0.87119	0.00002	2.12150	0.00007			
KeN	Slag	EIA	JD-2/22e	3468-19	FIERCE	17.961	0.002	15.638	0.002	38.092	0.005	0.87067	0.00002	2.12079	0.00009			
KeN	Copper	EIA	JD-2/22f	3469-19	FIERCE	17.964	0.003	15.637	0.003	38.099	0.007	0.87045	0.00003	2.12085	0.00010	DBM	-0.03	±0.01
KeN	Copper	EIA	JD-2/23b	3471-19	FIERCE	17.976	0.003	15.637	0.003	38.108	0.007	0.86991	0.00002	2.11992	0.00009	DBM	0.02	±0.01
KeN	Slag	EIA	JD-2/23c	3472-19	FIERCE	17.966	0.002	15.636	0.002	38.099	0.005	0.87032	0.00002	2.12053	0.00008			
KeN	Slag	EIA	JD-2/23d	3473-19	FIERCE	17.955	0.003	15.628	0.003	38.073	0.008	0.87043	0.00002	2.12045	0.00007			
KeN	Copper	EIA	JD-2/23e	3474-19	FIERCE	17.956	0.002	15.622	0.002	38.054	0.006	0.87004	0.00002	2.11938	0.00009			
KeN	Copper	EIA	JD-2/23f	3475-19	FIERCE	17.960	0.004	15.639	0.003	38.103	0.009	0.87076	0.00003	2.12150	0.00011			
KeN	Slag	EIA	JD-2/23g	3476-19	FIERCE	17.960	0.002	15.635	0.002	38.088	0.005	0.87049	0.00002	2.12061	0.00008			
KeN	Copper	EIA	JD-2/23h	3477-19	FIERCE	18.007	0.003	15.641	0.003	38.150	0.006	0.86862	0.00002	2.11853	0.00008			
KeN	Copper	EIA	JD-2/27b | 4644	5220-20	FIERCE	17.979	0.003	15.636	0.003	38.113	0.007	0.86967	0.00002	2.11989	0.00008	DBM	0.00	±0.01
KeN	Copper	EIA	JD-2/27d	3480-19	FIERCE	17.972	0.003	15.644	0.003	38.135	0.007	0.87048	0.00002	2.12188	0.00009			
KeN	Copper	EIA	JD-2/27d_II	5388-21	DBM	17.957	<0.001	15.628	<0.001	38.088	0.001	0.87036	<0.00001	2.12093	0.00002	DBM	0.09	±0.01
KeN	Copper	EIA	JD-2/27e	5395-21	DBM	17.960	<0.001	15.627	<0.001	38.085	<0.001	0.87020	<0.00001	2.12044	0.00003	DBM	0.16	±0.01
KeN	Copper	EIA	JD-2/27f	3481-19	FIERCE	17.953	0.003	15.631	0.003	38.065	0.007	0.87065	0.00002	2.12021	0.00009	DBM	-0.08	±0.01
KeN	Slag	EIA	JD-2/27x	3479-19	FIERCE	17.969	0.002	15.634	0.002	38.088	0.006	0.87008	0.00002	2.11972	0.00007			
KeN	Slag	EIA	JD-2/37	5219-20	FIERCE	17.968	0.002	15.634	0.002	38.092	0.006	0.87009	0.00002	2.12005	0.00008			
KeN	Slag	EIA	JD-2/38a	5214-20	FIERCE	17.952	0.002	15.633	0.002	38.080	0.006	0.87081	0.00002	2.12113	0.00009			
KeN	Slag	EIA	JD-2/38b	5216-20	FIERCE	17.954	0.003	15.635	0.003	38.085	0.007	0.87081	0.00001	2.12124	0.00005			
KeN	Slag	EIA	JD-2/38c	5217-20	FIERCE	17.956	0.003	15.630	0.002	38.077	0.006	0.87044	0.00002	2.12052	0.00007			

Location/ site	Type/ description	Date	Inv.-no. archeol.	Lab.-no. DBM	LIA	$^{206}Pb/^{204}Pb$	2SE	$^{207}Pb/^{204}Pb$	2SE	$^{208}Pb/^{204}Pb$	2SE	$^{207}Pb/^{206}Pb$	2SE	$^{208}Pb/^{206}Pb$	2SE	CIA	δ65Cu (NIST 976)	2SE
KeN	Slag	EIA	JD-2/38d	5218-20	FIERCE	17.979	0.002	15.637	0.002	38.108	0.006	0.86974	0.00002	2.11962	0.00009			
KeN	Slag	EIA	JD-2/4	5223-20	FIERCE	17.982	0.003	15.636	0.002	38.106	0.006	0.86954	0.00002	2.11921	0.00011			
KeN	Slag	EIA	JD-2/41	5215-20	FIERCE	17.959	0.003	15.635	0.003	38.093	0.006	0.87058	0.00002	2.12105	0.00008			
KeJ	Slag	Iron I	JD-11/2	5225-20	FIERCE	17.976	0.002	15.636	0.002	38.103	0.005	0.86985	0.00002	2.11967	0.00009			
KeJ	Copper	Iron I	JD-11/3a	3462-19	FIERCE	17.984	0.003	15.644	0.003	38.123	0.007	0.86991	0.00002	2.11979	0.00009			
KeJ	Copper	Iron I	JD-11/3b	3463-19	FIERCE	17.965	0.003	15.635	0.003	38.070	0.007	0.87029	0.00003	2.11909	0.00009	DBM	-0.05	±0.01
KeJ	Slag	Iron I	JD-11/3c	3460-19	FIERCE	18.021	0.002	15.642	0.002	38.157	0.005	0.86797	0.00002	2.11738	0.00008			
KeJ	Slag	Iron I	JD-11/3d	3461-19	FIERCE	18.002	0.003	15.639	0.003	38.143	0.007	0.86875	0.00002	2.11887	0.00006			
ReN	Copper	EBA II-III	JD-5/11e	5389-21	DBM	17.950	<0.001	15.623	<0.001	38.063	<0.001	0.87041	<0.00001	2.12036	0.00004	DBM	-0.06	±0.01
ReN	Copper	EBA II-III	JD-5/11a	5392-21	DBM	17.952	<0.001	15.623	<0.001	38.063	0.001	0.87038	<0.00001	2.12017	0.00003	DBM	0.00	±0.01
ReN	Copper	EBA II-III	JD-5/11b	5390-21	DBM	17.953	<0.001	15.624	<0.001	38.066	<0.001	0.87036	<0.00001	2.12021	0.00003	DBM	-0.01	±0.01
ReN	Copper	EBA II-III	JD-5/11d	5393-21	DBM	17.953	<0.001	15.623	<0.001	38.067	0.001	0.87031	<0.00001	2.12029	0.00004	DBM	-0.11	±0.01
ReN	Copper	EBA II-III	JD-5/11f	5394-21	DBM	17.959	<0.001	15.631	<0.001	38.084	0.001	0.87045	<0.00001	2.12050	0.00003	DBM	-0.42	±0.01
ReN	Slag	Iron II	JD-5/3a	5221-20	FIERCE	17.955	0.003	15.632	0.002	38.080	0.006	0.87064	0.00002	2.12083	0.00010			
ReN	Slag	Iron II	JD-5/3c	5226-20	FIERCE	17.937	0.002	15.629	0.002	38.062	0.006	0.87127	0.00002	2.12193	0.00009			
Qualb Ratiye	Geol. copper ore (MBS)		JD-12/2	5049-22	DBM	18.705	<0.001	15.673	<0.001	38.479	<0.001	0.83792	<0.00001	2.05716	0.00002	DBM	-0.60	±0.01
Qualb Ratiye	Geol. copper ore (MBS)		JD-12/5b	5050-22	DBM	18.678	<0.001	15.673	<0.001	38.763	<0.001	0.83912	<0.00001	2.07541	0.00002	DBM	-0.89	±0.01
Qualb Ratiye	Geol. copper ore (MBS)		JD-12/5c	5051-22	DBM	18.678	<0.001	15.669	<0.001	38.755	<0.001	0.83891	<0.00001	2.07496	0.00002	DBM	-0.51	±0.01
Qualb Ratiye	Geol. copper ore (MBS)		JD-12/6a	5052-22	DBM	18.251	<0.001	15.650	<0.001	38.360	<0.001	0.85751	<0.00001	2.10180	0.00002	DBM	-1.07	±0.01
Qualb Ratiye	Geol. copper ore (MBS)		GR-1	5047-22	DBM	18.673	<0.001	15.675	<0.001	38.747	0.001	0.83943	<0.00001	2.07499	0.00002	DBM	-1.47	±0.01
Qualb Ratiye	Geol. copper ore (MBS)		GR-2	5048-22	DBM	18.673	<0.001	15.669	<0.001	38.752	<0.001	0.83912	<0.00001	2.07537	0.00003	DBM	-1.20	±0.01
Faynan 9	Copper	EBA II-III	JD-23/30a	5382-21	DBM	17.935	<0.001	15.625	<0.001	38.056	0.001	0.87128	<0.00001	2.12173	0.00002	DBM	-0.19	±0.01
Faynan 9	Copper	EBA II-III	JD-23/30b	5386-21	DBM	17.943	<0.001	15.622	<0.001	38.053	0.001	0.87070	<0.00001	2.12060	0.00003	DBM	-0.09	±0.01
Faynan 9	Copper	EBA II-III	JD-23/30d	5391-21	DBM	17.943	<0.001	15.621	<0.001	38.049	0.001	0.87066	<0.00001	2.12037	0.00002	DBM	-0.13	±0.01
Faynan 9	Copper	EBA II-III	JD-23/30f	5387-21	DBM	17.933	<0.001	15.619	<0.001	38.033	0.001	0.87106	<0.00001	2.12076	0.00002	DBM	-0.07	±0.01
Faynan 9	Copper	EBA II-III	JD-23/30h	5384-21	DBM	17.964	<0.001	15.624	<0.001	38.075	<0.001	0.86981	<0.00001	2.11941	0.00002	DBM	-0.08	±0.01
Abu Kusheiba	Geol. copper ore (MBS)		JD-24/1b	5054-22	DBM	19.143	<0.001	15.707	<0.001	39.074	0.001	0.82051	<0.00001	2.04111	0.00002	DBM	-0.26	±0.01
Wadi Abiad	Geol. copper ore (MBS)		WA-4	5053-22	DBM	18.365	<0.001	15.656	<0.001	38.471	<0.001	0.85249	<0.00001	2.09478	0.00001	DBM	-0.31	±0.01
BeH. Locus 9 (1993)	Copper chunk	EBA II-III or rather EIA I	JD-31/22e	5383-21	DBM	17.950	<0.001	15.621	<0.001	38.046	0.001	0.87029	<0.00001	2.11938	0.00002	DBM	-0.04	±0.01
BeH. Locus 9 (1993)	Copper chunk	EBA II-III or rather EIA I	JD-31/22f	5385-21	DBM	17.957	<0.001	15.624	<0.001	38.058	0.001	0.87012	<0.00001	2.11923	0.00002	DBM	-0.08	±0.01

Location/ site	Type/ description	Date	Inv.-no. archeol.	Lab.-no. DBM	LIA	$^{206}Pb/^{204}Pb$	2SE	$^{207}Pb/^{204}Pb$	2SE	$^{208}Pb/^{204}Pb$	2SE	$^{207}Pb/^{206}Pb$	2SE	$^{208}Pb/^{206}Pb$	2SE	CIA	δ65Cu (NIST 976)	2SE
BeH. Locus 9 (1993)	Copper chunk	EBA II-III or rather EIA I	JD-31/22n	5380-21	DBM	18.082	<0.001	15.640	<0.001	38.201	0.002	0.86499	<0.00001	2.11247	0.00002	DBM	-0.84	±0.01
BeH. Locus 9 (1993)	Copper chunk	EBA II-III or rather EIA I	JD-31/22p	5563-20	DBM	17.947	<0.001	15.621	<0.001	38.052	0.002	0.87045	<0.00001	2.12006	0.00004			
BeH. Locus 9 (1993)	Copper chunk	EBA II-III or rather EIA I	JD-31/22q	5564-20	DBM	17.951	<0.001	15.621	<0.001	38.055	0.002	0.87027	<0.00001	2.11978	0.00004			
BeH. Locus 9 (1993)	Copper chunk	EBA II-III or rather EIA I	JD-31/22r	5565-20	DBM	17.948	<0.001	15.622	<0.001	38.051	0.002	0.87042	<0.00001	2.11988	0.00003			
BeH. Locus 9 (1993)	Copper chunk	EBA II-III or rather EIA I	JD-31/22s	5566-20	DBM	17.961	<0.001	15.622	<0.001	38.066	0.001	0.86982	<0.00001	2.11917	0.00003			
BeH. Locus 9 (1993)	Copper chunk	EBA II-III or rather EIA I	JD-31/22t	5567-20	DBM	17.948	<0.001	15.622	<0.001	38.056	0.001	0.87047	<0.00001	2.12019	0.00003			
BeH. Locus 9 (1993)	Copper chunk	EBA II-III or rather EIA I	JD-31/22u	5568-20	DBM	17.955	<0.001	15.623	<0.001	38.068	0.002	0.87021	<0.00001	2.12006	0.00004			
BeH. Locus 9 (1993)	Copper chunk	EBA II-III or rather EIA I	JD-31/22v	5569-20	DBM	17.950	<0.001	15.623	<0.001	38.062	0.002	0.87041	<0.00001	2.12031	0.00003	DBM	-0.13	±0.01
BeH. Locus 9 (1993)	Copper chunk	EBA II-III or rather EIA I	JD-31/22w	5570-20	DBM	17.955	<0.001	15.622	<0.001	38.045	0.002	0.87012	<0.00001	2.11881	0.00003	DBM	-0.06	±0.01
BeH. Locus 9 (1993)	Copper chunk	EBA II-III or rather EIA I	JD-31/22x	5571-20	DBM	17.950	<0.001	15.622	<0.001	38.058	0.002	0.87038	<0.00001	2.12011	0.00003	DBM	-0.12	±0.01
BeH. Locus 9 (1993)	Copper chunk	EBA II-III or rather EIA I	JD-31/22y	5572-20	DBM	17.948	<0.001	15.622	<0.001	38.058	0.002	0.87049	<0.00001	2.12033	0.00003			
BeH. Locus 9 (1993)	Copper chunk	EBA II-III or rather EIA I	JD-31/22z	5573-20	DBM	17.949	<0.001	15.622	<0.001	38.056	0.002	0.87041	<0.00001	2.12008	0.00003			
BeH. Locus 9 (1993)	Copper chunk	EBA II-III or rather EIA I	JD-31/22aa	5574-20	DBM	17.957	<0.001	15.620	<0.001	38.044	0.001	0.86992	<0.00001	2.11845	0.00003	DBM	-0.03	±0.01
BeH. Locus 9 (1993)	Copper chunk	EBA II-III or rather EIA I	JD-31/22ab	5575-20	DBM	17.948	<0.001	15.621	<0.001	38.052	0.001	0.87042	<0.00001	2.11999	0.00003			
BeH. Locus 9 (1993)	Copper chunk	EBA II-III or rather EIA I	JD-31/22ac	5576-20	DBM	17.944	<0.001	15.621	<0.001	38.047	0.002	0.87060	<0.00001	2.12021	0.00003			
BeH. Locus 9 (1993)	Copper chunk	EBA II-III or rather EIA I	JD-31/22ad	5577-20	DBM	17.975	<0.001	15.626	<0.001	38.067	0.002	0.86936	<0.00001	2.11764	0.00003			
BeH. Locus 9 (1993)	Copper chunk	EBA II-III or rather EIA I	JD-31/22ae	5578-20	DBM	17.958	<0.001	15.626	<0.001	38.061	0.002	0.87023	<0.00001	2.11935	0.00004	DBM	-0.10	±0.01
BeH. Locus 9 (1993)	Copper chunk	EBA II-III or rather EIA I	JD-31/22af	5579-20	DBM	17.968	<0.001	15.625	<0.001	38.074	0.002	0.86965	<0.00001	2.11887	0.00004			
BeH. Locus 9 (1993)	Copper chunk	EBA II-III or rather EIA I	JD-31/22ag	5580-20	DBM	17.942	<0.001	15.617	<0.001	38.033	0.001	0.87049	<0.00001	2.11966	0.00004	DBM	-0.15	±0.01
BeH. Locus 9 (1993)	Copper chunk	EBA II-III or rather EIA I	JD-31/22ah	5581-20	DBM	17.949	<0.001	15.621	<0.001	38.043	0.002	0.87035	<0.00001	2.11929	0.00003	DBM	-0.09	±0.01
BeH. Locus 9 (1993)	Copper chunk	EBA II-III or rather EIA I	JD-31/22ai	5582-20	DBM	17.960	<0.001	15.624	<0.001	38.076	0.001	0.86998	<0.00001	2.11988	0.00003			

Table 5. Lead isotope and copper isotope ratios of Timna samples.

Location/ site	Type/ description	Estimated date (BC)	Inv.-no. CTV	Lab.-no. DBM	LIA	$^{206}Pb/^{204}Pb$	2SE	$^{207}Pb/^{204}Pb$	2SE	$^{208}Pb/^{204}Pb$	2SE	$^{207}Pb/^{206}Pb$	2SE	$^{208}Pb/^{206}Pb$	2SE	CIA	δ65Cu (NIST 976)	2SE
2	Slag	1300-1150	LIA012	3012-18	FIERCE	18.138	0.003	15.633	0.002	38.253	0.006	0.861898	0.00004	2.10901	0.00017			
2	Slag	1300-1150	LIA013	3013-18	FIERCE	17.922	0.003	15.623	0.003	38.071	0.007	0.871728	0.00005	2.12424	0.00017			
2	Slag	1300-1150	LIA018	3018-18	FIERCE	17.963	0.005	15.620	0.005	38.095	0.013	0.869586	0.00004	2.12077	0.00016			
3	Copper chunk	1200-1100	LIA004	3004-18	FIERCE	18.297	0.002	15.649	0.002	38.399	0.005	0.855273	0.00003	2.09873	0.00016			
3	Slag	1200-1100	LIA021	3021-18	FIERCE	17.922	0.003	15.624	0.003	38.058	0.006	0.871818	0.00004	2.12374	0.00021			
3	Slag	1300-1100	TIM3-G1-04.3-CP	4299-16	FIERCE	18.243	0.001	15.683	0.002	38.405	0.005	0.859672	0.00003	2.10524	0.00014			
3	Slag	1300-1100	TIM3-G2-05-UT	4293-16	FIERCE	18.022	0.002	15.630	0.002	38.158	0.006	0.867271	0.00003	2.11734	0.00011			
3	Slag	1300-1100	TIM3-G3-06.3-CP	4300-16	FIERCE	17.983	0.002	15.648	0.002	38.118	0.005	0.870120	0.00003	2.11957	0.00014			
3	Slag	1300-1100	TIM3-G3-06-UT	4294-16	FIERCE	18.159	0.001	15.671	0.001	38.313	0.004	0.862985	0.00003	2.10994	0.00011			
3	Arch. copper ore	1300-1100	TIM3-Lay10	4287-16	FIERCE	18.171	0.002	15.638	0.002	38.323	0.006	0.860569	0.00002	2.10905	0.00010	DBM	-0.80	±0.01
15	Copper chunk	1100-1000	LIA017	3017-18	FIERCE	18.136	0.001	15.653	0.001	38.274	0.004	0.863051	0.00002	2.11035	0.00008			
15	Slag	1100-1000	LIA020	3020-18	FIERCE	17.960	0.002	15.630	0.002	38.098	0.006	0.870302	0.00005	2.12141	0.00017			
15	Copper	1100-1000	LIA034	3034-18	FIERCE	17.889	0.001	15.623	0.001	38.032	0.002	0.873361	0.00001	2.12612	0.00005			
15	Copper	1100-1000	LIA035	3035-18	FIERCE	18.147	0.001	15.640	0.001	38.262	0.003	0.861804	0.00002	2.10839	0.00006	DBM	-0.87	±0.01
15	Copper	1100-1000	LIA036	3036-18	FIERCE	18.053	0.001	15.631	0.001	38.165	0.004	0.865833	0.00002	2.11402	0.00008	DBM	-1.13	±0.01
15	Copper chunk	1100-1000	LIA040	3040-18	FIERCE	18.069	0.002	15.635	0.002	38.193	0.005	0.865273	0.00003	2.11372	0.00018			
15	Arch. copper ore	1100-1000	TIM15-307	4289-16	FIERCE	17.972	0.001	15.629	0.001	38.105	0.003	0.869593	0.00002	2.12015	0.00006	DBM	-1.09	±0.01
15	Metal	1100-1000	TIM15-308_1085	4279-16	FIERCE	18.212	0.002	15.776	0.002	38.547	0.004	0.866269	0.00002	2.11652	0.00005			
15	Metal	1100-1000	TIM15-308_1105	4282-16	FIERCE	18.045	0.010	15.622	0.009	38.146	0.023	0.865839	0.00006	2.11413	0.00015			
15	Arch. copper ore	1100-1000	TIM15-701	4288-16	FIERCE	18.121	0.002	15.636	0.002	38.243	0.004	0.862873	0.00002	2.11039	0.00006	DBM	-0.64	±0.01
15	Metal	1100-1000	TIM15-901_11011	4277-16	FIERCE	18.149	0.002	15.643	0.002	38.268	0.005	0.861881	0.00002	2.10851	0.00009			
30	Slag with visible prills	1150-930	LIA023	3023-18	FIERCE	17.899	0.002	15.620	0.002	38.014	0.005	0.872676	0.00003	2.12380	0.00017			
30	Slag	1150-930	LIA024	3024-18	FIERCE	18.229	0.004	15.642	0.003	38.338	0.009	0.858068	0.00005	2.10305	0.00016			
30	Slag	930-800	LIA026	3026-18	FIERCE	17.909	0.004	15.624	0.003	38.039	0.007	0.872436	0.00004	2.12413	0.00023			
30	Slag	930-800	LIA041	3041-18	FIERCE	17.906	0.003	15.623	0.002	38.039	0.008	0.872481	0.00005	2.12433	0.00032			
30	Slag	930-800	LIA042	3042-18	FIERCE	17.893	0.008	15.623	0.007	38.028	0.017	0.873183	0.00007	2.12532	0.00042			
30	Slag	930-800	LIA043	3043-18	FIERCE	17.893	0.005	15.623	0.004	38.025	0.010	0.873074	0.00006	2.12495	0.00027			
30	Slag	930-800	TIM30-806_1000B	4285-16	FIERCE	17.889	0.001	15.624	0.001	38.024	0.004	0.873360	0.00003	2.12549	0.00013			
30	Slag	1150-930	TIM30-901_552A	4284-16	FIERCE	17.982	0.001	15.659	0.001	38.164	0.004	0.870839	0.00002	2.12239	0.00010			

Location/ site	Type/ description	Estimated date (BC)	Inv.-no. CTV	Lab.-no. DBM	LIA	$^{206}Pb/^{204}Pb$	2SE	$^{207}Pb/^{204}Pb$	2SE	$^{208}Pb/^{204}Pb$	2SE	$^{207}Pb/^{206}Pb$	2SE	$^{208}Pb/^{206}Pb$	2SE	CIA	δ65Cu (NIST 976)	2SE
34	Copper prill	1030-930	LIA001	3001-18	FIERCE	18.223	0.002	15.659	0.002	38.339	0.004	0.859298	0.00002	2.10386	0.00009			
34	Slag with visible prills	1030-930	LIA002	3002-18	FIERCE	17.978	0.002	15.635	0.001	38.118	0.004	0.869667	0.00003	2.12024	0.00013			
34	Slag with visible prills	1030-930	LIA003	3003-18	DBM	17.900	<0.001	15.619	<0.001	38.029	0.002	0.872625	<0.00001	2.12442	0.00003	DBM	-0.71	±0.01
34	Slag with visible prills	1030-930	LIA005	3005-18	FIERCE	18.119	0.003	15.640	0.003	38.252	0.007	0.863183	0.00003	2.11119	0.00018			
34	Slag with visible prills	1030-930	LIA006	3006-18	FIERCE	18.115	0.002	15.637	0.002	38.232	0.005	0.863235	0.00003	2.11058	0.00018			
34	Copper prill	1030-930	LIA010	3010-18	FIERCE	18.065	0.002	15.634	0.002	38.209	0.006	0.865439	0.00004	2.11505	0.00013			
34	Tuyere with visible prills	1030-930	LIA016	3016-18	FIERCE	18.146	0.003	15.636	0.002	38.254	0.006	0.861695	0.00005	2.10792	0.00017			
34	Slag	1030-930	LIA019	3019-18	FIERCE	17.967	0.002	15.627	0.002	38.114	0.005	0.869740	0.00004	2.12134	0.00014			
34	Copper prill	1030-930	LIA028	3028-18	FIERCE	18.114	0.001	15.657	0.001	38.249	0.004	0.864355	0.00002	2.11155	0.00009			
34	Copper	1030-930	LIA033	3033-18	FIERCE	18.014	0.001	15.644	0.001	38.164	0.004	0.868452	0.00002	2.11867	0.00009			
34	Slag	1030-930	TIM34-129	4295-16	FIERCE	18.081	0.001	15.660	0.001	38.243	0.003	0.866129	0.00002	2.11513	0.00009			
34	Slag	1030-930	TIM34-132	4296-16	FIERCE	18.059	0.001	15.658	0.001	38.226	0.003	0.867044	0.00002	2.11672	0.00010			
34	Slag	1030-930	TIM34-17-1CP	4298-16	FIERCE	18.073	0.007	15.714	0.009	38.326	0.011	0.869	0.003	2.121	0.004			
34	Slag	1030-930	TIM34-18-1CP	4297-16	FIERCE	17.968	0.001	15.656	0.001	38.146	0.005	0.871344	0.00003	2.12304	0.00013			
34	Metal	1030-930	TIM34-410_5342	4280-16	FIERCE	17.892	0.001	15.626	0.001	38.042	0.003	0.873361	0.00002	2.12618	0.00009			
34	Arch. copper ore	1030-930	TIM34-510	4290-16	FIERCE	17.936	0.002	15.624	0.002	38.080	0.005	0.871073	0.00002	2.12310	0.00009	DBM	-1.02	±0.01
34	Arch. copper ore	1030-930	TIM34-517	4291-16	FIERCE	17.937	0.001	15.636	0.001	38.088	0.003	0.871747	0.00002	2.12351	0.00007	DBM	-1.42	±0.01
34	Arch. copper ore	1030-930	TIM34-521	4292-16	FIERCE	17.965	0.001	15.629	0.001	38.113	0.005	0.869959	0.00003	2.12151	0.00012	DBM	-0.72	±0.01
35	Copper prill	1200-1000	LIA007	3007-18	FIERCE	18.212	0.001	15.671	0.001	38.358	0.002	0.860454	0.00002	2.10618	0.00006			
35	Copper prill	1200-1000	LIA008	3008-18	FIERCE	18.067	0.001	15.635	0.001	38.184	0.003	0.865369	0.00001	2.11348	0.00006	DBM	-1.25	±0.01
35	Copper prill	1200-1000	LIA011	3011-18	FIERCE	18.153	0.002	15.636	0.002	38.255	0.006	0.861339	0.00004	2.10735	0.00014			
35	Copper prill	1200-1000	LIA022	3022-18	FIERCE	18.256	0.001	15.653	0.001	38.370	0.003	0.857376	0.00001	2.10173	0.00006			
35	Copper prill	1200-1000	LIA027	3027-18	FIERCE	18.256	0.001	15.652	0.001	38.370	0.003	0.857379	0.00002	2.10176	0.00007			
35	Copper prill	1200-1000	LIA029	3029-18	FIERCE	18.471	0.001	15.681	0.001	38.595	0.003	0.848944	0.00002	2.08952	0.00009			
35	Copper prill	1200-1000	LIA030	3030-18	FIERCE	18.088	0.002	15.632	0.002	38.201	0.004	0.864245	0.00004	2.11198	0.00016			
35	Copper prill	1200-1000	LIA031	3031-18	FIERCE	17.994	0.001	15.658	0.001	38.168	0.003	0.870151	0.00002	2.12116	0.00008			
35	Copper	1200-1000	LIA037	3037-18	FIERCE	18.128	0.001	15.635	0.001	38.232	0.003	0.862508	0.00002	2.10906	0.00007			
35	Copper	1200-1000	LIA038	3038-18	FIERCE	18.084	0.001	15.633	0.001	38.197	0.004	0.864473	0.00003	2.11215	0.00010			
35	Copper prill	1200-1000	LIA039	3039-18	FIERCE	18.156	0.002	15.693	0.001	38.354	0.005	0.864294	0.00003	2.11238	0.00010			
35	Copper prill	1200-1000	TIM35-1241_13251	4286-16	FIERCE	18.072	0.002	15.634	0.002	38.215	0.005	0.865104	0.00005	2.11455	0.00010			

analysed with concentrations of 200 ppb Pb and 50 ppm Tl (NIST SRM-997) in 5 % HNO_3.

Results of LIA are presented in Table 4 (Faynan samples) and Table 5 (Timna samples).

Copper isotope analysis (CIA) of copper and archaeological ore samples (MC-ICP-MS)

CIA was conducted using multi-collector ICP-MS (Neptune XT, Thermo Fisher Scientific) at the DBM. The methodology published by Jansen, et al. (2017) was adapted. 1 ppm Ni for mass bias correction was added to the samples and SRM which were diluted to 400 ppb Cu in 5 % HNO_3. Sample standard bracketing using the copper isotope SRM ERM-AE647 was applied. Delta values were calculated relative to NIST-976 using an offset of 0.21 ‰ (Moeller, et al., 2012). A small amount of NIST-976 was provided by FIERCE which was measured as unknown sample during the analytical campaigns. Repeat analyses yielded $\delta^{65}Cu_{ERM\text{-}AE647}$= -0.20 ± 0.02 ($n$ = 27, 2SD) for NIST-976 over a period of three month. For analytical criteria of sample selection see chapter V.2.

Copper isotope ratios of Faynan and Timna samples are presented in Tables 4 and 5.

Bulk chemical analysis of copper samples (SF-ICP-MS)

In the laboratory of the Deutsches Bergbau-Museum Bochum (DBM), about 50 mg of metal was mixed with 3 ml HCl and 2 ml HNO_3, both half-concentrated. After digestion, the copper metal solutions were diluted with ultra-pure water up to a concentration of about 1000 mg/l. For the slag powder digestions, after drying for 8 hours at 105°C, about 100 mg was mixed with concentrated 5 g HCl, 5 g HNO_3 and 1.2 g HF in teflon beakers and then heated up in a microwave (µPREP-A microwave (MLS GmbH): first, for 80 min at 260°C (1 bar, 1200 W) and afterwards in a second step after addition of 10 ml H_3BO_3 (50 g/l) for 40 min at 220°C (1 bar, 1200 W). The solution was also diluted up to a concentration of ca. 1000 mg/l.

The chemical composition was determined using sector field inductively coupled plasma mass spectrometry (SF-ICP-MS, ELEMENT XR, Thermo Fisher Scientific). Quantification was done with external calibration. For elements in trace amounts, the stock solution was diluted 1:10 with 5 % HNO_3, for copper and 1:100 for minor elements. The analyses were carried out with a FAST SC-system, ST 5532 PFA µ-FLOW nebulizer, Peltier-cooled PFA spray chamber and 1.8 mm sapphire injector in triple detector mode for all three different mass resolutions (m/Δm). Metal analyses have been controlled with copper standard BAM 376 (Bundesanstalt für Materialforschung, Berlin) and tin bronze standard BRONZE C (British Chemical Standards, Middlesbrough, UK), slag measurements with compatible standard materials FER-1 and FER-2 (Canadian Certified Reference Materials Project), GBW07107 (LGC Standards, Teddington, Middlesex, UK). Relative standard deviation for trace elements varied between 0.5 and 4.5 %, for major elements between 0.6 and 1.2 % and for copper around 2 %.

15 elements were measured: Ag, As, Bi, Co, Cu, Fe, Ni, P, Pb, S, Sb, Se, Sn, Te, Zn. The data set of the analytical results (not normalized to Cu) is presented in Tables 6 and 7, while in the text and in the figures we operate with Cu-normalized values.

Microstructural analysis of copper samples (OM, SEM-EDX)

Analysis was conducted in the Institute of Nanoscience and Nanotechnology (INN) at N.C.S.R. "Demokritos", Athens. The samples were preliminarily examined and photographed through a binocular stereoscope. Subsequently, they were embedded into polyester resin and –upon resin curing- were subjected to grinding and polishing in order to acquire polished cross-sections. Cross sections were investigated through an optical microscope (OM, Leica, model DMRPX) in both the as-polished and etched (by an alcoholic $FeCl_3$ solution, Scott, 1991) condition, at magnifications ranging from 25 x to 200 x. Sections were also examined through a scanning electron microscope coupled with an energy dispersive X-ray analyser (SEM-EDX by FEI, model Quanta Inspect D 8334, equipped with a sutw EDX detector). Prior to SEM-EDX examination, the sections were sputter-coated with conductive carbon through a Balzers' CED 030 carbon vaporizer for conductivity purposes. The samples were mainly examined using the backscattered electron (BSE) detector which allows for the differentiation of the observed phases on the basis of their atomic number (the higher the atomic number of a phase – the brighter it appears), and occasionally with the secondary electron (SE) detector which reveals topographic details (Egerton, 2005). The samples' bulk quantitative elemental compositions were estimated using the SEM's built-in 'Genesis-Spectrum' software (EDAX Company); the corresponding spectra were collected for 200 seconds with the SEM-EDX device operating at 25 kV voltage and ~100 µA current (high vacuum mode). The adopted standard-less quantification method incorporates ZAF matrix corrections (Heinrich, 1991), which, in combination with high accelerating voltage (25 kV) and optimal spectra collection parameters (high count rate, long

Table 6. Bulk chemical analysis of Faynan samples (SF-ICP-MS).

Location/ site	Type/ description	Date	Inv.-no. archeol.	Lab.-no. DBM	Chemistry	wt.% Cu	wt.% Ag	wt.% As	wt.% Bi	wt.% Co	wt.% Fe	wt.% Ni	wt.% P	wt.% Pb	wt.% S	wt.% Sb	wt.% Se	wt.% Sn	wt.% Te	wt.% Zn	wt.% sum
Faynan 1	Copper	Roman-Byzantine	JD-1/30	5381-21	DBM	85.2	0.010	0.080	0.000	0.30	1.32	0.17	0.028	9.91	0.21	0.001	0.001	0.001	0.000	0.28	98
Faynan 5	Copper	EIA	JD-1/53a	3482-19	DBM	95.8	0.025	0.092	0.000	0.17	1.77	0.094	0.085	0.99	0.31	0.004	0.001	0.002	0.000	0.16	100
Faynan 5	Copper	EIA	JD-1/53d	3485-19	DBM	65.2	0.001	0.096	0.000	0.073	5.20	0.045	0.35	5.99	0.74	0.004	0.001	0.003	0.000	0.13	78
Faynan 5	Copper	EIA	JD-1/53e	3486-19	DBM	58.8	0.017	0.12	0.000	0.31	6.73	0.15	0.63	10.1	1.52	0.004	0.001	0.002	0.001	0.49	79
Faynan 5	Copper	EIA	JD-1/54a	3487-19a	DBM	91.3	0.001	0.16	0.000	0.044	1.83	0.060	0.43	4.86	0.11	0.003	0.001	0.002	0.001	0.32	99
KeN	Copper	EIA	JD-2/22f	3469-19	DBM	67.0	0.001	0.14	0.000	0.034	3.46	0.060	0.61	5.50	0.41	0.005	0.001	0.003	0.001	0.20	77
KeN	Copper	EIA	JD-2/23b	3471-19	DBM	84.9	0.002	0.14	0.000	0.084	5.79	0.080	0.83	1.72	0.28	0.005	0.001	0.002	0.000	0.27	94
KeN	Copper	EIA	JD-2/23e	3474-19	DBM	67.2	0.000	0.019	0.000	0.061	0.17	0.062	0.030	0.12	0.23	0.004	0.001	0.002	0.001	0.090	68
KeN	Copper	EIA	JD-2/23f	3475-19	DBM	43.5	0.002	0.30	0.001	0.47	23.6	0.29	2.29	4.91	0.94	0.006	0.001	0.006	0.001	0.51	77
KeN	Copper	EIA	JD-2/23h	3477-19	DBM	59.0	0.000	0.048	0.000	0.16	1.57	0.12	0.14	2.39	1.12	0.004	0.002	0.002	0.002	0.32	65
KeN	Copper	EIA	JD-2/27d	3480-19	DBM	87.8	0.001	0.22	0.001	0.075	2.02	0.042	0.39	7.66	0.078	0.004	0.001	0.002	0.001	0.053	98
KeN	Copper	EIA	JD-2/27d_II	5388-21	DBM	88.6	0.002	0.21	0.000	0.089	2.31	0.050	0.44	6.48	0.085	0.002	0.001	0.001	0.000	0.069	98
KeN	Copper	EIA	JD-2/27e	5395-21	DBM	86.3	0.012	0.086	0.000	0.068	1.88	0.044	0.43	7.30	0.060	0.002	0.001	0.002	0.002	0.095	96
KeN	Copper	EIA	JD-2/27f	3481-19	DBM	93.7	0.001	0.089	0.000	0.086	2.89	0.11	0.43	1.15	0.066	0.004	0.001	0.002	0.001	0.17	99
KeJ	Copper	Iron I	JD-11/3a	3462-19	DBM	58.2	0.000	0.045	0.000	0.076	3.40	0.030	0.21	0.57	0.56	0.007	0.001	0.003	0.002	0.21	63
KeJ	Copper	Iron I	JD-11/3b	3463-19	DBM	92.8	0.000	0.10	0.000	0.13	2.54	0.038	0.24	0.99	0.33	0.005	0.001	0.004	0.001	0.10	97
ReN	Copper	EBA II-III	JD-5/11e	5389-21	DBM	95.2	0.003	0.043	0.001	0.003	0.13	0.044	0.12	1.08	0.12	0.001	0.001	0.003	0.000	0.024	97
ReN	Copper	EBA II-III	JD-5/11a	5392-21	DBM	95.0	0.005	0.062	0.001	0.001	0.003	0.033	0.10	0.33	0.10	0.002	0.001	0.000	0.000	0.004	96
ReN	Copper	EBA II-III	JD-5/11b	5390-21	DBM	97.3	0.005	0.062	0.001	0.001	0.002	0.033	0.19	0.29	0.19	0.001	0.001	0.000	0.001	0.010	98
ReN	Copper	EBA II-III	JD-5/11d	5393-21	DBM	98.0	0.002	0.040	0.001	0.000	0.016	0.020	0.30	0.059	0.30	0.001	0.001	0.000	0.000	0.009	99
ReN	Copper	EBA II-III	JD-5/11f	5394-21	DBM	97.4	0.009	0.058	0.000	0.075	1.29	0.050	0.33	0.42	0.33	0.002	0.001	0.001	0.001	0.020	100
Faynan 9	Copper	EBA II-III	JD-23/30a	5382-21	DBM	95.7	0.003	0.038	0.002	0.000	0.025	0.043	0.010	1.44	0.094	0.001	0.001	0.001	0.000	0.007	97
Faynan 9	Copper	EBA II-III	JD-23/30b	5386-21	DBM	96.3	0.001	0.023	0.002	0.002	0.032	0.015	0.017	0.64	0.16	0.001	0.001	0.000	0.001	0.011	97
Faynan 9	Copper	EBA II-III	JD-23/30d	5391-21	DBM	96.4	0.002	0.022	0.000	0.001	0.015	0.025	0.004	0.84	0.23	0.001	0.001	0.000	0.000	0.010	98
Faynan 9	Copper	EBA II-III	JD-23/30f	5387-21	DBM	96.2	0.004	0.050	0.001	0.001	0.001	0.044	0.003	1.78	0.50	0.001	0.001	0.000	0.001	0.008	99
Faynan 9	Copper	EBA II-III	JD-23/30h	5384-21	DBM	96.2	0.002	0.008	0.000	0.000	0.035	0.005	0.009	0.16	0.091	0.001	0.001	0.000	0.000	0.007	97
BeH. Locus 9 (1993)	Copper chunk	EBA II-III or rather EIA I	JD-31/22e	5383-21	DBM	96.5	0.001	0.060	0.000	0.014	0.55	0.040	0.008	0.33	0.15	0.001	0.001	0.000	0.000	0.021	98
BeH. Locus 9 (1993)	Copper chunk	EBA II-III or rather EIA I	JD-31/22f	5385-21	DBM	92.6	0.001	0.072	0.000	0.13	3.20	0.056	0.32	0.75	0.31	0.001	0.001	0.001	0.000	0.236	98
BeH. Locus 9 (1993)	Copper chunk	EBA II-III or rather EIA I	JD-31/22n	5380-21	DBM	85.3	0.024	0.059	0.000	0.033	11.7	0.041	0.027	0.21	0.41	0.006	0.010	0.000	0.000	0.068	98

Location/ site	Type/ description	Date	Inv.-no. archeol.	Lab.-no. DBM	Chemistry	wt.% Cu	wt.% Ag	wt.% As	wt.% Bi	wt.% Co	wt.% Fe	wt.% Ni	wt.% P	wt.% Pb	wt.% S	wt.% Sb	wt.% Se	wt.% Sn	wt.% Te	wt.% Zn	wt.% sum
BeH. Locus 9 (1993)	Copper chunk	EBA II-III or rather EIA I	JD-31/22p	5563-20	DBM	86.2	0.003	0.058	0.001	0.093	2.57	0.072	0.098	3.89	0.46	0.003	0.001	0.002	0.002	0.13	94
BeH. Locus 9 (1993)	Copper chunk	EBA II-III or rather EIA I	JD-31/22q	5564-20	DBM	90.7	0.002	0.064	0.000	0.10	2.60	0.068	0.037	1.84	0.28	0.003	0.007	0.002	0.001	0.12	96
BeH. Locus 9 (1993)	Copper chunk	EBA II-III or rather EIA I	JD-31/22r	5565-20	DBM	91.0	0.003	0.079	0.000	0.076	3.54	0.098	0.014	1.78	0.25	0.003	0.000	0.001	0.001	0.16	97
BeH. Locus 9 (1993)	Copper chunk	EBA II-III or rather EIA I	JD-31/22s	5566-20	DBM	74.9	0.003	0.066	0.001	0.083	2.22	0.057	0.026	7.90	0.31	0.002	0.001	0.002	0.001	0.11	86
BeH. Locus 9 (1993)	Copper chunk	EBA II-III or rather EIA I	JD-31/22t	5567-20	DBM	70.3	0.002	0.051	0.001	0.036	6.14	0.032	0.071	2.92	0.29	0.002	0.001	0.014	0.001	0.14	80
BeH. Locus 9 (1993)	Copper chunk	EBA II-III or rather EIA I	JD-31/22u	5568-20	DBM	90.1	0.002	0.085	0.000	0.043	3.62	0.064	0.33	2.98	0.18	0.002	0.000	0.004	0.001	0.14	98
BeH. Locus 9 (1993)	Copper chunk	EBA II-III or rather EIA I	JD-31/22v	5569-20	DBM	95.3	0.001	0.044	0.001	0.003	0.020	0.028	0.005	1.72	0.23	0.002	0.002	0.002	0.001	0.01	97
BeH. Locus 9 (1993)	Copper chunk	EBA II-III or rather EIA I	JD-31/22w	5570-20	DBM	92.5	0.000	0.049	0.000	0.059	2.68	0.039	0.127	0.39	0.21	0.002	0.001	0.002	0.001	0.15	96
BeH. Locus 9 (1993)	Copper chunk	EBA II-III or rather EIA I	JD-31/22x	5571-20	DBM	96.7	0.001	0.057	0.001	0.027	1.07	0.043	0.056	1.53	0.30	0.002	0.001	0.003	0.000	0.07	100
BeH. Locus 9 (1993)	Copper chunk	EBA II-III or rather EIA I	JD-31/22y	5572-20	DBM	85.7	0.019	0.071	0.001	0.074	3.58	0.041	0.016	3.42	0.48	0.002	0.000	0.005	0.001	0.06	94
BeH. Locus 9 (1993)	Copper chunk	EBA II-III or rather EIA I	JD-31/22z	5573-20	DBM	87.3	0.002	0.064	0.001	0.056	2.93	0.048	0.010	2.27	0.49	0.002	0.001	0.002	0.002	0.12	93
BeH. Locus 9 (1993)	Copper chunk	EBA II-III or rather EIA I	JD-31/22aa	5574-20	DBM	99.0	0.000	0.018	0.000	0.029	0.24	0.040	0.008	0.28	0.49	0.001	0.003	0.001	0.001	0.03	100
BeH. Locus 9 (1993)	Copper chunk	EBA II-III or rather EIA I	JD-31/22ab	5575-20	DBM	92.2	0.002	0.078	0.001	0.038	2.72	0.060	0.006	2.26	0.81	0.002	0.001	0.002	0.001	0.10	98
BeH. Locus 9 (1993)	Copper chunk	EBA II-III or rather EIA I	JD-31/22ac	5576-20	DBM	85.7	0.002	0.040	0.000	0.028	1.12	0.047	0.014	1.86	0.36	0.002	0.000	0.017	0.001	0.06	89
BeH. Locus 9 (1993)	Copper chunk	EBA II-III or rather EIA I	JD-31/22ad	5577-20	DBM	91.6	0.005	0.036	0.000	0.078	2.31	0.032	0.25	0.37	0.22	0.002	0.001	0.004	0.001	0.11	95
BeH. Locus 9 (1993)	Copper chunk	EBA II-III or rather EIA I	JD-31/22ae	5578-20	DBM	93.5	0.000	0.14	0.000	0.062	2.51	0.061	0.005	0.33	0.55	0.002	0.001	0.002	0.001	0.05	97
BeH. Locus 9 (1993)	Copper chunk	EBA II-III or rather EIA I	JD-31/22af	5579-20	DBM	90.5	0.000	0.064	0.000	0.23	2.40	0.085	1.58	1.50	0.070	0.002	0.000	0.012	0.001	0.16	97
BeH. Locus 9 (1993)	Copper chunk	EBA II-III or rather EIA I	JD-31/22ag	5580-20	DBM	92.7	0.001	0.016	0.002	0.013	0.79	0.021	0.026	0.35	0.21	0.001	0.002	0.004	0.001	0.13	94
BeH. Locus 9 (1993)	Copper chunk	EBA II-III or rather EIA I	JD-31/22ah	5581-20	DBM	92.5	0.000	0.036	0.000	0.037	0.13	0.027	0.006	0.32	0.67	0.002	0.002	0.002	0.001	0.04	94
BeH. Locus 9 (1993)	Copper chunk	EBA II-III or rather EIA I	JD-31/22ai	5582-20	DBM	90.3	0.044	0.028	0.000	0.10	1.82	0.020	0.023	2.94	0.32	0.001	0.002	0.002	0.000	0.09	96

Table 7. Bulk chemical analysis of Timna samples (SF-ICP-MS).

Location/ site	Type/ description	Estimated date (BC)	Inv.-no. CTV	Lab.-no. DBM	Chemistry	wt.% Cu	wt.% Ag	wt.% As	wt.% Bi	wt.% Co	wt.% Fe	wt.% Ni	wt.% P	wt.% Pb	wt.% S	wt.% Sb	wt.% Se	wt.% Sn	wt.% Te	wt.% Zn	wt.% sum
15	Copper chunk	1100-1000	LIA017	3017-18	DBM	83.8	0.0050	0.025	0.0001	0.0050	1.44	0.0070	0.021	0.09	0.19	0.0055	0.0045	0.0002	0.0005	0.049	86
15	Copper	1100-1000	LIA034	3034-18	DBM	92.0	0.058	0.038	0.0015	0.0030	1.84	0.0065	0.0020	0.73	0.38	0.0045	0.0020	0.009	0.0005	0.019	95
15	Copper	1100-1000	LIA035	3035-18	DBM	93.7	0.022	0.067	0.0005	0.018	2.59	0.019	0.0085	0.35	0.17	0.018	0.011	0.087	0.0015	0.081	97
15	Copper	1100-1000	LIA036	3036-18	DBM	93.7	0.046	0.059	0.0002	0.016	1.46	0.023	0.0075	0.17	0.27	0.01	0.0075	0.0015	0.0005	0.045	96
15	Metal	1100-1000	TIM15-308_1085	4279-16	DBM	68.6	0.003	0.019	0.0003	0.0040	0.61	0.0050	0.012	0.07	0.37	0.0030	0.0040	0.006	0.0010	0.0410	70
15	Metal	1100-1000	TIM15-308_1105	4282-16	DBM	76.3	0.040	0.051	0.0004	0.0140	1.13	0.0200	0.008	0.14	0.35	0.0060	0.0055	0.005	0.0010	0.0370	78
15	Metal	1100-1000	TIM15-901_11011	4277-16	DBM	79.6	0.016	0.049	0.0003	0.0200	2.82	0.0170	0.013	0.29	0.28	0.0095	0.0065	0.004	0.0010	0.0640	83
34	Copper prill	1030-930	LIA001	3001-18	DBM	87.9	0.0045	0.051	0.0004	0.0080	5.03	0.036	0.013	0.08	0.17	0.0080	0.0080	0.0004	0.0009	0.084	93
34	Slag with visible prills	1030-930	LIA003	3003-18	DBM	95.0	0.026	0.016	0.0001	0.0032	2.26	0.0035	0.0007	0.73	0.037	0.0031	0.0010	0.0080	0.0004	0.024	98
34	Copper prill	1030-930	LIA010	3010-18	DBM	10.1	0.0055	0.036	0.0001	0.018	22.1	0.012	0.25	0.06	0.13	0.0035	0.0075	0.0002	0.0005	0.11	33
34	Copper prill	1030-930	LIA028	3028-18	DBM	57.2	0.0007	0.036	0.0002	0.034	14.4	0.037	0.20	0.10	0.13	0.0045	0.0015	0.0003	0.0009	0.038	72
34	Copper	1030-930	LIA033	3033-18	DBM	78.3	0.032	0.052	0.0002	0.0095	2.52	0.018	0.037	0.09	0.16	0.0060	0.0045	0.047	0.0005	0.014	81
34	Metal	1030-930	TIM34-410_5342	4280-16	DBM	86.1	0.092	0.029	0.0015	0.0030	1.36	0.0055	0.009	0.58	0.55	0.0025	0.0015	0.005	0.0010	0.0180	89
35	Copper prill	1200-1000	LIA007	3007-18	DBM	41.4	0.0015	0.036	0.0001	0.034	17.3	0.026	0.20	0.25	0.52	0.0075	0.0035	0.0003	0.0005	0.091	60
35	Copper prill	1200-1000	LIA008	3008-18	DBM	92.7	0.077	0.18	0.0001	0.014	4.60	0.038	0.016	0.58	0.58	0.037	0.019	0.0034	0.0005	0.23	99
35	Copper prill	1200-1000	LIA022	3022-18	DBM	73.9	0.010	0.056	0.0001	0.022	7.44	0.023	0.0050	0.37	0.072	0.0085	0.0020	0.0003	0.0005	0.12	82
35	Copper prill	1200-1000	LIA027	3027-18	DBM	74.2	0.0075	0.050	0.0001	0.017	6.03	0.020	0.0060	0.29	0.054	0.0080	0.0020	0.0002	0.0005	0.11	81
35	Copper prill	1200-1000	LIA029	3029-18	DBM	70.1	0.0025	0.084	0.0001	0.024	7.52	0.053	0.096	0.15	0.084	0.017	0.0085	0.0002	0.0005	0.17	78
35	Copper prill	1200-1000	LIA030	3030-18	DBM	38.4	0.0080	0.004	0.0001	0.0050	0.04	0.0040	0.014	0.02	0.36	0.001	0.0020	0.0002	0.0005	0.25	39
35	Copper prill	1200-1000	LIA031	3031-18	DBM	16.1	0.0003	0.027	0.0001	0.0015	2.37	0.0035	0.068	0.11	0.063	0.0030	0.0010	0.0002	0.0005	0.036	19
35	Copper	1200-1000	LIA037	3037-18	DBM	56.1	0.0006	0.090	0.0001	0.0095	0.88	0.014	0.0040	0.16	0.29	0.016	0.0070	0.0010	0.0005	0.021	58
35	Copper	1200-1000	LIA038	3038-18	DBM	74.8	0.0025	0.070	0.0001	0.016	1.81	0.023	0.015	0.23	0.12	0.0085	0.0050	0.0008	0.0005	0.050	77
35	Copper prill	1200-1000	LIA039	3039-18	DBM	61.3	0.0010	0.074	0.0002	0.026	13.7	0.026	0.064	0.11	0.21	0.011	0.0095	0.013	0.0005	0.025	76

Table 8. Results of EDX analyses conducted on inclusions spotted within the solid metal cores of the studied samples. Analyses are normalized to 100 wt.%. Abbreviations: n.d.: not detected.
[1] Consider that there are practical difficulties in detecting low amounts of silver in Pb-rich phases by EDX, because the L_α spectra line of Ag almost coincides with an M-series line of lead (2.99 and 3.07 keV respectively). For this reason question marks accompany the relevant entries.

ID (date – site)	Inclusion type	Size (μm)	Relative presence	Detected elements							
				O	P	S	Pb	Mn	Fe	Cu	Other
3480-19 (EIA – Khirbet en-Nahas)	Fe-P-Mn-Co	5-30	**	0.1	19.3	n.d.	0.2	5.3	68.1	3.4	Co/Ni (3.5/0.1)
	Mn-S-Cu	8-40	*	n.d.	0.1	30.2	n.d.	49.3	0.5	19.9	
	Pb-Cu	5-30	***	0.5	n.d.	n.d.	85.2	0.1	n.d.	14.3	
	Composite	10-30	**	0.1	10.8	n.d.	8.5	15.9	0.9	60	As/Ni (3.7/0.1)
3481-19 (EIA – Khirbet en-Nahas)	Fe-P-Mn-Co	<1-50	***	0.1	19.7	n.d.	n.d.	1.4	69.4	5.4	Co/Ni (3.1/0.9)
	Mn-S-Cu	5-30	**	1.1	0.1	29.9	n.d.	47.9	0.7	20.3	
	Cu-P	5-20	*	0.5	14.1	n.d.	0.4	0.7	0.7	82.6	As/Ni (0.8/0.2)
	Pb-Cu-Fe	4-20	*	0.4	6.1	n.d.	55.6	2.1	14.3	20.5	Co/Ni (0.5/0.6)
3482-19 (EIA – Faynan 5)	Cu-S	15-40	***	0.9	n.d.	20.7	0.8	n.d.	0.6	77.1	
	Cu-S-Fe-Mn	4-15	*	1.2	n.d.	24	0.9	2.5	6.9	64.5	
	Fe-O-Cu	5-40	*	18.9	0.6	0.8	0.2	n.d.	56.3	15.6	Co/Ni/Zn/Cl (3.2/2.8/0.9/0.6)
	Pb-Cu	2-30	**	5.2	4	n.d.	43.2	n.d.	2	44.2	Cl (1.5)
3003-18 (1030-930 BC – Timna)	Cu-S-Fe-Pb	5-50	***	1	n.d.	22.1	8.2	n.d.	9.2	59	Se/Ag(?)[1] 0.5/tr(?)
	Cu-S-Fe-O-Se	4-35	**	1	n.d.	23.4	n.d.	n.d.	10	64.7	Se (0.8)
	Pb-rich	5-50	*	1.1	n.d.	n.d.	80.5	n.d.	1	17.4	
	Slag	25-130	*	19.9	1.1	0.1	0.6	n.d.	33.4	1.7	Si/Ca/Al/K/Ti/Mg (29.8/9.5/2.2/1.1/0.2/0.2)
3034-18 (1100-1000 BC – Timna)	Cu-S-Fe	5-50	***	0.9	n.d.	24.7	n.d.	n.d.	9.6	64.7	
	Cu-S	5-50	***	0.9	n.d.	19.4	n.d.	n.d.	0.7	79	
	Pb-rich	5-40	*	2	n.d.	3.4	53.4	n.d.	1.2	28	Cl/Ag(?)/K/Ca (10.4/1.1(?)/0.3/0.3)
	Fe-Cu-O-S	8-20	*	11.6	n.d.	6.7	1.8	n.d.	43.3	35.9	Cl (0.7)

Table 9. Summary of EDX bulk analyses and metal matrices' analyses, posted versus the corresponding bulk analyses with SF-ICP-MS. EDX analyses are normalized to 100 wt.%. Abbreviations: n.d.: not detected; n.m.: not measured.
[1] Corresponds to the mean values of EDX analyses conducted on "pure" (i.e. excluding all types of inclusions) metal matrix areas.

ID (date-site)		O	P	S	Pb	Cl	Mn	Fe	Cu	Other
3480-19 (EIA – Khirbet en-Nahas)	Bulk-Chem (SF-ICP-MS)	n.d.	0.39	0.08	7.66	n.m.	1.16.	2.02	87.8	Ni/Co (0.04/0.08)
	Bulk-EDX	0.5	0.7	n.d.	3	n.d.	2.5	1.8	91.6	
	Matrix-EDX[1]	*0.4*	*n.d.*	*n.d.*	*n.d.*	*n.d.*	*1.1*	*2.6*	*95.9*	
3481-19 (EIA – Khirbet en-Nahas)	Bulk-Chem (SF-ICP-MS)	n.m.	1.15	0.07	1.15	n.m.	0.25	2.89	93.7	Ni/Co (0.11/0.009)
	Bulk-EDX	0.6	1	0.4	0.7	n.d.	1.4	2.3	93.5	
	Matrix-EDX	*0.2*	*0.3*	*n.d.*	*n.d.*	*n.d.*	*0.3*	*2.5*	*96.7*	
3482-19 (EIA – Faynan 5)	Bulk-Chem (SF-ICP-MS)	n.m.	0.08	0.31	0.99	n.m.	0.024.	1.77	95.8	Ni/Co (0.09/0.17)
	Bulk-EDX	0.9	0.1	0.6	1.1	0.4	n.d.	2	94.4	Ni/Co (0.1/0.3)
	Matrix-EDX	*0.5*	*n.d.*	*n.d.*	*n.d.*	*n.d.*	*n.d.*	*2.1*	*97.4*	
3003-18 (1030-930 BC – Timna)	Bulk-Chem (SF-ICP-MS)	n.m.	0.001	0.037	0.73	n.m.	<0.002	2.26	95	Ni/Co (0.004/0.003)
	Bulk-EDX	0.4	n.d.	0.2	0.5	n.d.	n.d.	1.9	97	
	Matrix-EDX	*0.4*	*n.d.*	*n.d.*	*n.d.*	*n.d.*	*n.d.*	*1.8*	*97.8*	
3034-18 (1100-1000 BC – Timna)	Bulk-Chem (SF-ICP-MS)	n.m.	0.002	0.38	0.73	n.m.	n.m.	1.84	92	Ni/Co (0.007/0.003)
	Bulk-EDX	0.8	n.d.	0.8	1	0.2	n.d.	2.1	95.1	
	Matrix-EDX	*0.3*	*n.d.*	*n.d.*	*n.d.*	*n.d.*	*n.d.*	*2.6*	*97.1*	

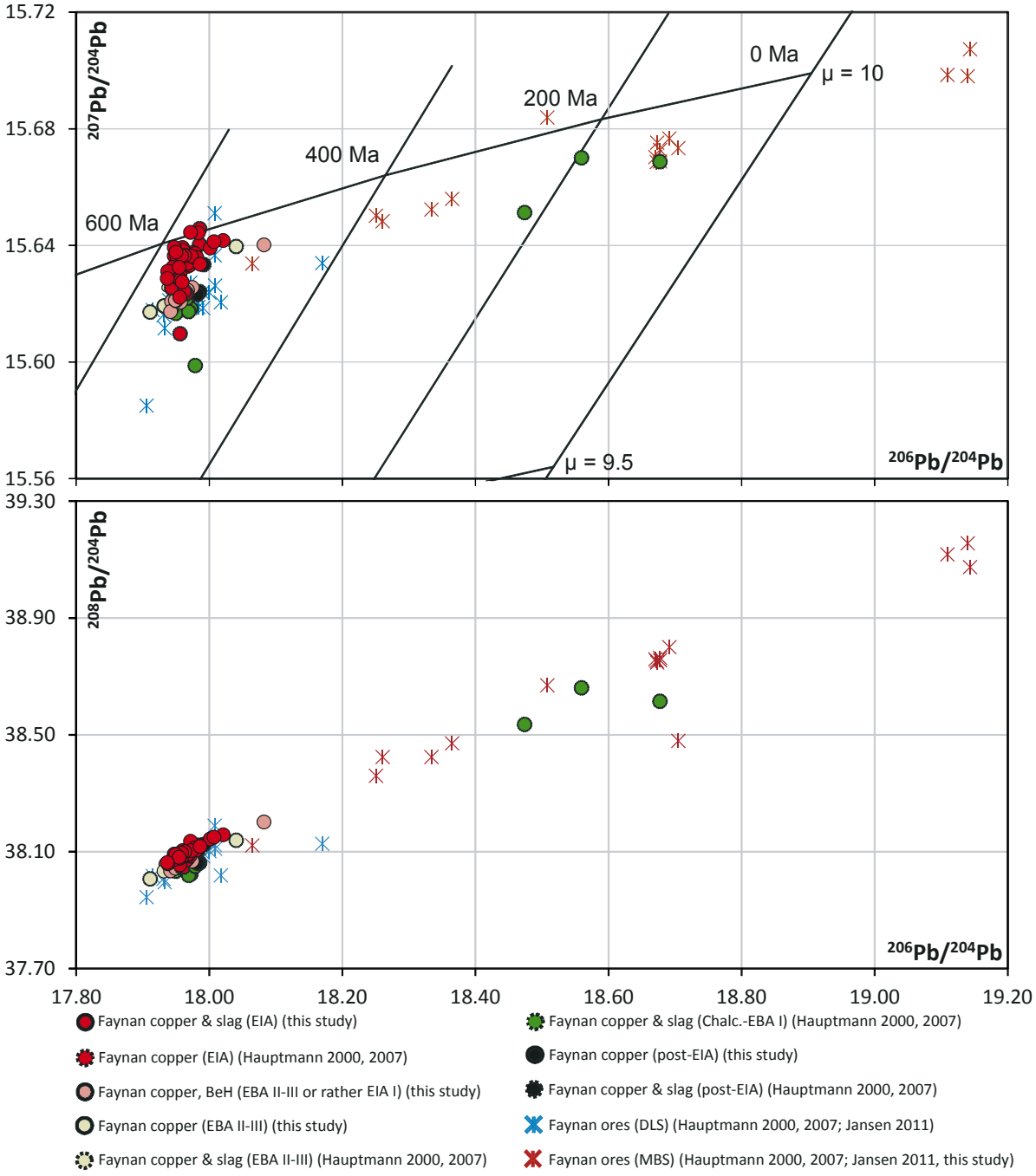

Figure 4. Lead isotopic field of copper and slag from EIA smelting sites in Faynan (red dots), compared with copper and slag from other archaeological periods (dots in other colours) and with ores (crosses). Errors are smaller than symbols except TIMS measurements from Hauptmann (2000; 2007). Graph: M. Bode. See continuation on the opposite page.

collection times, adequate DT % etc., tuned in order to achieve high elemental peaks to background ratios) led to increased reliability of the semi-quantitative analytical data. The accuracy of the results was checked through the analysis of five certified reference copper-alloys (BCR© 691, European Commission, Institute for Reference Materials and Measurements): high concentration element contents (>15 %) are estimated by errors in the order of ±3 %, while the low concentration ones (<5 %) are estimated with errors in the order of ±15-20%. The data set is presented in Tables 8 and 9.

Discussion

Lead isotope ratios

Lead isotope fields of Faynan raw copper and slags compared to ores

Complete analytical data of copper smelting remains, copper slag and their metal inclusions from the different archaeological periods of mining and smelting in Faynan are combined and plotted on a graph in Figure 4. These metallurgical samples are divided into:

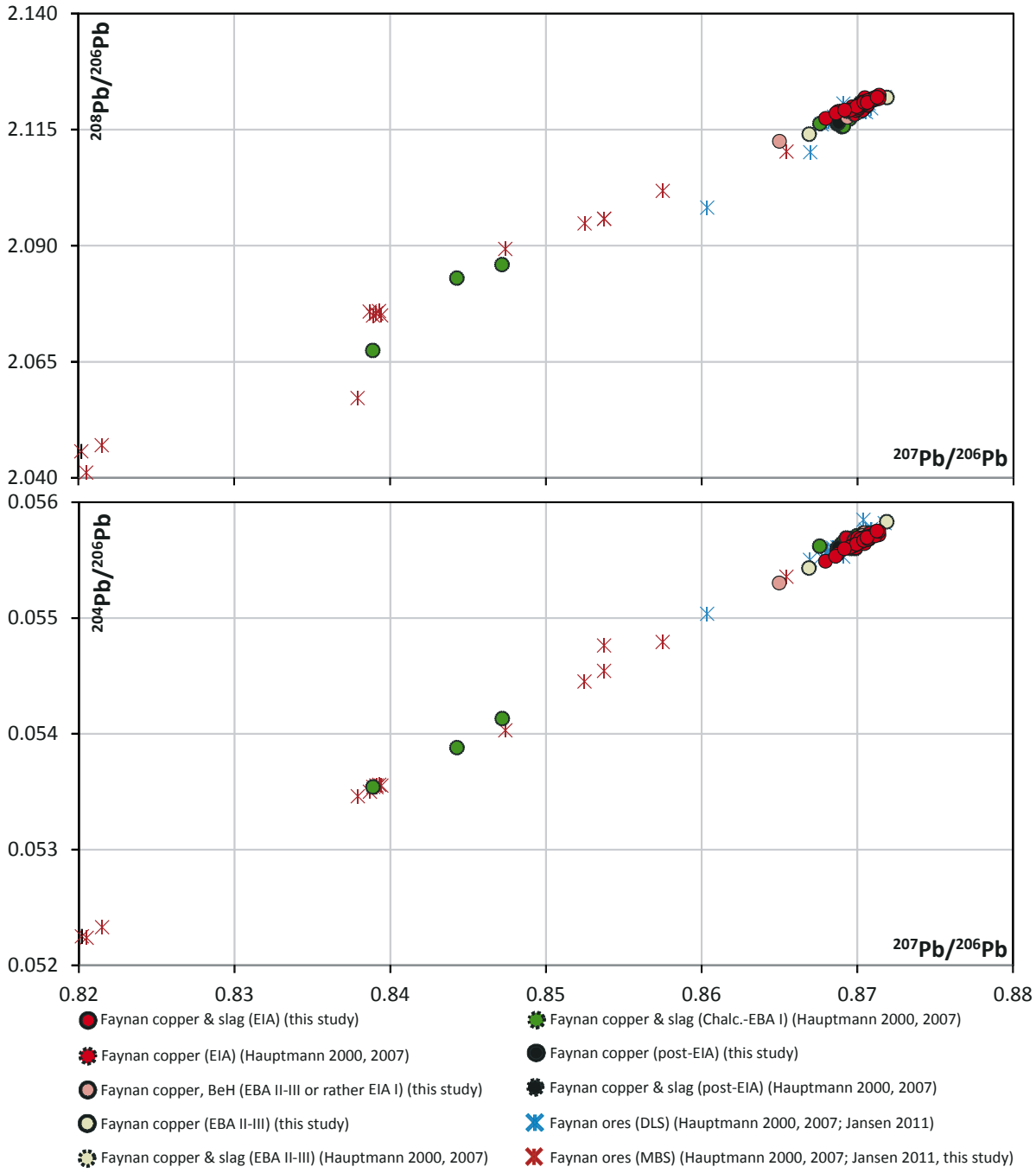

Continuation of Figure 4.

1. EBA I (published data);
2. EBA II-III (published data and this study);
3. IA (this study and published data);
4. Post-Iron Age (Roman and Mamluk; published data);
5. material from Barqa el-Hetiye, the dating of which, however, is not certain: EBA II-III or rather IA I (this study).

For comparison, ore data of the two different ore-bearing layers in the Faynan mining district are plotted:

1. DLS;
2. MBS.

Except for two outliers, the ore analyses of the DLS formation define a relatively narrow isotopic field in the diagrams with a Pb model age of about 600 to about 550 million years. The ores from the MBS formation are geologically part of the younger, overlying Lower Cretaceous. Accordingly, the MBS data plot away from the DLS data, with model ages between c. 500 million years and even negative ages (see Hauptmann, 2007, pp.79-83).

In the diagram $^{207}Pb/^{204}Pb$ vs. $^{206}Pb/^{204}Pb$ both ore types lie on the same Pb evolution trendline, but with a different distribution range. All metallurgical remains

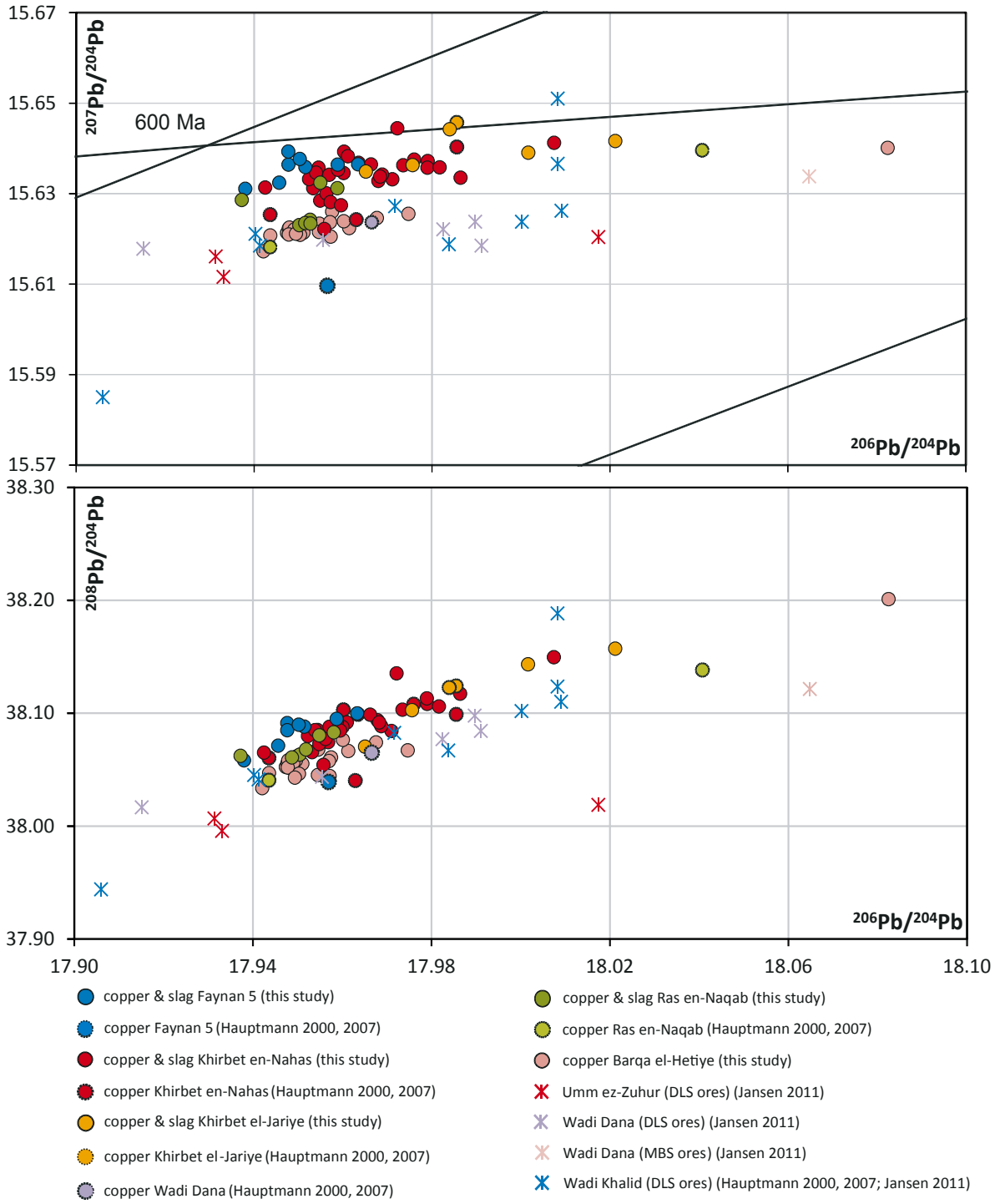

Figure 5. Lead isotopic fields of copper and slag from EIA smelting sites in Faynan plotted according site (dots) and compared with DLS-ores from various locations (crosses). Note: the material from Barqa el-Hetiye is unclear in date (EBA II-III or rather IA I). Ore data and six measurements of EIA copper are taken from the literature (Hauptmann, 2000; 2007; Jansen, 2011), the rest are new measurements. Errors are smaller than symbols except TIMS measurements from Hauptmann (2000; 2007). Graph: M. Bode. See continuation on the opposite page.

of all epochs are in the DLS ore distribution range. The only exception are three Chalcolithic-EBA I-samples and one (EBA II-III or rather IA I)-Barqa el-Hetiye-sample which are in the MBS ore range. This fits with the mining archaeological observations that miners in most epochs exploited exclusively DLS, but in the Chalc.-EBA I and again in Roman times also MBS. Some internal differentiation within DLS is noticeable: Bronze Age metallurgical wastes are directly overlapping the DLS ore sample data, while the IA metallurgical samples are in a peripheral area that is higher up in the diagram. This is probably because the ore samples were predominantly taken from the area of Bronze Age mines and less frequently from the area of EIA mines .

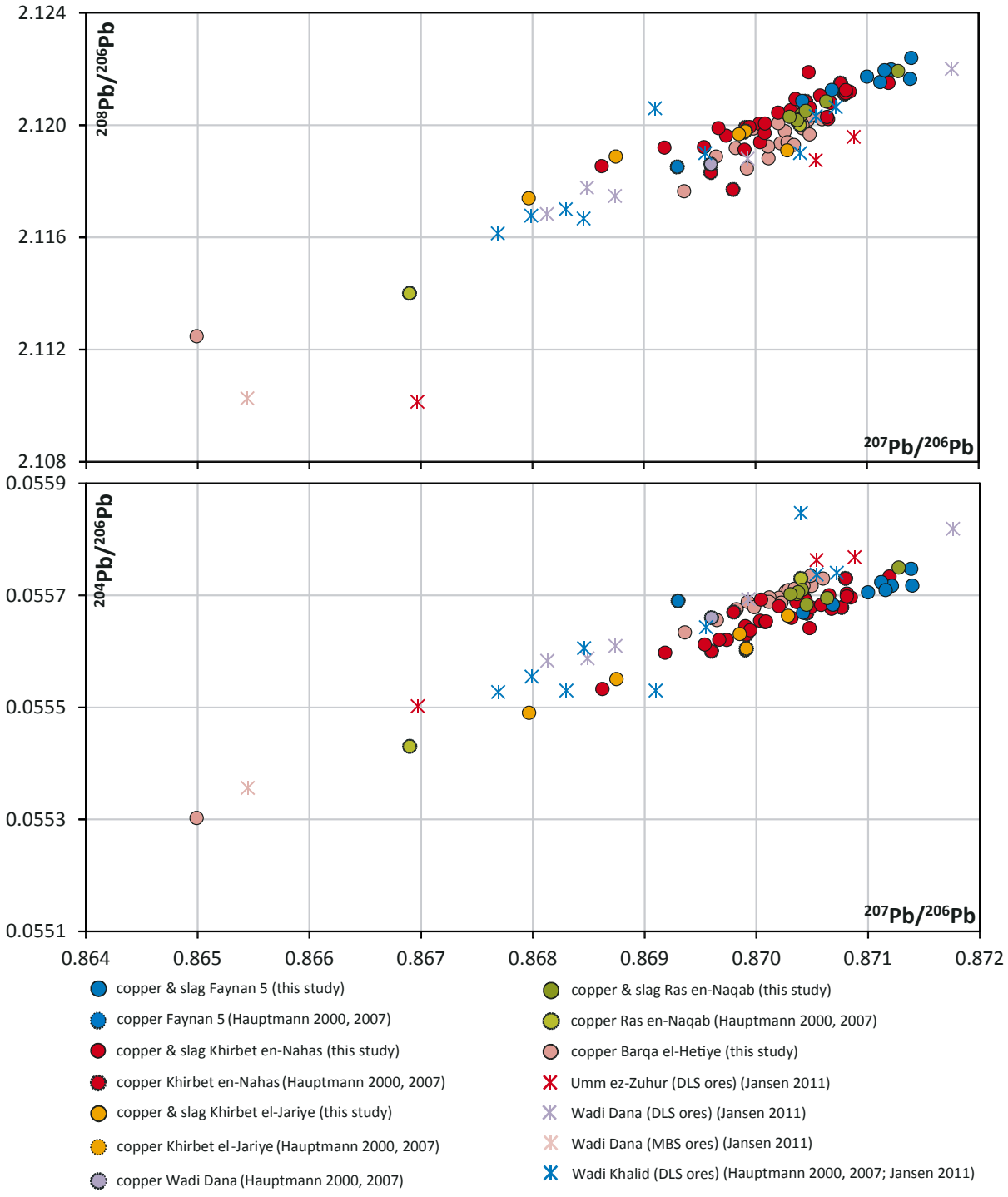

Continuation of Figure 5.

Comparison between different EIA smelting sites in Faynan

In Figure 5 data from Faynan are divided according to EIA smelting sites and plotted for comparison. In the version $^{207}Pb/^{204}Pb$ vs. $^{206}Pb/^{204}Pb$ two units can be seen. The first unit includes the quantitatively most important EIA smelting sites. They are almost all on the same trendline. At its geologically older end is Faynan 5 (blue dots). In the middle and in the area of geologically younger ores is Khirbet el-Jariye (orange dots). Khirbet en-Nahas (red dots) is distributed over almost the entire trendline, as is Ras en-Naqb (grey dots). The second unit consists of the samples from Barqa el-Hetiye (pink dots) and the data point from Wadi Dana (purple dot). They lie on a slightly offset trendline. This grouping is confirmed by the other plots.

Comparison to different published groups of ingots

In Figure 6 different groups of ingots are compared to our samples. In the version $^{207}Pb/^{204}Pb$ vs. $^{206}Pb/^{204}Pb$, the loaf ingots from the LBA-EIA wreck off Neve Yam (blue diamonds) lie very densely clustered on the geologically

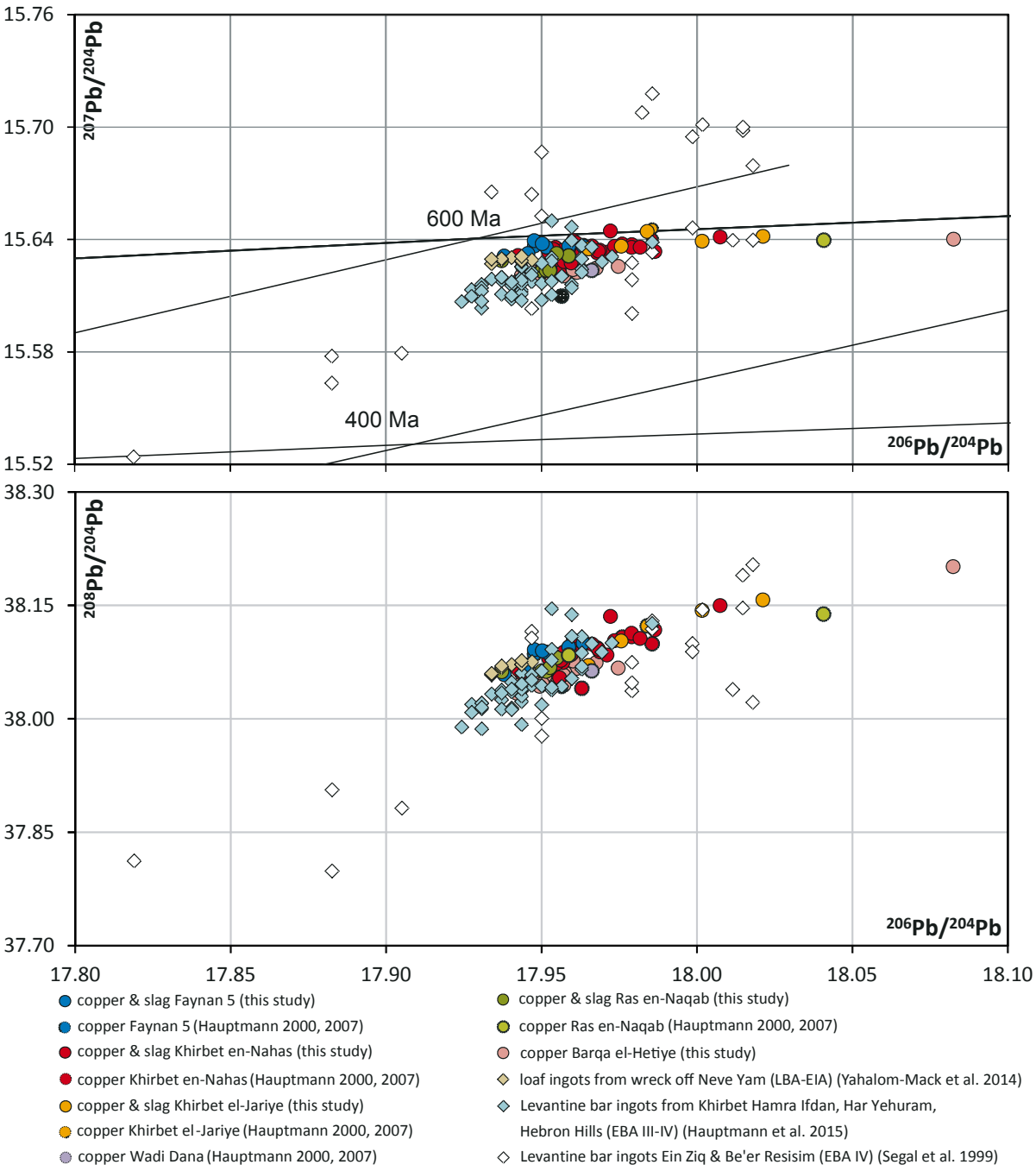

Figure 6. Lead isotopic fields of copper and slag from EIA smelting sites in Faynan (dots), compared to copper ingots of Southern Levantine contexts of different archaeological periods (diamonds):
- loaf ingots from the LBA-EIA wreck site off Neve Yam (Carmel coast); data from Yahalom-Mack, et al. (2014);
- Levantine bar ingots from Khirbet Hamra Ifdan in Faynan, Har Yehuram in the Negev, and Hebron Hills (EBA III-IV); data from Hauptmann, et al. (2015);
- Levantine bar ingots from ʿEin Ziq and Beʾer Resisim in the Negev (EBA IV); data from Segal, Halicz and Cohen (1999) (with large analytical error).

Measurements of material from Faynan smelting sites are new except six TIMS analyses taken from Hauptmann (2007). Errors of new data are smaller than symbols. Graph: M. Bode. See continuation on the opposite page.

older end of the trendline of the large smelting sites of EIA Faynan. The EBA III-IV Levantine bar-ingots from Khirbet Hamra Ifdan in Faynan, Har Yehuram in the Negev, and Hebron Hills (Hauptmann, et al., 2015) plot on both trendlines of the EIA smelting sites, but also in between, a feature which may be caused by the slightly less precise analytical method used for these ingots (TIMS). The Levantine EBA IV bar-ingots from ʿEin Ziq and Beʾer Resisim in the Negev analysed by Segal, Halicz, and Cohen (1999) are much more scattered and lie largely outside the DLS ores. This scatter is essentially an artefact related to a rather imprecise analytical method (quadru-

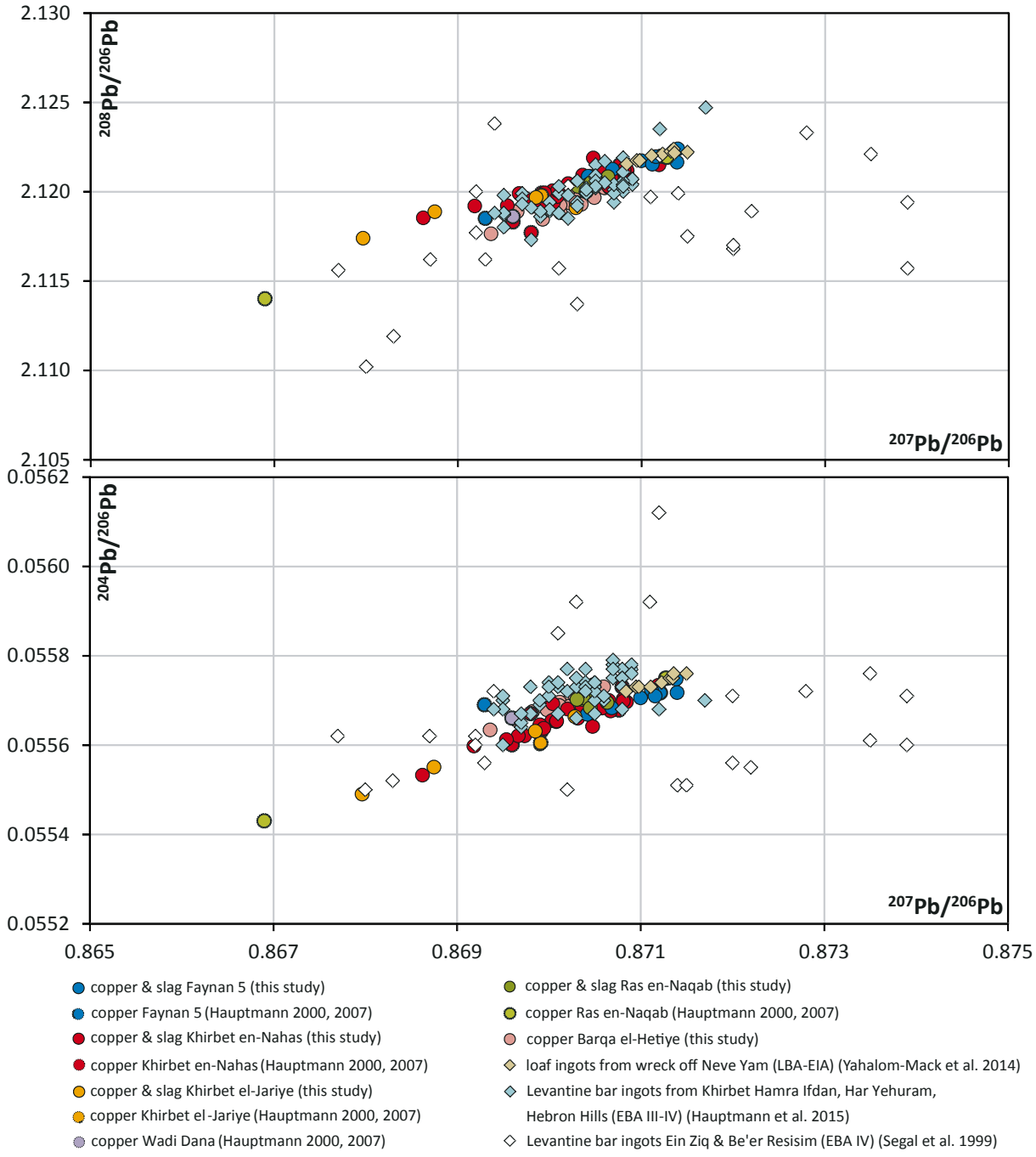

Continuation of Figure 6.

pole ICP-MS) and the analyses should be repeated using modern analytical tools.

Lead isotope fields of Timna raw copper and slags compared to ores and fluxes

In Figure 7, analyses of copper smelting remains, dated to the Late Bronze and and Early Iron Ages from different smelting sites in Timna are combined and plotted. Ore bearing formations from the Timna mining district are included in the diagrams for comparison. We also included ore samples from the Wadi Amram mining district as it is a closeby ore deposit which was also exploited during the LBA-EIA according to mining archaeological data (see Avner, et al., 2018, pp.151-158; Langford, et al., 2018, p.220, 226; Shilstein and Shalev, 2018, p.233). Since only small amounts of LBA-EIA slags were found in the Wadi Amram district compared to the EIA mining, it is suspected that the ores were taken elsewhere for smelting, and a possible candidate would be Timna.

Based on the $^{207}Pb/^{204}Pb$ vs. $^{206}Pb/^{204}Pb$ diagram, a relatively tight grouping of the geological formation of the Cambrian shales and lower Cretaceous sandstones (Amir/Avrona ores) with a geological model age of about 600 to 400 million years can be recognised (red crosses).

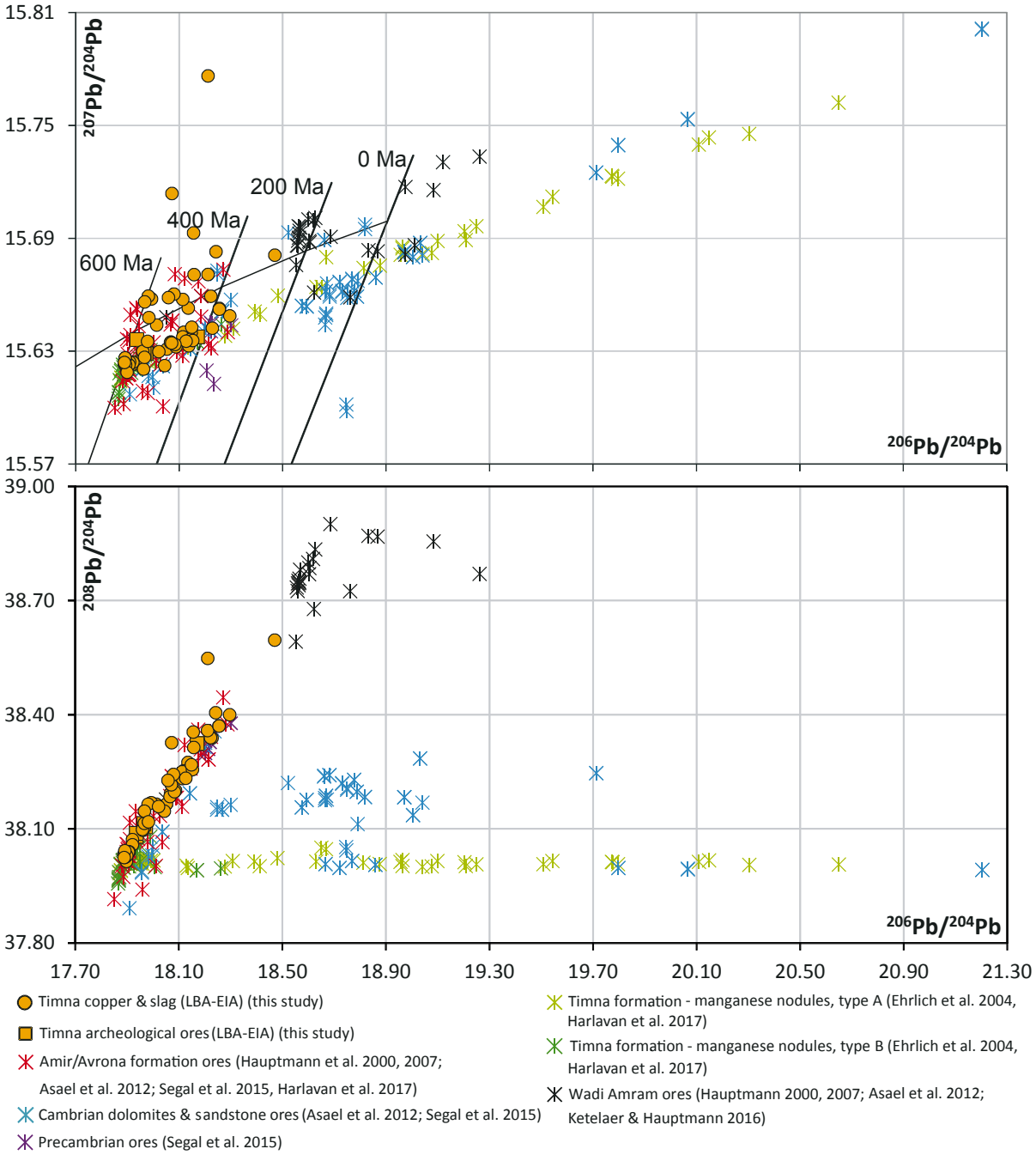

Figure 7. Lead isotope field of copper, slag, and archaeological ores from LBA-EIA smelting sites at Timna (dots) compared to several ore types occurring at Timna plus Wadi Amram (crosses). Measurements of industrial remains are from this study, ore data are from the literature (Hauptmann, 2000; 2007; Ehrlich, et al., 2004; Asael, et al., 2012; Segal, et al., 2015; Ketelaer and Hauptmann, 2016; Harlavan, et al., 2017). Errors of new data are smaller than symbols. Graph: M. Bode. See continuation on the opposite page.

A narrower sub-cluster within this field is formed by the genetically identical ores from Merkavot (grey crosses). The type B manganese nodules also plot at the geologically older margin (dark green crosses), although they originate geologically from a different stratum, namely the Timna formation. Interestingly, the Precambrian ores ("Precambrian magmatic mineralizations", purple crosses, see Segal, et al., 2015) stay on the right margin of the red cluster and show surprisingly young model ages of about 400 million years. This is in contrast to the estimated time of formation of primary ore in the Wadi Arabah via Pb-model ages of between approximately 620 to 470 million years (see Hauptmann, 2007, p.81).

The Cambrian dolomite & sandstone data of the Timna formation (blue crosses) stretch over a long geological timeline starting at about 600 million years, but the majority of the samples are younger than 200 million years, with some having negative geological ages. The manganese nodules type A of the Timna formation (bright green crosses) also are very variable in model age, starting at

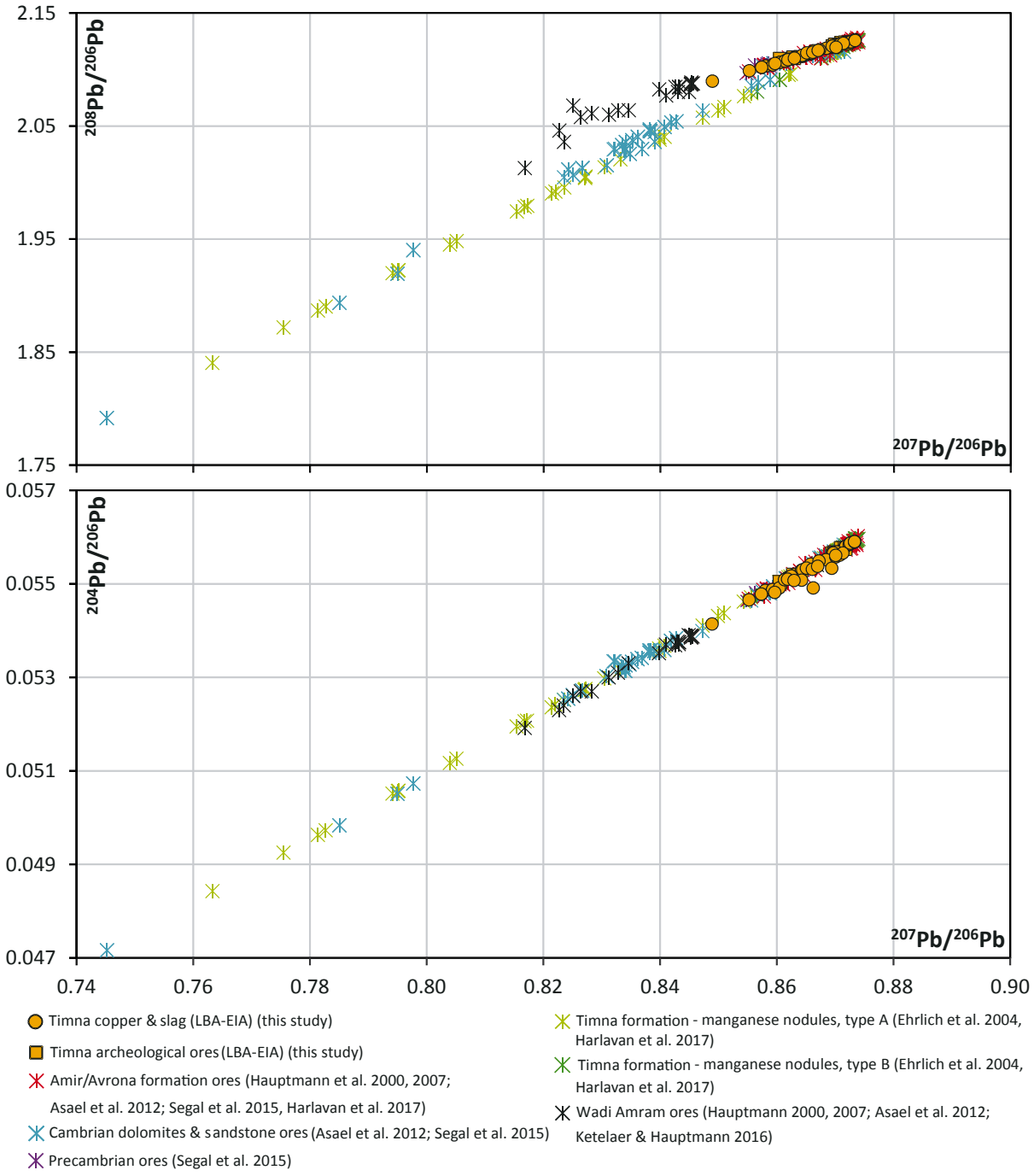

Continuation of Figure 7.

about 400 million years (see Ehrlich, et al., 2004, pp.1927-1930), and also like the Cambrian dolomite & sandstones, in some cases have negative ages. Wadi Amram ores (black crosses) do not overlap the afore mentioned Timna ores, since they are on the exact trendline of the Cambrian shales and Lower Cretaceaous sandstones (Amir/Avrona formation ores), but model ages start only at 250 million years (with one exception). The grouping of the ores is also shown for the other Pb isotope plot variants.

Most of the smelting remains (orange dots) and archaeological ores (orange cubes) from Timna are tightly grouped together. This main cluster is fully congruent with the Amir/Avrona formation ores. A part of it is also overlapped by the geologically older part of the Cambrian dolomites and sandstones of the Timna formation.

In diagram $^{207}Pb/^{204}Pb$ vs. $^{206}Pb/^{204}Pb$ there are at least four outliers. Three of them do not fit to any of the plotted ores (sample 3039-18 from site 35, sample 4279-16 from site 15, and sample 4298-16 from site 34). The unique LI ratios in these samples should either echo an undetected ore source, or reflect other uncommon components of the smelting charge (i.e. flux). The fourth outlier is on a possible mixing line to the Wadi Amram ores (sample no. 3029-18 from site 35).

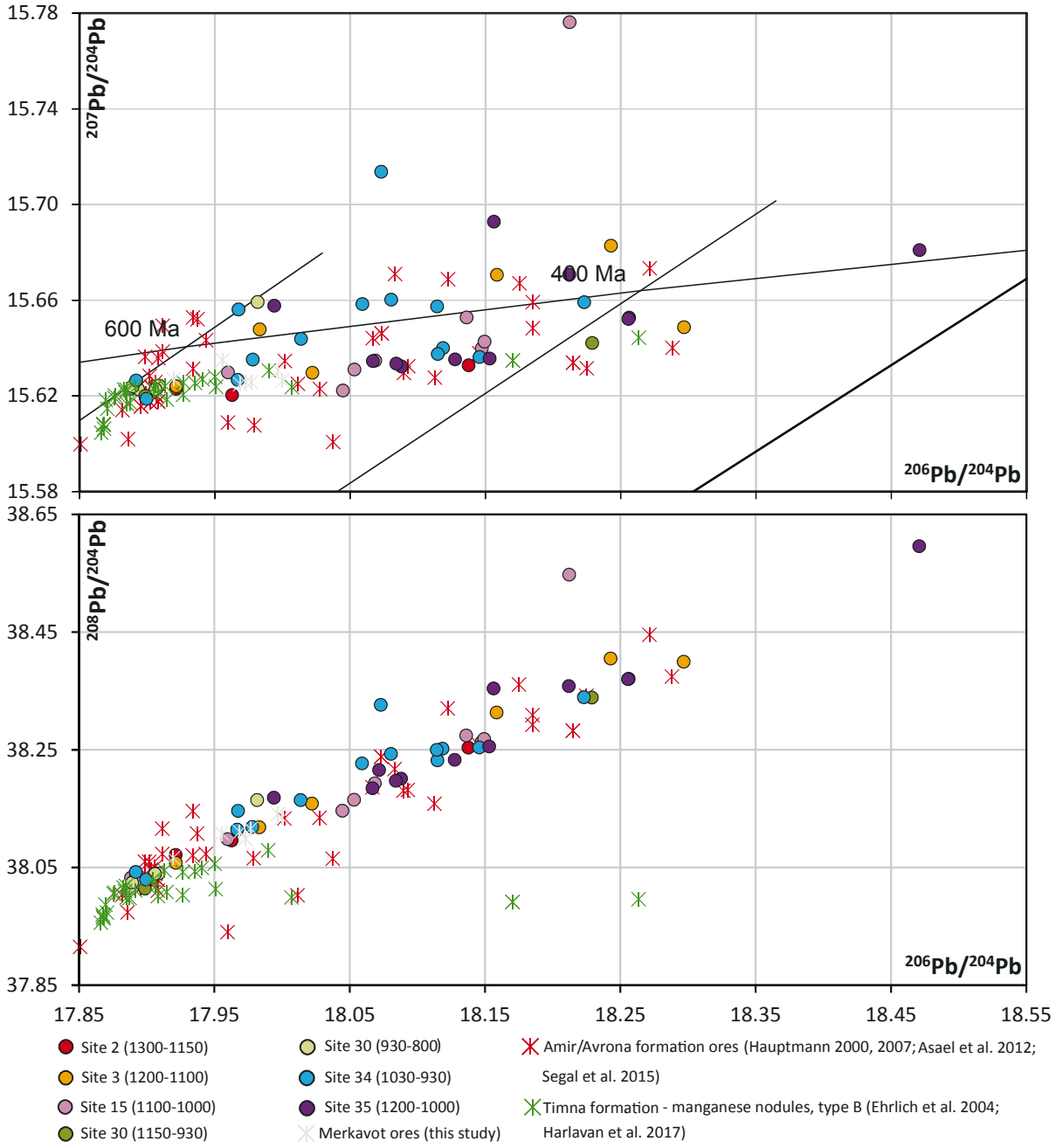

Figure 8. Lead isotope data of Timna LBA-EIA copper, slag, and archaeological ores (dots) differentiated according smelting sites and compared with ores (crosses). Measurements of industrial remains are from this study, ore data are from the literature (Hauptmann, 2000; 2007; Ehrlich, et al., 2004; Asael, et al., 2012; Segal, et al., 2015; Harlavan, et al., 2017). Errors of new data are smaller than symbols. Graph: M. Bode. See continuation on the opposite page.

According to LI data we may therefore distinguish three types of copper smelted at Timna:

- the Timna main group, which is equivalent to the ores of the Amir/Avrona formation and therefore can be termed "Type Amir/Avrona";
- "Timna Type 2", evidently produced in relatively small quantities, and seemingly smelted from yet undetected ore/flux sources;
- "Timna Type 3", represented by only one sample, and perhaps smelted using ores mined at Wadi Amram.

Comparison between different smelting sites at Timna

In Figure 8 the metallurgical remains from LBA-EIA Timna are distinguished according to the different smelting sites. In addition, we differentiated within Site 30 between an 11th-10th centuries BC technological phase (material associated with fayalite slags of type B) and a late 10th-9th centuries BC technological phase (material associated with knebelite slags of type A).

In general, the smelting remains do not show a systematic distribution in this plot according to site. In other words, Type Amir/Avrona dominates at all smelting

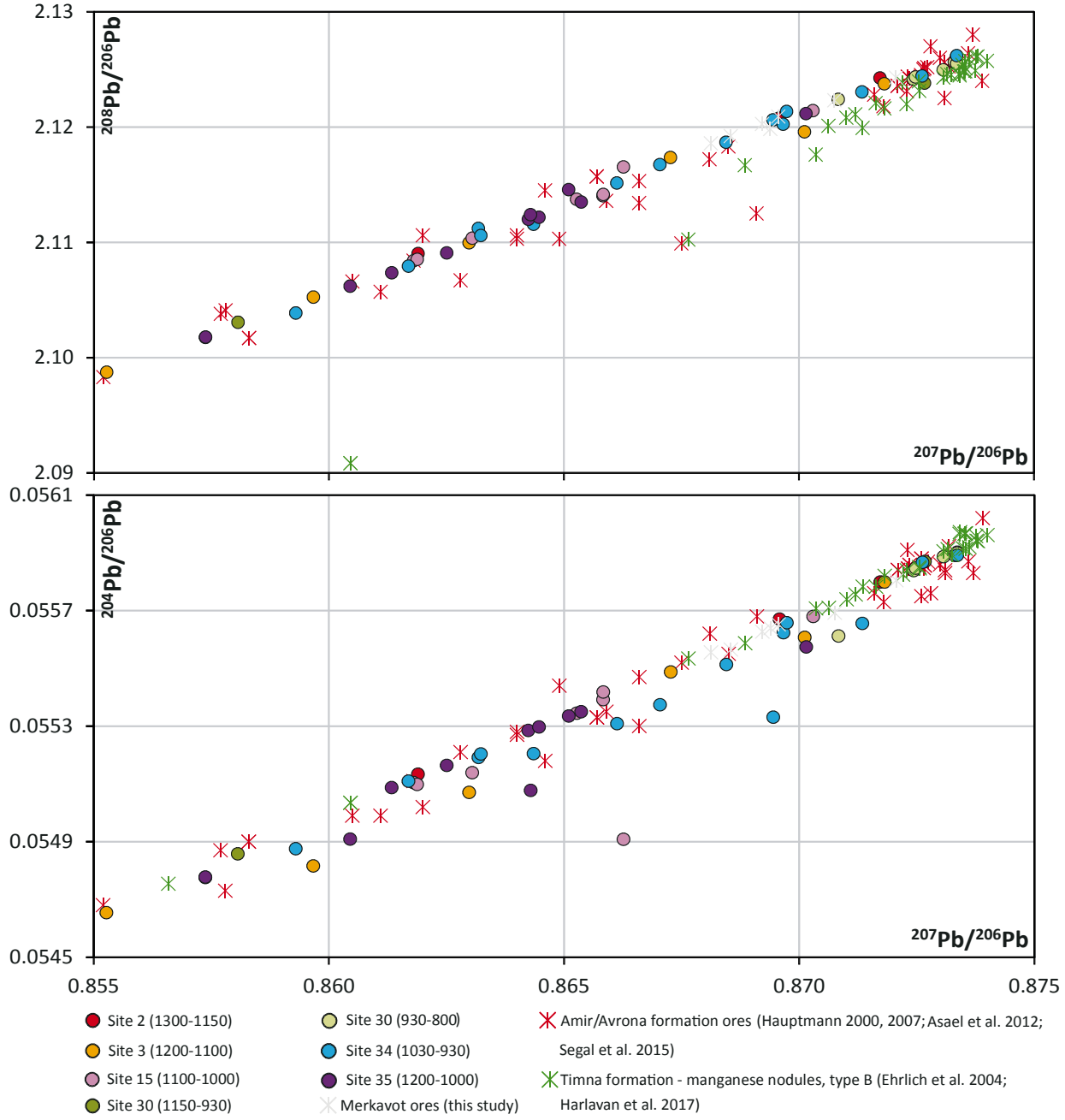

Continuation of Figure 8.

sites and periods. Type 2 is present at three sites (sites 15, 34, and 35), but even at these sites does not play an important role. Also the role of Type 3 at site 35 is limited.

Nevertheless, if we go more in details, there is a conspicuous feature within Type Amir/Avrona: a sub-cluster of data of smelting remains from sites 15, 34 and site 30 (late) coincides with the manganese nodules type B (Ehrlich, et al., 2004) as well as with a sub-cluster of red crosses (site 15: metal sample 3034-18, site 34: metal samples 4280-16, 3003-18; site 30 [late]: slag samples 4285-16, 3026-18, 3041-18, 3042-18, 3043-18). The question arises whether this reflects a specific technology that used manganese nodules type B as a flux. An alternative explanation would be that copper ores from a very specific mining area within the Amir/Avrona formation were used. Taking into account the archaeological context, this sub-cluster probably represents both options. The relevant five slag samples from Site 30 (late) belong to the Mn-rich slag type A (Mn contents were checked with p-XRF and are between 24 and 30 wt.%), which is characteristic of production system 3 at Timna (see above Chapter II.2). Since Mn nodules were found in Site 30 in the same context with this slag type, there is little doubt that fluxing with such nodules is the source of the high Mn contents in the slag in question. The observed clustering of LI ratios fits this scenario. The picture is dif-

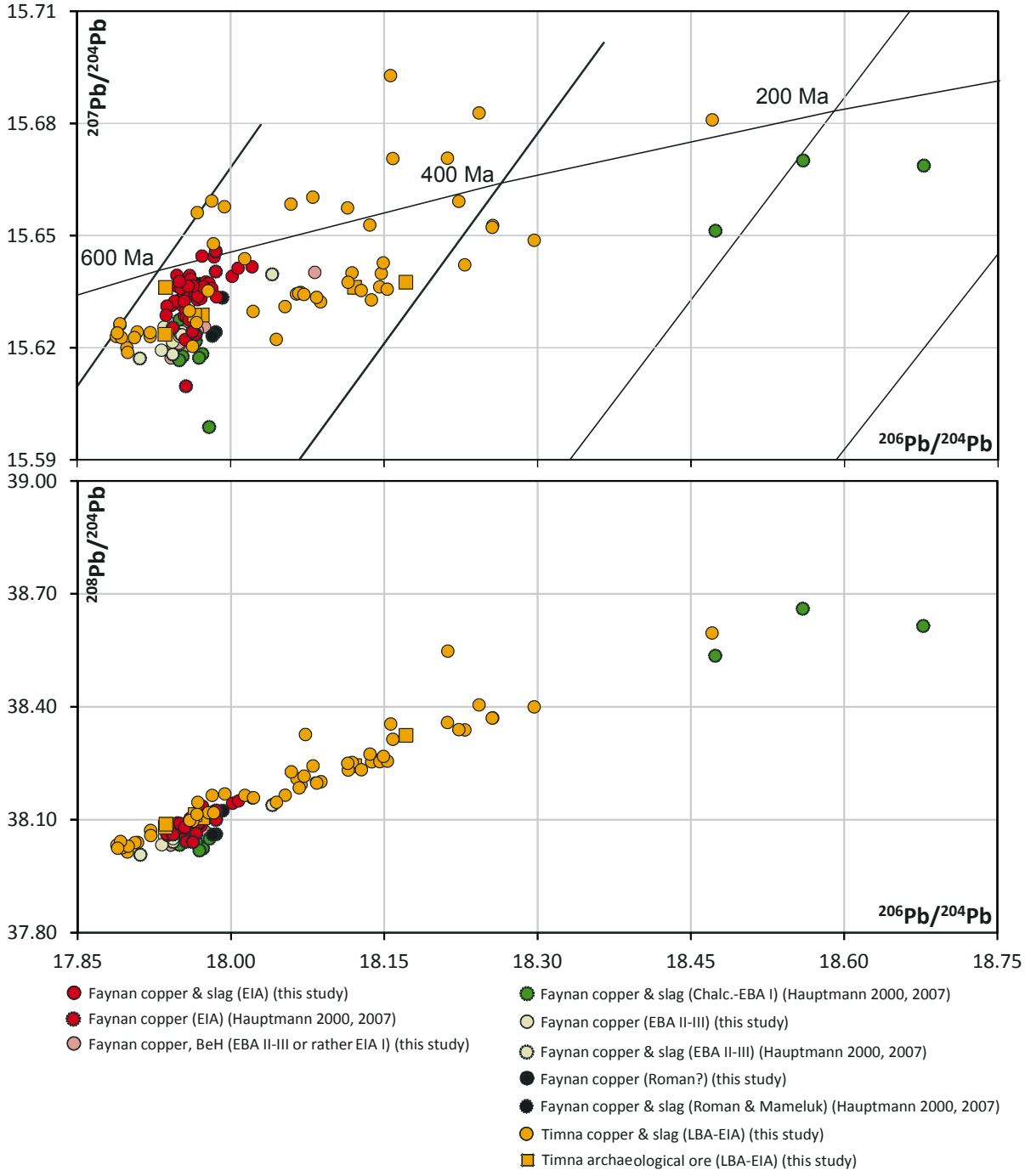

Figure 9. Lead isotope data of industrial remains from smelting sites of EIA Faynan and LBA-EIA Timna compared with each other and with material from other archaeological periods. Data are measurements of this study except seven EIA Faynan and all post- and pre-EIA samples taken from Hauptmann (2000; 2007). Errors of new data are smaller than symbols. Graph: M. Bode. See continuation on the following pages.

ferent for the samples from sites 15 and 34. There is no evidence of Mn-based fluxing at these sites and the LI ratios should be associated solely with the ore source.

EIA Faynan vs. LBA-EIA Timna

In Figure 9 we compare the fields of smelting remains of Faynan with smelting remains of Timna.

In the diagram $^{207}Pb/^{204}Pb$ vs. $^{206}Pb/^{204}Pb$, the „semi-circular“ cluster of the EIA Faynan smelting remains (red dots) lies in the left part of the fan-shaped triangular field spanned by the LBA-EIA Timna symbols (orange dots). In other words, most samples and sub-clusters of smelting remains from LBA-EIA Timna are far outside the cluster of EIA Faynan smelting remains.

For EIA Faynan, we can define the copper type produced on an industrial scale (“Type DLS”) as follows:

$^{208}Pb/^{206}Pb$: 2.1174-2.1224,

$^{207}Pb/^{206}Pb$: 0.8680-0.8714,

$^{204}Pb/^{206}Pb$: 0.0555-0.0558,

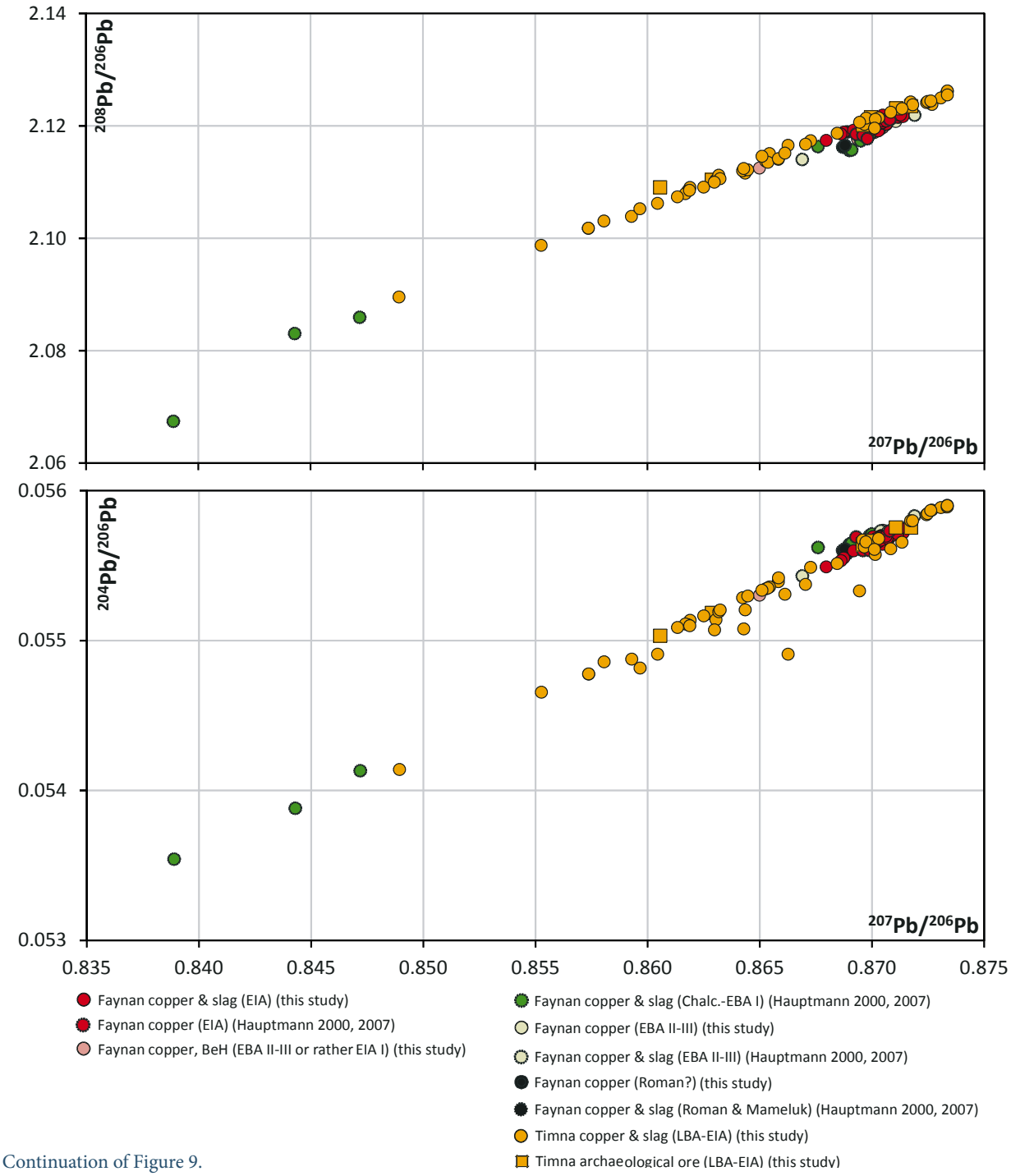

Continuation of Figure 9.

$^{208}Pb/^{204}Pb$: 38.033-38.157,
$^{207}Pb/^{204}Pb$: 15.610-15.646,
$^{206}Pb/^{204}Pb$: 17.937-18.021,
μ ($^{238}U/^{204}Pb$): 9.90-10.00,
κ ($^{232}Th/^{204}Pb$): 3.97-4.01.

Geological model age: 531 Ma - 581 Ma (μ, κ, and model age after Stacey and Kramers, 1975).

The Chalc.-EBA I smelting remains from Faynan scatter a little wider and some are in the MBS range. The samples from the EBA II-III period, the sample suite from Barqa el-Hetiye (EBA II-III or rather IA I), and also the Roman and Mameluk samples plot in the EIA field or only slightly outside.

At Timna, the main copper type of industrial scale production in LBA-EIA ("Type Amir/Avrona") can be defined as follows:

$^{208}Pb/^{206}Pb$: 2.0896-2.1262,
$^{207}Pb/^{206}Pb$: 0.8490-0.8734,
$^{204}Pb/^{206}Pb$: 0.0542-0.0559,
$^{208}Pb/^{204}Pb$: 38.014-38.596,

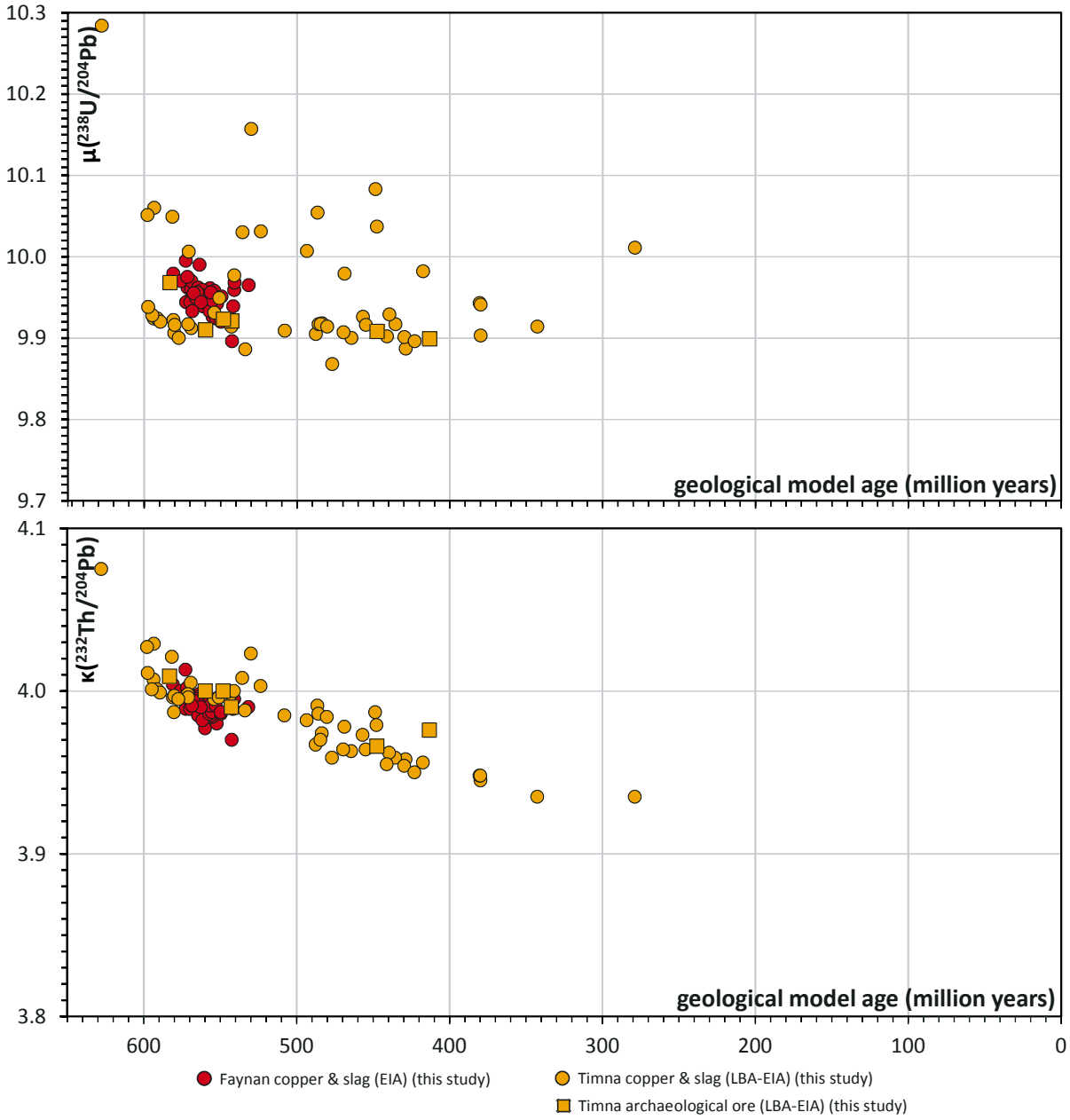

Continuation of Figure 9.

$^{207}Pb/^{204}Pb$: 15.619-15.777,
$^{206}Pb/^{204}Pb$: 17.889-18.471,
μ ($^{238}U/^{204}Pb$): 9.87-10.53,
κ ($^{232}Th/^{204}Pb$): 3.94-4.12.
Geological model Age: 279 Ma - 642 Ma (μ, κ, and model age after Stacey and Kramers, 1975).

Furthermore, of some economic importance might have been also Timna Type 2, which based on only three samples we provisionally define as follows:
$^{208}Pb/^{206}Pb$: 2.1123-2.1206,
$^{207}Pb/^{206}Pb$: 0.8642-0.8695,
$^{204}Pb/^{206}Pb$: 0.0549-0.0554,
$^{208}Pb/^{204}Pb$: 38.326-38.548,
$^{207}Pb/^{204}Pb$: 15.692-15.777,
$^{206}Pb/^{204}Pb$: 18.073-18.213.

Timna Type 3 seems to have been of only very limited economic importance and is therefore left aside here.

Copper isotope ratios

Jansen, et al. (2017) described differences in the copper isotope composition of ores from Faynan and Timna: ore samples from Faynan DLS and samples from EBA II-III bar ingots from Khirbet Hamra Ifdan in the Faynan showed higher $^{65}Cu/^{63}Cu$ ratios than it had been observed for Amir/Avrona ores from Timna by Asael,

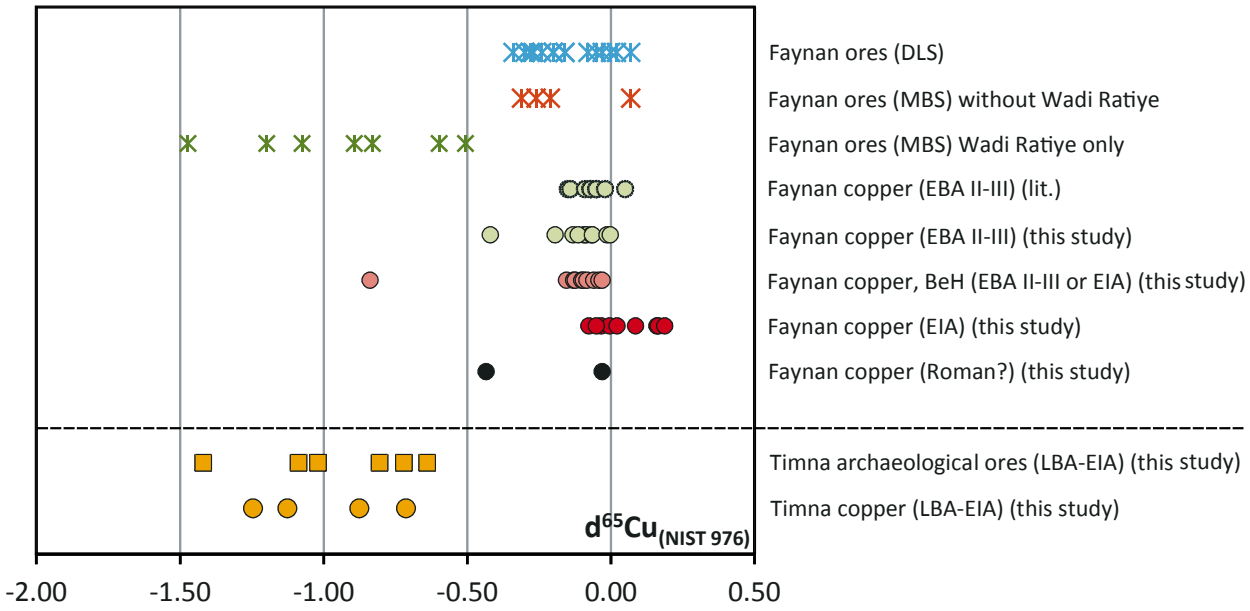

Figure 10. Copper isotope ratios of material from smelting sites in Faynan and Timna (metal samples and archaeological ores), compared to ore data. Graph: M. Jansen.

et al. (2007; 2009; 2012). This suggested that CI ratios might be a good criterium for provenance studies to distinguish between archaeological copper deriving from Faynan and Timna.

In order to follow up this opportunity, a subset of our metal samples was chosen for CIA. Only samples free of any corrosion were analysed to exclude fractionation through post-depositional processes that could mask the initial Cu isotope composition. From Timna four metal samples proved suitable for analysis, which are augmented by six archaeological ore samples from Timna smelting sites. From Faynan we analysed altogether 30 metal samples, of which nine are from the EIA large central smelting sites Faynan 5, Khirbet en-Nahas, and Khirbet el-Jariye. Ten are from Locus 9 at Barqa el-Hetye (IA I?), five from the EBA II-III activity at Ras en-Naqab, five from Faynan 9 (EBA II-III), and two from Faynan 1 (Roman?). Furthermore, we analysed eight geological ore samples from outcrops of Faynan MBS at Qualb Ratiye, Abu Kusheiba, and Wadi Abiad. Analytical results are presented in Tables 4 and 5 and are combined with published data in Figure 10.

Ore samples from Faynan

According to Jansen, et al. (2017), the narrow spread of Cu-isotope ratios of DLS ore samples defines a main field. In this main field plot also several outcrops of MBS, such as those in Abu Kusheiba and Wadi Abiad. An exception are samples from the MBS outcrop in Wadi Ratiye, which systematically have a lower $^{65}Cu/^{63}Cu$ ratio.

Metal samples from Faynan

All the metal samples that are lead isotopically related to DLS ores are copper isotopically consistent with the main field of Faynan ores. At the lower end ($\delta^{65}Cu$ = -0.43) plot a Roman sample from Faynan I and a EBA II-III sample from Ras en Naqab, at the higher end ($\delta^{65}Cu$ = 0.19) plot a EIA sample from Khirbet en Nahas and the two EIA samples from Faynan 5. It seems that the Faynan main field is not yet fully covered through the analysed DLS ores, especially towards the higher values where the metal samples from the large EIA smelting sites are concentrating.

A metal chunk from Barqa el Hetiye is outside the cluster, its ratio being much lower (sample JD-31/22n). This sample is consistent with MBS ores from nearby Wadi Ratiye both for its copper and lead isotope composition.

Ore samples from Timna

Our six archaeological ore samples are lead isotopically consistent with ore samples from the Amir/Avrona-formation (see chapter above). Copper isotope ratios form a cluster from $\delta^{65}Cu$ values of -1.42 to -0.64. These values are within the range of the measurements obtained by Asael, et al. (2007; 2009; 2012) for the oxidic fraction of the Amir/Avrona ores.

Metal samples from Timna

The four metal samples from Timna belong to the Timna copper main type, according to their lead isotope ratios, and therefore presumably were smelted from Amir/Av-

rona ores. As expected, their copper isotope ratio is consistent with the archaeological ore samples of our study. To sum up, despite the small number of metal samples it seems probable that the Cu-isotope ratio of the LBA-EIA Timna copper main type (= Type Amir/Avrona) rarely was lower than $\delta^{65}Cu = -1.42$, and rarely higher than -0.64.

EIA Faynan vs. LBA-EIA Timna

The CI values of Timna Amir/Avrona ore do not overlap with those of Faynan DLS ore. Correspondingly, Timna Amir/Avrona copper type and Faynan DLS copper type do not overlap either. However, the Timna Amir/Avrona copper type cannot be distinguished by either LIA or CIA from the Faynan copper smelted from the MBS outcrop in Wadi Ratiye. But, according to LIA and CIA, this MBS copper played a minor role in EIA Faynan production and was only observed in a single sample representing a minor portion of the third rate Barqua el-Hetiye smelting site. To summarise, it is indeed possible to distinguish between the economically important copper types of the Faynan EIA and the Timna LBA-EIA on the basis of the CI ratio, with the exceptions being economically insignificant.

Bulk chemical composition

Bulk chemical analysis with ICP-MS comprises 72 samples:

- 15 samples of copper prills and lumps from smelting sites of EIA Faynan. Of special importance here are the samples from the three large central smelting sites Faynan 5, Khirbet en-Nahas, Khirbet el-Jariye;
- 23 samples of the copper lumps from Barqa el-Hetiye in Faynan, with unclear archaeological dates either in EBA II-III or rather IA I;
- 10 samples of copper prills and lumps from EBA II-III contexts in Faynan (Faynan 9 and Ras en-Naqb);
- 1 Roman (?) copper sample from Faynan 1;
- 23 samples of copper prills and lumps from LBA-EIA smelting sites in Timna.

Our data are presented as bi-elemental plots (Figure 11) and line plots (Figure 12). We include published comparative data in the bi-elemental plots and in additional line plots (Figure 13 and Figure 14). Values in plots and in the text are given in wt.% normalized to Cu.

Samples from Faynan

Our samples in Figure 11 and Figure 12 represent all three central smelting sites of the EIA period: Faynan 5, Khirbet en-Nahas, and Khirbet el-Jariye. As the samples from these sites do not show an internal grouping according to site they are all plotted with the same symbols (red dots/lines). The samples from Barqa el-Hetiye are plotted in pale red because of their unclear archaeological date.

Characteristic for the chemical signature of the EIA samples are the high contents of Fe (Ø 7.41 wt.%) and Pb (Ø 5.75 wt.%). Iron enters the produced copper metal through intensive intergrowths, e.g. of the DLS ore rocks with oxidic manganese ores, which are rich in Fe_2O_3. The manganese ores contain Ø 8-10 wt.% Fe. The significant Pb contents also come from the manganese ore minerals (coronadites). Also phosphorus is quite abundant in the raw copper (Ø 0.81 wt.%). The same applies to sulphur (Ø 0.74 wt.%). In the trace element range, Zn, Co, As, and Ni and follow with values around 0.3 to 0.1 wt.%, Sb and Ag are around 0.006 wt.%, Te, Se, and Bi around 0.001 to 0.0005 wt.%, Sn in average is 0.004 wt.%.

The samples from the EBA II-III industrial period of Faynan (green lines/dots) are significantly lower in Fe, Co, P, Pb, and also lower in Ni, Sb, Sn, and Te (averages and medians). The values for Ag, As, Bi, S and Se are quite similar to EIA values.

The samples from Barqa el-Hetiye with unclear chronological context (pale red lines/dots) are very similar to the EIA samples in averages, medians, and degree of scattering. This confirms published measurements of this material with AAS (cf. Hauptmann, 2007, p.204) and supports a date in EIA I rather than in EBA II-III.

Comparison of our EIA samples with published AAS-data for EIA copper prills and lumps shows nearly identical results for Ag, As, Co, Fe, Ni, Pb, and Sb in averages, medians, and degree of scattering, with the exception of different medians for Sb (Figure 13). These similarities suggest that our sample collection is large enough to give a statistically reliable overview of the EIA production. The difference in the medians of Sb may be related to inaccuracies of AAS when Sb-contents are near to the detection limit.

Comparison of our EIA samples with published AAS-data for EBA II-III copper prills and lumps from Ras en-Naqab and Barqa el-Hetiye repeats the above observations (Figure 13):

Generally, data for As, Co, Fe, Ni, and Pb are less scattered in the EIA copper than in the EBA II-III copper. In other words, peak values of these elements in both periods are quite similar, but very low values do not occur in EIA copper prills and lumps. If we look at the median and average values, Ag contents do not change much with time. All other elements in plot Figure 13 rise significantly in EIA raw copper. The rise is even stronger in Roman and Mameluk raw copper (Figure 11).

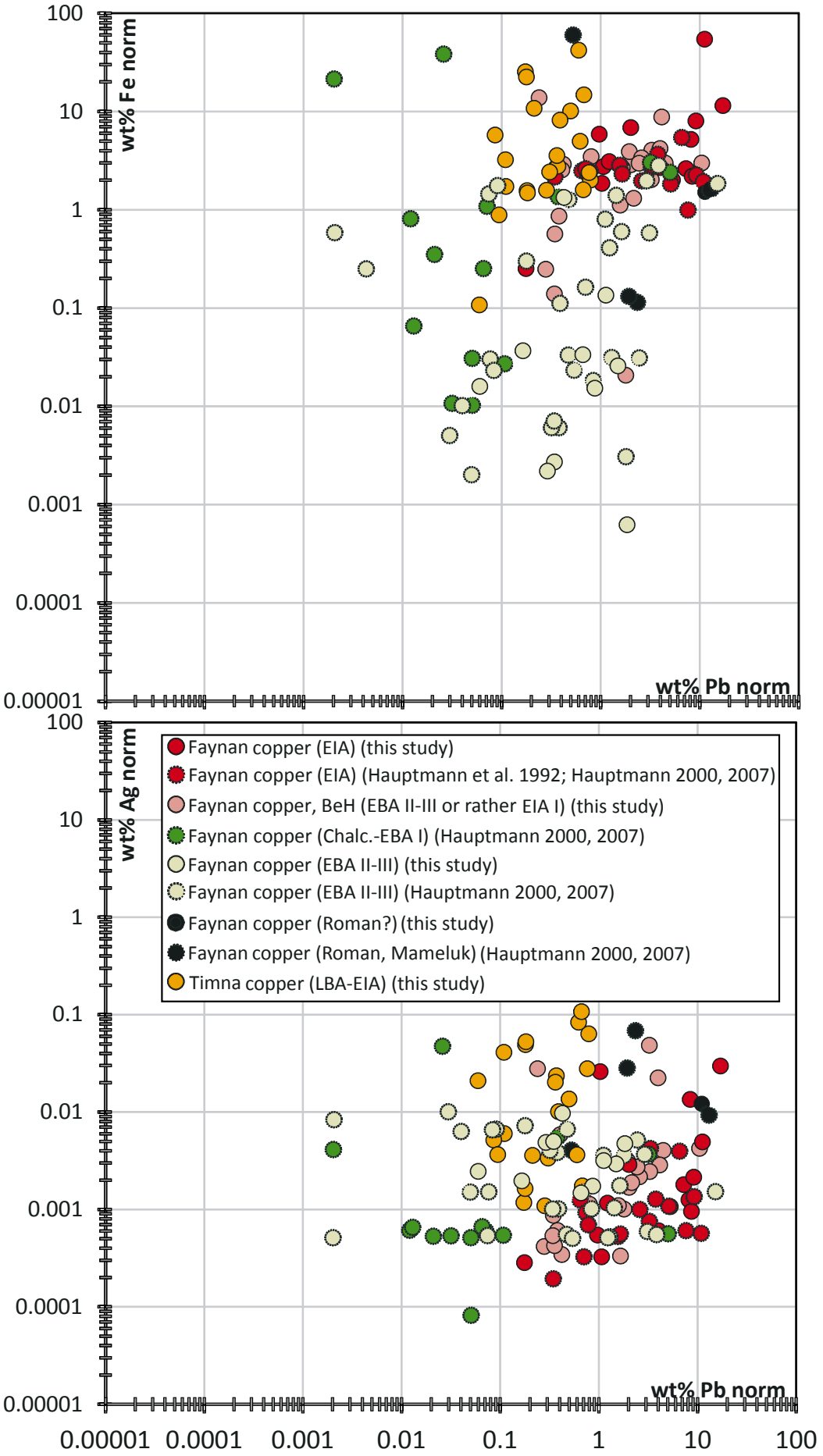

Figures 11. Selected bi-elemetal plots of results of bulk chemical analysis with ICP-MS (this study). Comparative data from the literature are included, all obtained with AAS or sometimes NAA. Graph: M. Bode. See continuation on the following pages.

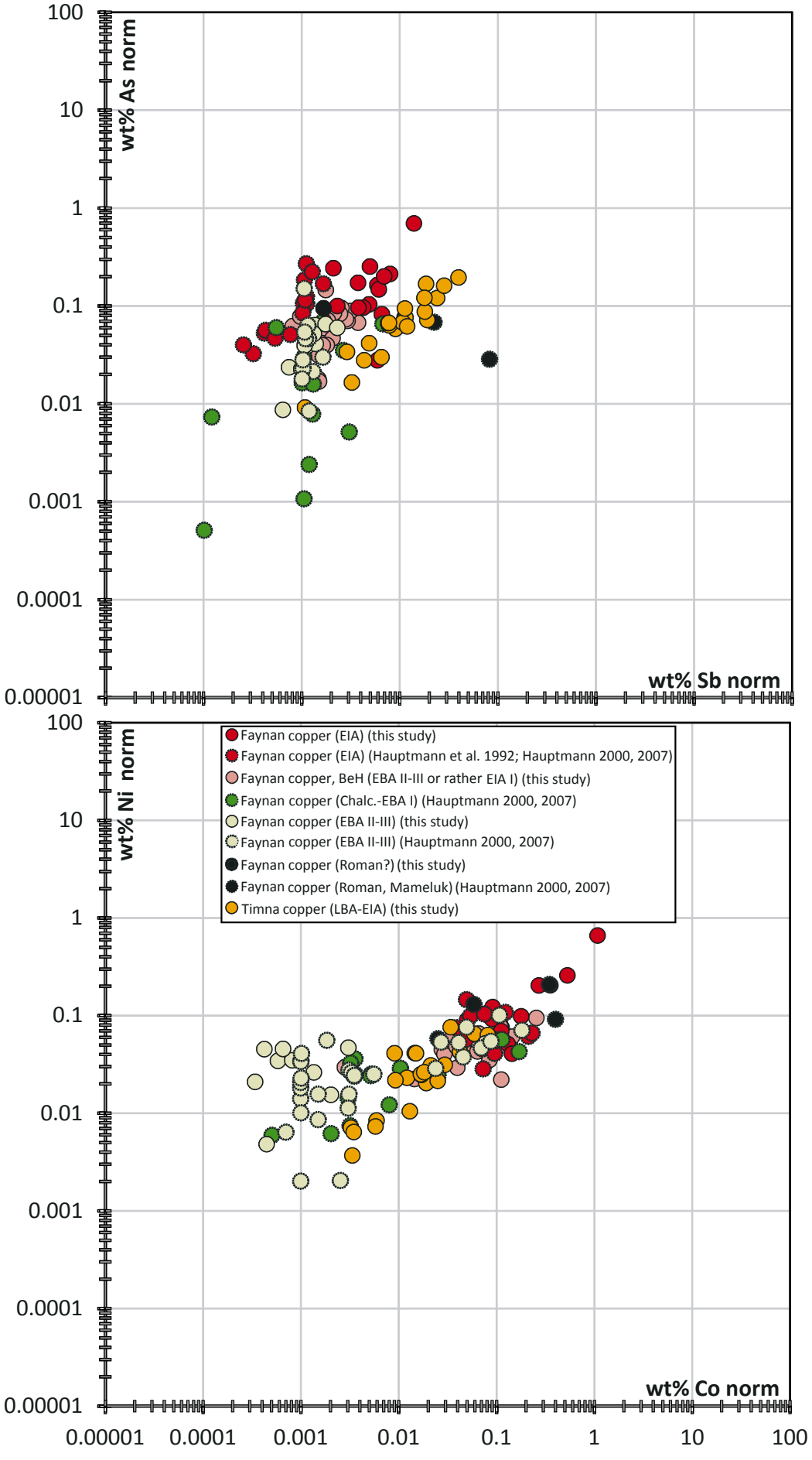

Continuation of Figure 11.

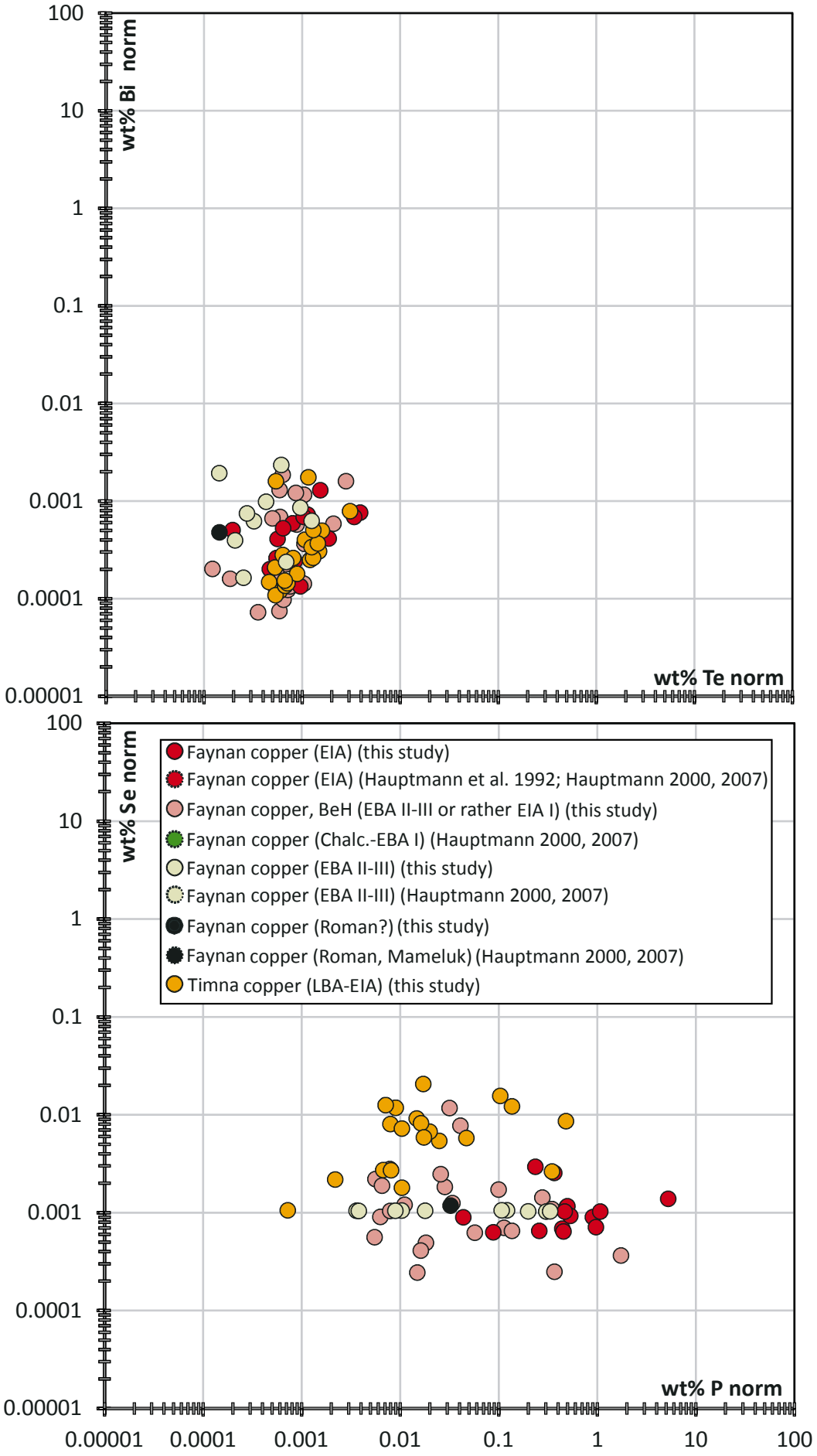

Continuation of Figure 11.

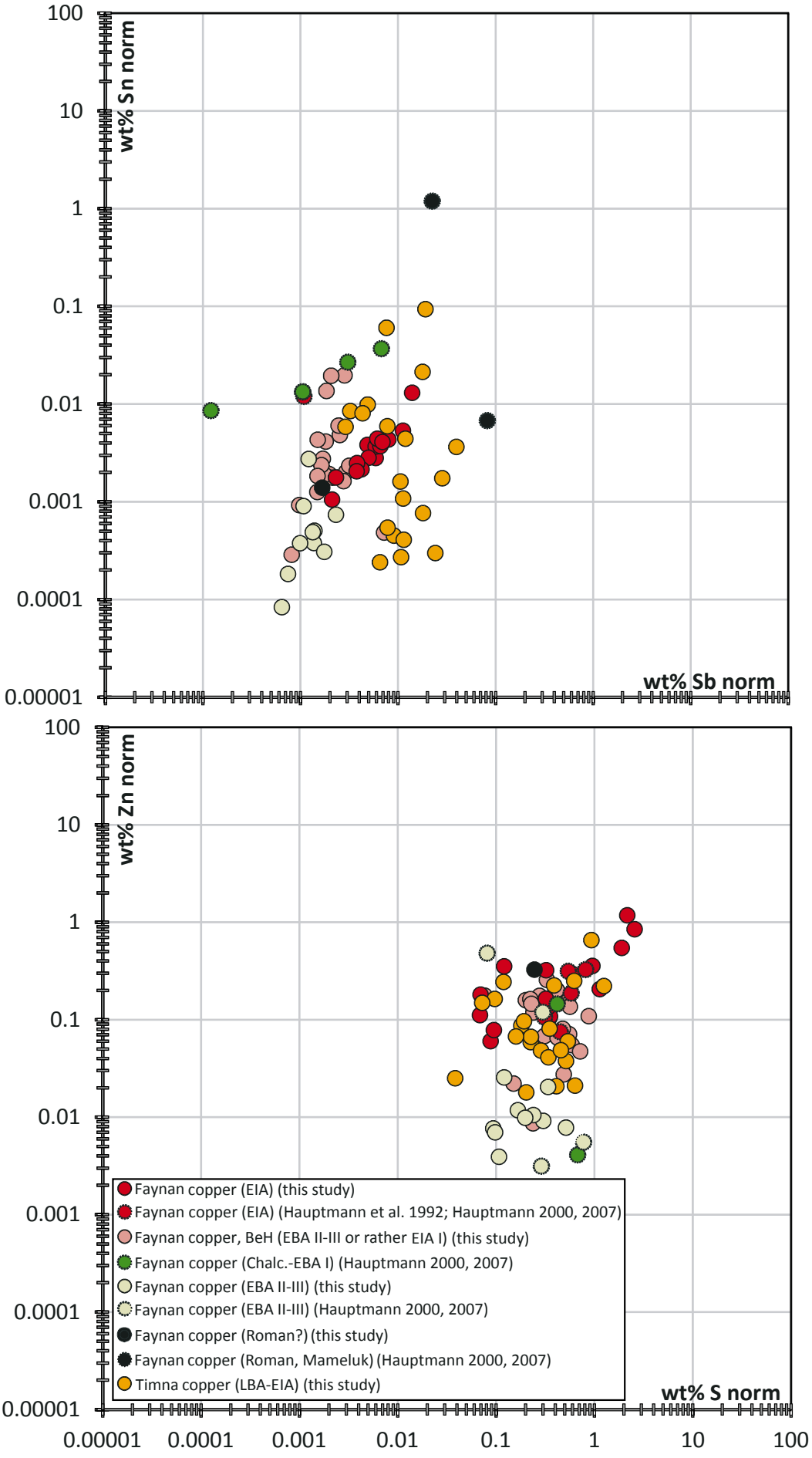

Continuation of Figure 11.

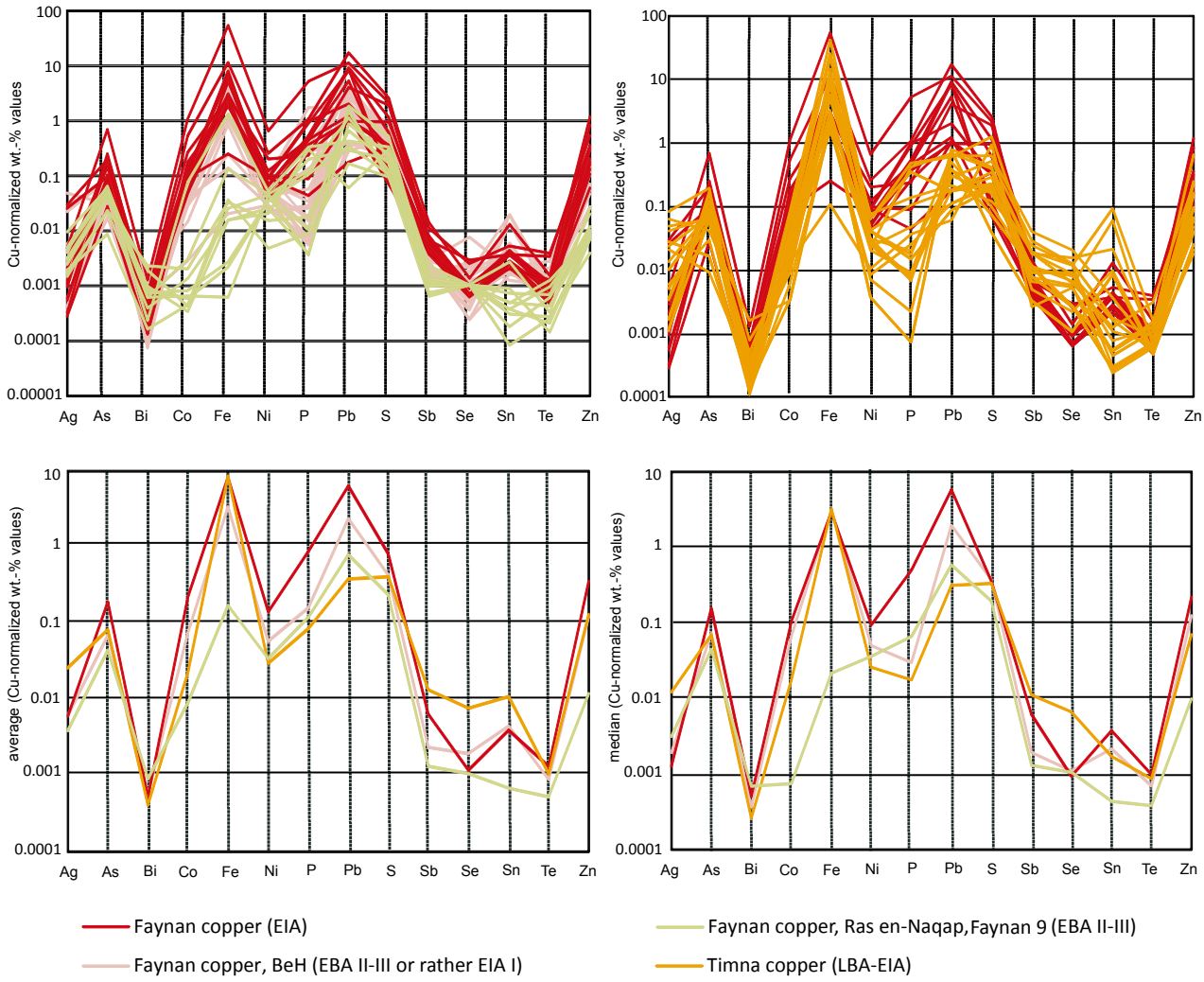

Figure 12. Bulk chemical composition (ICP-MS) of copper prills and lumps from EIA and EBA II-III smelting sites in Faynan and from LBA-EIA smelting sites in Timna. The material from Barqa el-Hetiye is distinguished here from the other Faynan sites by colour, as its dating is uncertain (EBA II-III or rather EIA I). a, b) individual samples; c) averages; d) medians. Graphs: M. Bode.

The same is true if we compare EIA prills and lumps with the EBA III-IV Levantine bar ingots from Khirbet Hamra Ifdan in Faynan, Har Yehuram in the Negev, and Hebron Hills (Figure 13).

Comparison of our EIA samples with published ICP-AES-data for the loaf ingots from the LBA-EIA wreck off Neve-Yam shows extremely low scattering on the side of the ingot group (Figure 14). Averages and medians of Pb, As, and Ni are similar on both sides. Averages and medians are significantly higher for Ag on the side of the ingots, but much lower for Fe, Zn, and Co.

Samples from Timna

The LBA-EIA samples from Timna do not show an internal grouping according to different smelting sites and are therefore all plotted with the same symbols (orange dots/lines) (Figure 11 and Figure 12). Note that from the following discussion samples 3010-18, 3030-18 and 3031-18 are excluded because of their too low bulk chemical sums.

As expected, the chemical signatures of our LBA-EIA samples from Timna equivalent to Amir/Avrona formation ores (n = 17) are very similar to the EIA samples from Faynan. Characteristic are again the high contents of Fe (Ø 7.07 wt.%). Iron enters the produced copper metal through intensive intergrowths of copper ore with iron ore, which is quite common in Timna (see Hauptmann, 2007, p.81). Contents of Pb (Ø 0.38 wt.%), although significantly lower than in Faynan, are higher relative to other known copper ore bodies exploited in antiquity.

Sulphur is in the range of a minor element with Ø 0.35 wt.%. In the trace element range, Zn, As, P, Ag, Ni, Co, Sb follow with values around 0.09 to 0.01 wt.%. Se, Te and Bi are around 0.007 to 0.0004 wt.%. Sn in average is 0.01 wt.%, but the median only 0.002 wt.%.

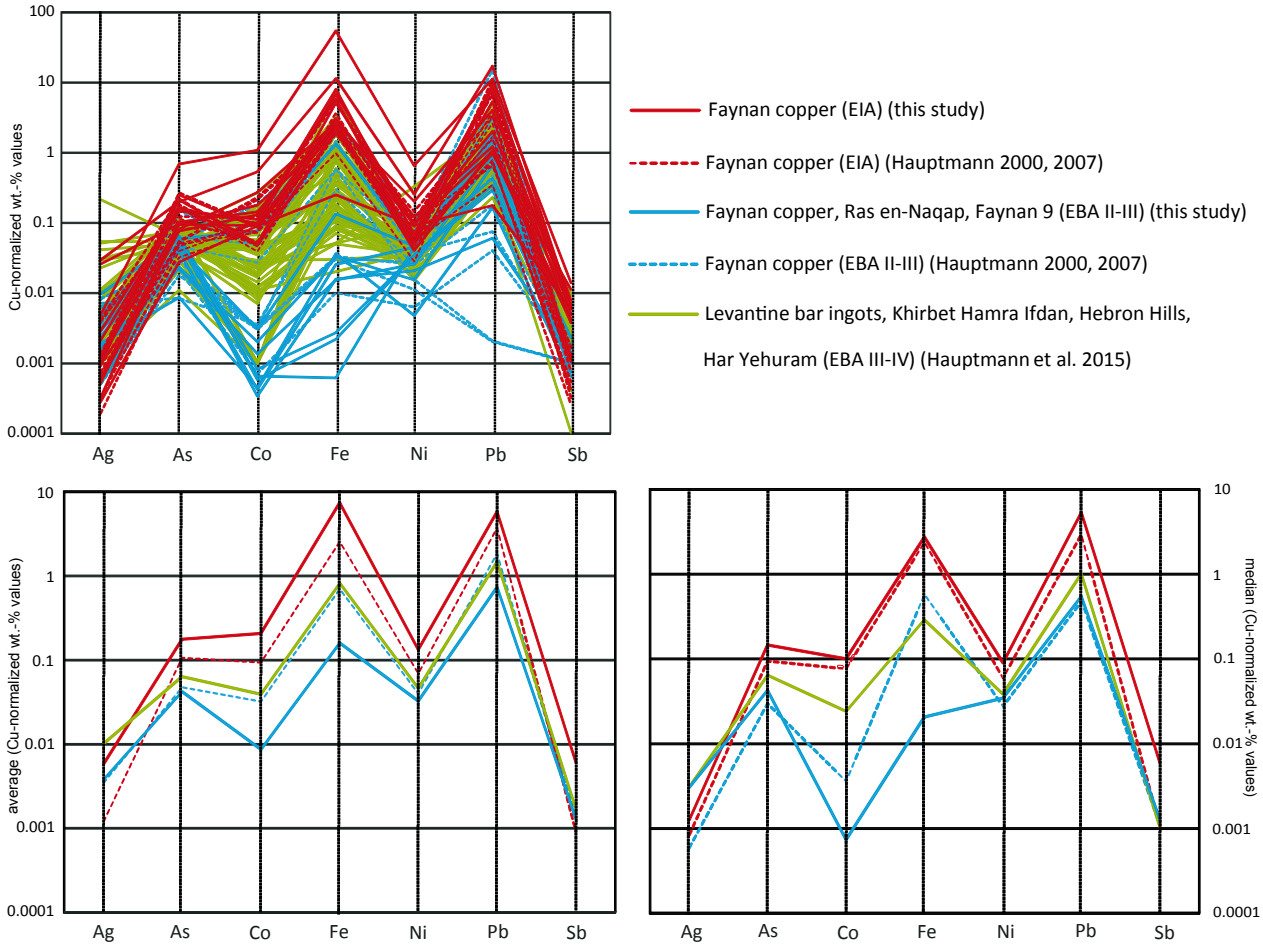

Figure 13. Bulk chemical composition of copper prills and lumps from EIA and EBA II-III smelting sites in Faynan (this study) plotted together with published data of comparative material measured with AAS (Hauptmann 2000; 2007) and OES (Hauptmann, et al., 2015). a) individual samples; b) averages; c) medians. Graphs: M. Bode.

Common features of copper types Faynan DLS and Timna Amir/Avrona, differences, and assessment of shifts related to smelting technique and refining

At Faynan, we have the opportunity to observe the changes in chemical composition of industrially produced raw copper through a very long chronological sequence. Since both mining archaeological evidence and LIA results show that both in EBA and EIA only DLS-ores were used, the observed differences in elemental content should be the result of different smelting techniques, those of the EIA evidently achieving better controlled conditions with a more reducing atmosphere and higher temperatures. This resulted in higher efficiency, but lower quality copper with more impurities (cf. Craddock and Meeks, 1987; Hauptmann, et al., 1992; Pernicka, 1999; Hauptmann, 2000; 2007). The high contents in Pb were especially problematic, since they limited suitability of the copper for hammered sheets like bronze vessels and for heavy duty objects like bronze weapons (see Papadimitriou, 2001). Once the Pb was in the metal, the problem was impossible to settle, since ancient refining techniques evidently were not capable of removing Pb. This is exemplified by the cargo of the LBA/EIA wreck off Neve-Yam, whose loaf ingots as seen by their low iron contents evidently consist of intentionally refined metal, but nevertheless still have very high Pb contents (see below).

Unfortunately, we do not have enough chronological resolution and/or coverage in the corpus of our samples to trace the effects of technological development within the subperiods of EIA mining industry in the Arabah. Therefore, a correlation with the four stages of EIA industrial development defined by Ben-Yosef, et al. (2019) is not possible at the moment.

With respect to provenance determination, our ICP-MS-data underline and detail already known aspects. First, Pb contents of EIA copper of both Faynan and Timna are much higher than those of most other ancient centres of copper production. Secondly, contents of all other elements are generally low, with the exception of Fe and P, which were easy to remove during remelting/refining. Nevertheless, if occasionally high contents of P

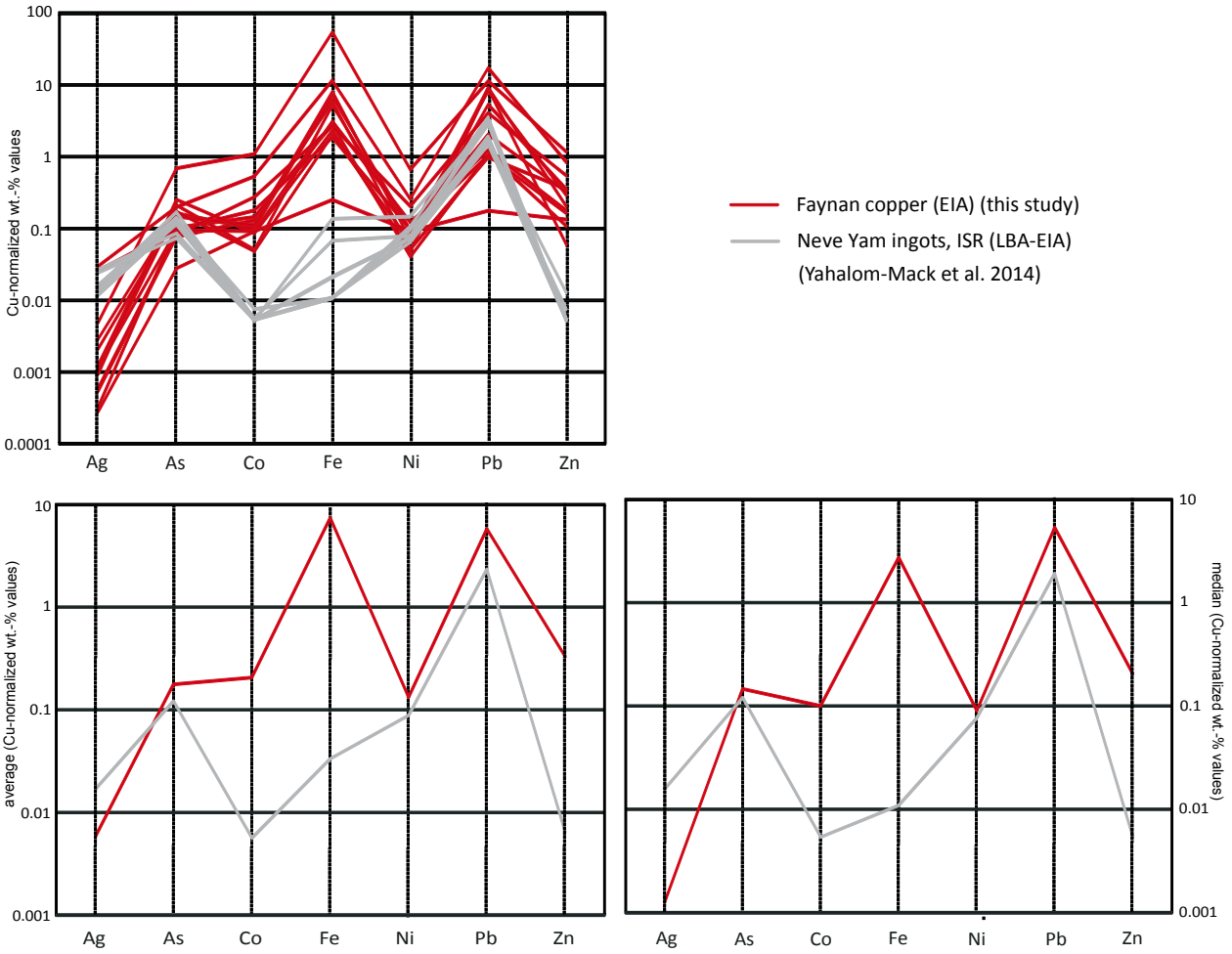

Figure 14. Bulk chemical composition of copper prills and lumps from EIA smelting sites in Faynan (this study) plotted together with LBA-EIA loaf ingots from the wreck site off Neve Yam at the Carmel coast (ISR) (Yahalom-Mack, et al., 2014). a) individual samples; b) averages; c) medians. Graphs: M. Bode

occur in a series of finished objects, this may be a good indicator for a connection with Faynan, since no other ancient centres of copper production are known with high P contents. Generally useful are the contents of Ag, Sb, and As, since these elements (like also Pb) are robust against fractionation effects during further processing (remelting/refining; cf. Pernicka, 1999; 2014 discussing Merkel's (1983; 1990) refining experiments). Ni and Co are less robust, and S, Se not at all.

If we compare EIA Faynan with LBA-EIA Timna (Figure 12), we note some differences in the averages and medians, despite the general similarities: Faynan analyses have more Pb, As, Co and Ni, P and S. Timna has on average higher contents of Ag, Sb and Se. Furthermore, the As/Sb-ratios are different in Faynan and Timna, resulting in a rather discreet grouping in the bi-elemental plot (Figure 11).

For the discrimination of Faynan vs. Timna in EIA finished objects, the differences in Pb, Ag, Sb, and As, are the most useful since these elements are robust against fractionation effects during remelting/refining.

If we apply these findings to the example of the loaf ingots of the LBA/EIA wreck off Neve-Yam (Figure 14), their very high lead content (average and median) fit with a production at Faynan and clearly exclude Timna (s. Yahalom-Mack, et al., 2014, p.171). The very low scattering of element contents in the loaf ingots points to homogenisation effects during the casting of the ingots. The very low content of Fe in these ingots points to intentional refining, as also do results of microstructural analysis conducted by Yahalom-Mack, et al. (2014, p.164). Refining may also explain the much lower values for Co and Zn compared to EIA copper prills and lumps. The similarities to the EIA prills and lumps in averages and medians of Pb, As, and Ni would then indicate that indeed these elements were not reduced through refining (surprising here is the seemingly very different behaviour of Ni compared to Co). The high averages and medians of Ag in the loaf ingots, settling at the upper end of the range of the prills and lumps, should be directly related to the ores and point to the mining of a sub-cluster within Faynan DLS ores, a suggestion that is

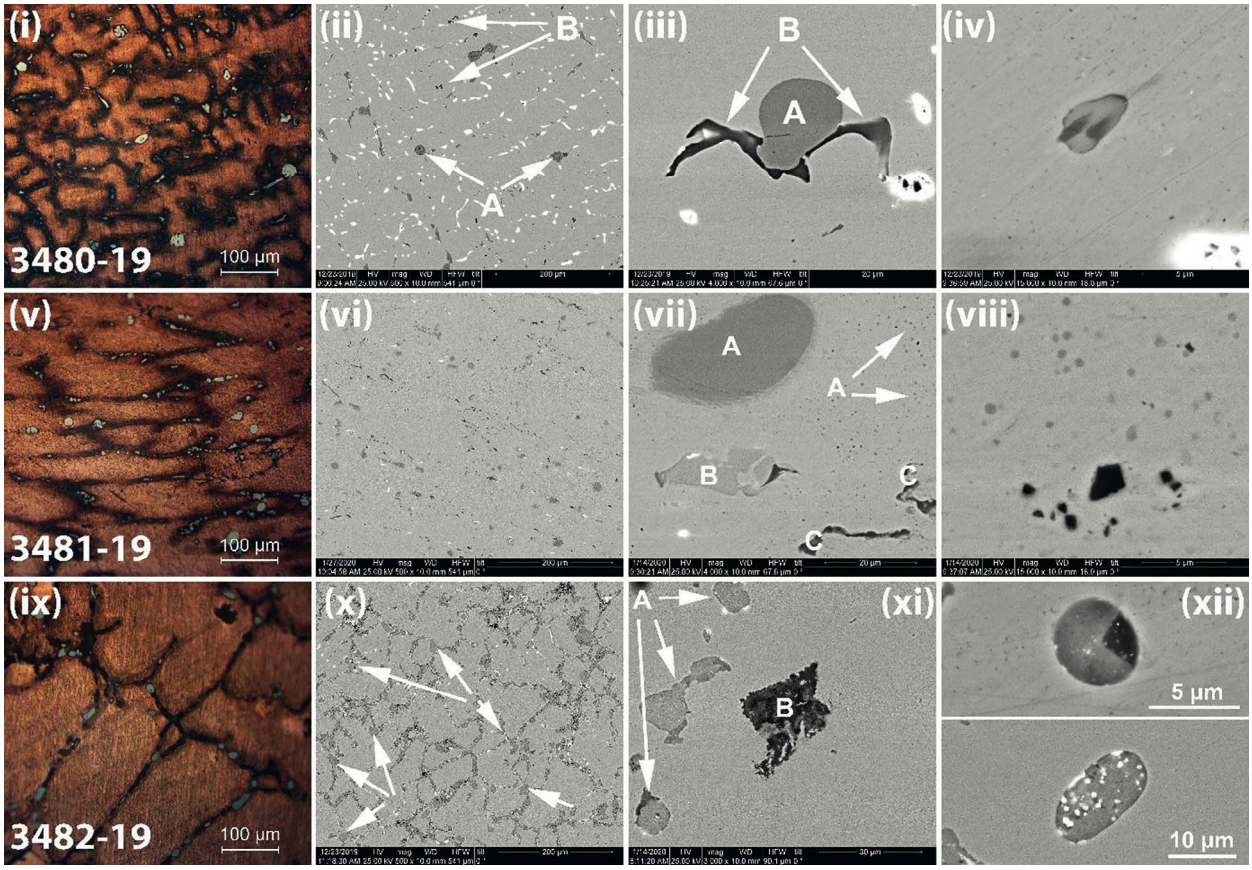

Figure 15. Sample 3480-19 **(i)** OM, 200×, etched. **(ii)** Numerous Pb-particles (white spots) along with a few Fe-P **(A)** and Mn-S ones (B) (BSE, 500×). **(iii)** Typical Fe-P dominated inclusion **(A)** in proximity with Mn-S **(B)** and Pb particles (white) (BSE, 4000×). **(iv)** Composite inclusion, containing minor As and traces of Ni (BSE, 15000×). Sample 3481-19 **(v)** OM, 200×, etched. **(vi)** Overview through SEM (BSE, 500×); compare with **(ii)**. **(vii)** Inclusions containing Fe, P, Mn and Co **(A)**, Cu-P dominated **(B)**, and inclusions composed primarily of Mn, S and Cu **(C)**; white spots correspond to Pb-rich inclusions (BSE, 4000×). **(C)** Grey circular spots are "type ii" Fe-P inclusions (<1μ); black spots correspond to Si-C remnants (due to grinding). Sample 3482-19 **(ix)** OM, 200×, etched. **(x)** Overview (BSE, 500×); the irregular linear patterns correspond to corrosion. Cu-S inclusions (arrows) lead inclusions (white particles) are also visible. **(xi)** Cu-S inclusions **(A)** next to a Fe-grain **(B)** (BSE, 3000×). **(xii)** Cu-S-Fe-Mn inclusions. Up: dark area is Mn- enriched; bottom: white spots are Pb-rich. Photos: G. Mastrotheodoros.

corroborated by the very tight lead isotopic clustering of these ingots at the geologically old end of Faynan DLS (Figure 6).

Microstructure

Three raw copper samples from Faynan sites and two from Timna sites preserve uncorroded metal cores and therefore were suitable for microstructural analysis. We discuss them one by one. Results on inclusion types and inclusions' elemental compositions (EDX) are listed in Table 8, and the elemental compositions (EDX) of the metals' matrices are listed in Table 9. Note that oxygen contents have been also estimated upon quantitation, the relevant data being utilized in order to differentiate the various inclusions and as a means to roughly estimate the extent of corrosion of the samples. For the sake of convenience, information on archaeological contexts/date and results of bulk chemical analysis is repeated in the entries. Characteristic OM and SEM photomicrographs are presented in Figures 15-17; for reasons of comparison the first two images of every single sample correspond to a 200× OM and a 500× SEM photomicrographs respectively.

Sample 3480-19 (EIA – Khirbet en-Nahas)

Sample 3480-19 is notably rich in (Pb) (Table 8), and this probably accounts for its dendrite-like microstructure (Figure 15 (i) and (ii)). In addition, the sample contains a substantial number of Fe-enriched inclusions along with some inclusions that are rich in Mn and S (Figure 15 (ii)); the elemental compositions of the aforementioned inclusions are reported in Table 8. Interestingly, the Pb particles contain minor Cu while the Fe-dominated ones are notably rich in P (>15%) and bear several minor ingredients such as Mn and Co. As

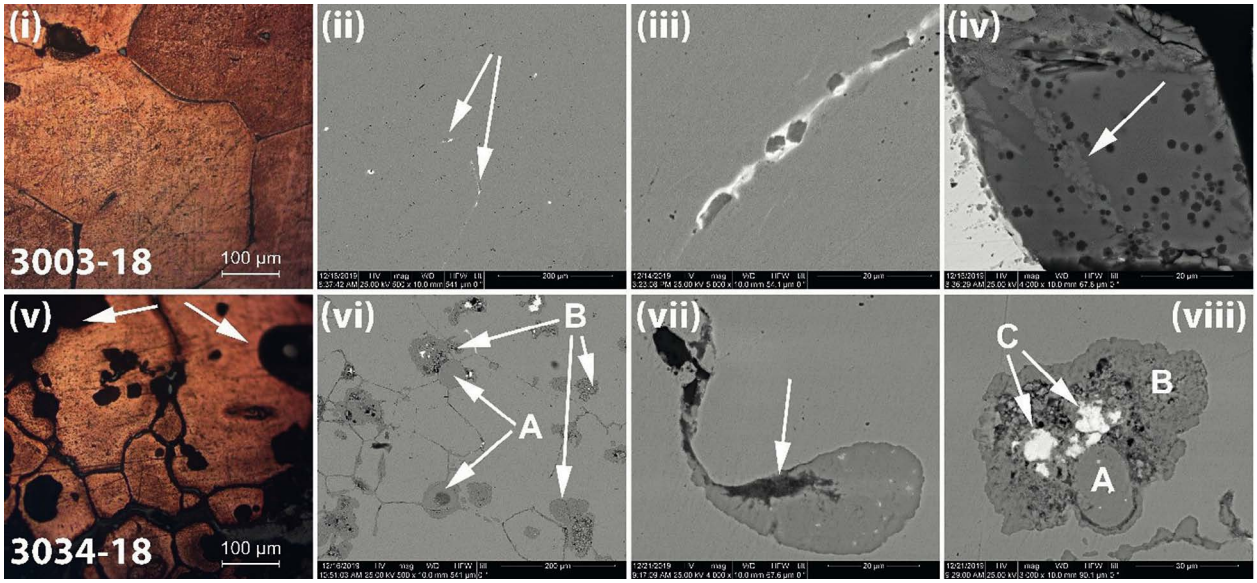

Figure 16. Sample 3003-18 **(i)** OM, 200×, etched. **(ii)** Cu-S-Fe (arrow) and Pb-rich inclusions (white spots) (BSE, 500×). **(iii)** Se-containing Cu-S-Fe inclusions (grey), surrounded by Pb-phase (BSE, 5000×). **(iv)** slag remnant; arrow points on a fayalite dendrite, dark spots on the grey glassy matrix correspond to O & Si enriched phases (BSE, 4000×). Sample 3034-18 **(v)** OM, 200×, etched; arrows point on voids. **(vi)** copper sulphide inclusions **(A)** and corroded areas **(B)** (BSE, 500×). **(vii)** Fe-rich inclusion (arrow) within a copper sulphide particle (BSE, 4000×). **(viii)** copper sulphide inclusion **(A)** surrounded by corrosion **(B)** and Pb particles **(C)** (BSE, 3000×). Photos: G. Mastrotheodoros.

for the latter element, it shall be noted that its quantification is problematic because Co's major peak (K_α @ 6.93 keV) partially coincides with the Fe K_β spectra line (7.06 keV), hence in case of Fe-rich phases Co contents are expected to be considerably overestimated. On the other hand, the Mn-S inclusions contain only traces of Fe and P (Table 8, Figure 15 (iii)), while detailed probing revealed the presence of a few multi-phased inclusions and a couple of composite ones that contain minor As and traces of Ni (Figure 15 (iv)).

Sample 3481-19 (EIA – Khirbet en-Nahas)

Under OM, sample 3481-19 appears dominated by rather elongated equiaxial grains, a microstructure resembling that of hammered items (Figure 15 (v)). Probably this prill was deformed when the surrounding slag was crushed. As for its inclusions, one may note apparent similarities with sample 3480-19. In detail, sample 3481-19 is rich in Fe-P inclusions which are of an identical composition to those found in sample 3480-19 (Table 9), while it bears the same manganese sulphide inclusions as the ones spotted in 3480-19 (Table 8, Figure 15 (vi)). It is worth noting that these two types of inclusions are of the same micromorphology – and composition– with those found in Iron Age slags from Khirbet-en-Nahas (Hauptmann, 2007). However, in case of sample 3481-19 the Fe-P inclusions appear more frequently (hence higher P content is detected in the bulk, see Table 9) and in two distinct morphologies, namely i) as relatively large grains (5-50 μm) and ii) as tiny particles (<1 μm) (Figure 15 (vii) and (viii)). Moreover, the sample in consideration bears far–fewer Pb particles in comparison to sample 3480-19, and this is readily noted upon comparison of the Figure 15 (ii) and (vi) (see also Table 9 for the relevant bulk elemental compositions). Finally, sample 3481-19 bears a few Cu-P inclusions (Figure 15 (vi)); similar particles were not seen in the sample 3480-19.

Sample 3482-19 (EIA – Faynan 5)

Compared to the two previously discussed samples, sample 3482-19 has a coarser grain, which presumably indicates slower cooling. (Figure 15 (ix)). However, the sample in consideration is largely altered by corrosion (Figure 15 (x)), the latter being mostly developed in the characteristic intergranular pattern (Scott, 1991). Interestingly, two distinct (in terms of composition) corrosion patterns were spotted, namely chlorine-induced (Cl>20 wt.%) and oxygen-related (O>4 wt.%). Although the extensive corrosion hinders the detailed probing of the initial micromorphology (Figure 15 (x)), it turned out that the sample 3482-19 contains dispersed Pb inclusions along with numerous copper sulphide particles, which occasionally bear inherent Pb-rich inclusions (Figure 15 (x) and (xii)). A second type of copper sulphides that contain enhanced Fe and Mn were also spot-

ted (Figure 15 (xii)), as well as a few Fe & O dominated inclusions (Figure 15 (xi) and (xii)). The pertinent analytical data are summarized in Table 8.

Sample 3003-18 (1030-930 BC - Timna site 34)

Prill 3003-18 from Timna bears only few Cu-S-Fe grains along with some Pb-rich inclusions (Figure 16 (i) and (ii)). Numerous Cu-S-Fe inclusions contain Se in detectable levels (>0.1 wt.%) along with minor Pb, while in some instances these very inclusions appear next to or surrounded by Pb-rich phases (Figure 16 (iii)); therefore Pb was quite often detected in appreciable levels upon their EDX analyses. The relevant EDX data are summarized in Table 8. In addition, the sample contains a couple of bigger multi-phase grains of rather enhanced dimensions (Figure 16 (iv)) which are composed of a Fe-Si-O-Ca glassy matrix that bears partially formed fayalite dendrites (Fe-Si-O). Therefore these inclusions shall be interpreted as slag remnants (Bourgarit, 2019) (Table 8).

Sample 3034-18 (1100-1000 BC - Timna site 15)

Sample 3034-18 has undergone severe corrosion and appears far richer in inclusions in comparison with the other copper prill from Timna (sample 3003-18). Indeed, it contains several copper sulphide inclusions, some Pb-rich grains, and a few Fe enriched particles. Extensive areas of corrosion are also spotted (i.e. areas with enhanced levels of oxygen and chlorine, distinct in terms of microstructure from the sound metal core) which have been mostly developed in the characteristic intergranular pattern (Figure 16 (vi) and (viii)) (Scott, 1991). In addition, numerous voids of enhanced diameters (>100 μm) are seen scattered within the metallic matrix (Figure 16 (v)), a morphological characteristic that has been occasionally spotted in pertinent ingots as well (Hauptmann, Maddin and Prange, 2002; Yahalom-Mack, et al., 2014). The analysed copper sulphide particles contain considerable Fe, and in fact their composition is very similar to that of sample's 3003-18 Cu-S-Fe particles (Table 8). It is also worth noting that the Pb particles are often seen in the rims of voids and inside corroded areas, and this may imply a process of gradual lead-leaching upon corrosion (Figure 16 (vi) and (viii)). Finally, the Fe-rich particles contain remarkable O and this may indicate that they correspond to remnants of parent minerals that were partly (or insufficiently) reduced upon smelting.

Comparison of microstructural observations

Fe-rich inclusions were detected in all five prill samples. Analyses of the metallic – not contaminated by inclusions – matrix of the samples (Figure 17) showed that the metallic matrix itself, also contains a considerable amount of iron (Table 9). For the phenomenon compare Salje and Feller-Kniepmeier (1977). The high amount of Fe is related to the fact that both Faynan DLS copper ores and Timna Amir/Avrona copper ores are intergrown with Fe ores, resulting in self fluxing qualities, and to the use of advanced smelting techniques employing high temperatures and strongly reducing conditions (s. above chapter on - Technical and organisational development of mining and smelting in the Wadi Arabah – with references).

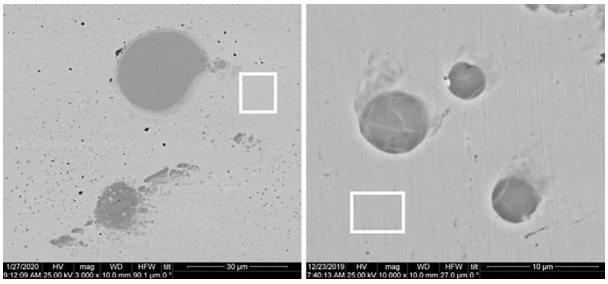

Figure 17. Samples 3481-19 (left) & 3491-19 (right): rectangles mark inclusion-free areas of prills' metallic matrices where corresponding EDX analyses were conducted. Photos: G. Mastrotheodoros.

Mn-rich inclusions are specific for the Faynan samples and are not observed on the Timna samples (Table 8). This is reflected in the bulk contents of Mn as measured with EDX and ICP (Table 9). As stated above in the chapter on the - Copper ore deposits -, the intergrowth of Mn ore and Cu ore is characteristic for Faynan DLS and made this ore type self-fluxing, in addition to the effect of the intergrown Fe-ore. Timna Amir/Avrona-ore is not intergrown with Mn ores but only with Fe ore. At Timna, Mn-contents in raw copper are only expected if Mn nodules of the Timna formation were intentionally added as a flux.

The high amount of S-rich inclusions in both Faynan and Timna samples (Table 8) is surprising at first sight, as both Faynan DLS and Timna Amir/Avrona are secondary copper ores with only low amounts of S-rich mineralization. Evidently, the smelting technique of the EIA Arabah industry with its strong reducing conditions prevented the S-rich inclusions from oxidation so that a large percentage of the initial S-content entered into the raw copper.

P-bearing inclusions, Co-bearing inclusions, and As-bearing inclusions seem more common in Faynan raw copper (samples 3480-19 and 3481-19), while the two Timna samples bear Pb inclusions that presumably contain traces of Ag, and Se-bearing sulphides are only spotted in Timna sample 3003-18. These findings fit the differences in averages and medians of elemental bulk contents as measured with ICP.

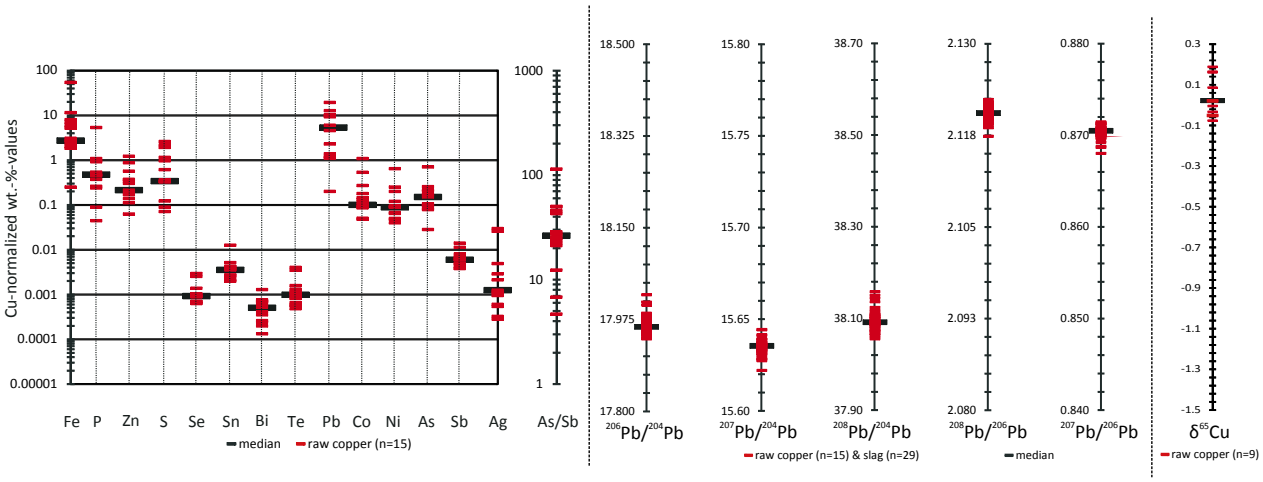

Figure 18. Chemical fingerprint of EIA Faynan copper (bulk chemical composition, As/Sb ratio, LI ratios and CI ratio). Data of this study. There is only one copper type at Faynan: copper of type Faynan DLS. Graph: M. Bode.

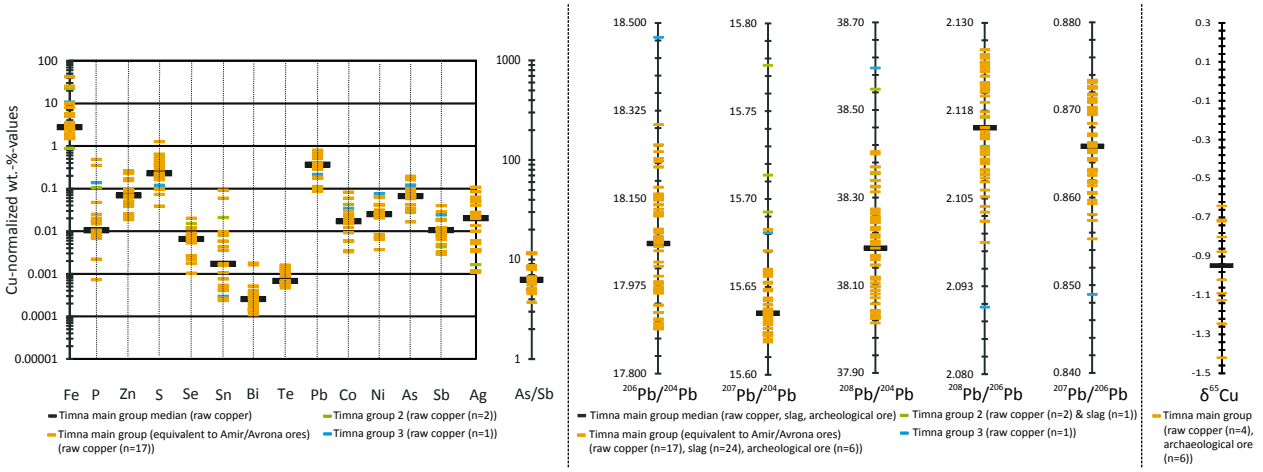

Figure 19. Chemical fingerprint of LBA-EIA Timna copper (bulk chemical composition, As/Sb ratio, LI ratios and CI ratio). Data of this study. Three copper types can be distinguished at Timna: Timna main type (equivalent to Amir/Avrona ores), Timna Type 2, and Timna Type 3. Graph: M. Bode.

Conclusions

This study was based on a relatively large sample suite of raw copper, slag, and archaeological ores collected at the economically most significant smelting sites of the industrial regions of EIA Faynan and LBA-EIA Timna. In the above chapters we demonstrated that LI ratios, CI ratios, bulk chemical composition, and microstructure fit very well with geological and mining archaeological information and result in coherent models for the copper types that were actually produced and marketed.

Four copper types can be distinguished (Figure 18 and Figure 19):

Copper Type Faynan DLS (Figure 18)

At EIA Faynan, copper was smelted exclusively from ores of the Dolomite Limestone Shale formation (DLS), but not of the Massive Brown Sandstone formation (MBS). Due to this homogeneity of the raw materials and enhanced by homogenisation along the *chaîne opératoire*, copper and slag samples cluster very densely both in terms of lead isotope ratios and of copper isotope ratios. There are no outliers except one sample from a third-rate smelting site (sample 5380-21 from Barqa el-Hetiye). We therefore can define in quite a strict way LI and CI ratios characteristic for EIA copper from Faynan. Microstructure analysis of raw copper samples shows high amounts of Pb-particles and of Fe-containing phases (Fe-P-Mn-Co, Pb-Cu, Mn-S-Cu). Iron is also present within the matrix. Cu-S-phases can sometimes be abundant, despite the oxidic character of DLS-ore. Most interesting is the high amount and the diversity of Mn-containing phases. It reflects the intergrowth of Cu-, Mn- and Fe-minerals in the DLS-ores which made them self-fluxing, – an important advantage for the ancient smelters. P is present in many phases,

which is an unusual feature for Ancient copper types. Bulk chemical analysis of raw copper samples shows large amounts of Fe and Pb, but relatively low amounts for all other minor elements. Generally, bulk elemental contents fit with the metallogenesis of the oxidic DLS ores and to the advanced smelting technology of EIA with high temperatures and strongly reducing conditions.

Mn contents with ICP-MS were only measured for the three samples selected for metallography, but an average may be roughly estimated to be around 0.5 wt.%.

As far as provenance research is concerned, it is primarily the bulk contents of those elements that do not deplete so much during remelting and refining that are relevant. The very high Pb content and the relatively low scattering of Bi, Te, Ni, As, Sb and Ag should be emphasised here. In the case of objects made of unrefined metal, a high Mn or P content can be an indication of the use of Faynan DLS copper.

Copper Type Timna Amir/Avrona (Figure 19)

The main copper type produced at LBA-EIA Timna was smelted from Amir/Avrona ore. Due to radiogenic lead isotopes present in this ore, the LI ratios of raw copper and slags form relatively broad ranges, integrating the ranges of the Faynan DLS copper type. The range of CI ratios is narrow, analogous to the range of the Amir/Avrona ore, and distant from the range of the Faynan DLS copper.

Microstructure analysis and bulk chemical analysis of raw copper samples show similarities to copper of type Faynan DLS because of the shared geological history of the ores and similar smelting techniques. An important difference visible in the microstructure analysis is the absence of Mn-phases, corresponding with a low bulk content in Mn as measured by EDX and ICP-MS. Absence of Mn-phases agrees with the fact that Amir/Avrona copper-ore is not intergrown with Mn-ore (in contrary to Faynan DLS-ore), but only with Fe-ore, which equally results in self-fluxing properties. A second difference is the absence of P-phases, corresponding to a lower bulk content as measured with ICP-MS. Abundant microphases are Cu-S-Fe-Pb, Cu-S-Fe-O-Se, Cu-S-Fe, Cu-S.

The main impurities in the bulk composition are Fe and Pb as with copper type Faynan DLS, even if the median of Pb content is one order of magnitude lower. Compared to copper type Faynan DLS, the medians of Ni and Co are lower, those of Bi, Te, Sb, and As are quite similar, and the median for Ag higher. The median of the ratio As/Sb is lower.

At Timna site 30 (late), the centre of the last phase of smelting activity at Timna, we note a sub-cluster of LI-ratios. Probably it is related to the fluxing with Mn-nodules of Type B stemming from the Timna formation.

Copper Type Timna 2 (Figure 19)

Of limited relative importance compared to the Amir/Avrona type at Timna was a Type 2 with somewhat offset LI-ratios, influenced from ores that we can not pinpoint yet. CI-ratios of this copper type are not available yet.

Copper Type Timna 3 (Figure 19)

Of little relative importance was Timna Type 3, again with offset LI-ratios compared to Amir/Avrona copper type. It probably was smelted from ores mined at Wadi Amram. CI-ratios of this copper type are not available yet.

Relevance of CI-ratios in provenance studies for the detection of mixtures between copper of type Faynan DLS, Timna Type Amir/Avrona, and third parties

Copper of type Faynan DLS contains several orders of magnitude more natural lead than most other ancient copper types, and especially than Cypriot copper. To a lower degree this is true also for copper of type Timna Amir/Avrona. Therefore, if concurring copper types from other source regions are low in lead, with their mixture, their LI-signal is overpowered by the abundant natural lead in the Faynan and Timna copper types. Consequently, any copper imports from Faynan and Timna should leave strong signals in the LI-ratios of the metal pools of their respective distribution areas. This effect is very welcome if one just wants to sketch the geographic scope and extent of the distribution systems of Faynan and Timna, but at the same time makes it more difficult to assess the exact market shares, since the amount of mixture with copper from other source regions is impossible to establish with LI alone. For a first crosscheck of the probability of large amounts of admixtures in assemblages dominated by Faynan DLS and/or Timna Amir/Avrona it will therefore be necessary to consider the medians, averages, and spreads of bulk chemical contents. In a next step, for a consideration of the quantities of admixture of third parties and for internal differentiation between Faynan DLS and Timna Amir/Avrona, the interpretation of CI-ratios offers an effective approach, since the ranges of unmixed copper from Faynan and Timna are both very narrow and at the same time different from each other without overlapping. Consequently, any admixture should cause a strictly proportional shift, visible as a deviation from the expected CI-range. The reasons for such a shift can then be searched and tested by multi-dimensional modelling of potential mixtures (method: arithmetic simulation of effects of admixtures

of, e.g. Cypriot copper with step-by-step-modelling of LI-ratios & CI-ratios and elemental contents/ratios).

Acknowledgements

We thank Regina Friese for the chemical preparation of the samples and Sabine Klein for the lead isotope measurements at FIERCE. We also thank the anonymous reviewers for their comments and suggestions, and also the native speaker for checking the Englisch. We thank the GlobaLID-team for their support and are, as always, grateful to have access to the large OXALID data base.

References

Asael, D., Matthews, A., Bar-Matthews, M. and Halicz, L., 2007. Copper isotope fractionation in sedimentary copper mineralization (Timna Valley, Israel). *Chemical Geology*, 243, pp.238-254. https://doi:10.1016/j.chemgeo.2007.06.007.

Asael, D., Matthews, A., Oszczepalski, S., Bar-Matthews, M. and Halicz, L., 2009. Fluid speciation controls of low temperature copper isotope fractionation applied to the Kupferschiefer and Timna ore deposits. *Chemical Geology*, 262, pp.147-158. https://doi:10.1016/j.chemgeo.2009.01.015.

Asael, D., Matthews, A., Bar-Matthews, M., Harlavan Y. and Segal, I., 2012. Tracking redox controls and sources of sedimentary mineralization using copper and lead isotopes. *Chemical Geology*, 310-311, pp.23-35. https://doi.org/10.1016/j.chemgeo.2012.03.021.

Avner, U., Ginat, H., Shalev, S., Shilstine, S., Langford, B., Frumkin, A., Shem-Tov, R., Filin, S., Arav, R., Basson, U., Shamir, O. and Scott-Cummings, L., 2018. Ancient copper mines at Nahal 'Amram, Southern Aabah. In: E. Ben-Yosef, ed. 2018. *Mining for ancient copper. Essays in memory of Beno Rothenberg. Tel Aviv University, Sonia and Marco Nadler Institute for Archaeology Monograph Series*, 37. University Park, PA/Tel Aviv: Eisenbrauns & Emery and Claire Yass Publications in Archaeology of the Institute of Archaeology, Tel Aviv University. pp.147-177.

Bartura, Y. and Würzburger, U., 1974. The Timna copper deposit. *Annales de la Société géologique de Belgique*, *Publications spéciales. Gisements stratiformes et provinces cuprifères - Centenaire de la Société Géologique de Belgique,* pp.277-285, [online] Available at: https://popups.uliege.be/0037-9395/index.php?id=3505.

Bartura, Y., Hauptmann, A. and Schöne-Warnefeld, G., 1980. Zur Mineralogie und Geologie der antik genutzten Kupferlagerstätte im Timna-Tal. In: H.G. Conrad and B. Rothenberg, eds. 1980. *Antikes Kupfer im Timna-Tal. Der Anschnitt, Beiheft*, 1. Bochum: Deutsches Bergbau-Museum. pp.41-56.

Ben-Dor Evian, S., Yagel, O.,Harlavan, Y., Seri, H., Lewinsky, J., and Ben-Yosef, E., 2021. Pharaoh's copper: The provenance of copper in bronze artifacts from post-imperial Egypt at the end of the second millennium BCE. *Journal of Archaeological Science: Reports*, 38, pp.1-13. https://doi.org/10.1016/j.jasrep.2021.103025.

Ben-Yosef, E., 2010. *Technology and Social Process: Oscillations in Iron Age Copper Production and Power in Southern Jordan*. Ph. D. University of California, San Diego.

Ben-Yosef, E., 2016. Back to Solomon's Era: Results of the First Excavations at Slaves' Hill (Site 34, Timna, Israel). *Bulletin of the American Schools of Oriental Research,* 376, pp.169-98.

Ben-Yosef, E., 2018. The Central Timna Valley Project: Research Design and Preliminary Results. In: E. Ben-Yosef, ed. 2018. *Mining for Ancient Copper: Essays in Memory of Beno Rothenberg*. University Park, PA/Tel Aviv: Eisenbrauns & Emery and Claire Yass Publications in Archaeology of the Institute of Archaeology, Tel Aviv University. pp.28-63.

Ben-Yosef, E. and Sergi, O., 2018. The Destruction of Gath by Hazael and the Arabah Copper Industry: A Reassessment. In: *I. Shai, J.R. Chadwick, L. Hitchcock, A. Dagan, C. McKinny and J. Uziel, eds*. 2018. *Tell it in Gath. Studies in the History and Archaeology of Israel. Essays in Honor of Aren M Maeir on the Occasion of his Sixtieth Birthday.* Ägypten und Altes Testament. Münster: Zaphon. pp.461-480.

Ben-Yosef, E., Langgut, D. and Sapir-Hen, L., 2017. Beyond Smelting: New Insights on Iron Age (10th c. BCE) Metalworkers Community from Excavations at a Gatehouse and Associated Livestock Pens in Timna, Israel. *Journal of Archaeological Science: Reports*, 11, pp.411-26. https://doi.org/10.1016/j.jasrep.2016.12.010.

Ben-Yosef, E., Shaar, R., Tauxe, L. and Hagai, R., 2012. A New Chronological Framework for Iron Age Copper Production at Timna (Israel). *Bulletin of the American Schools of Oriental Research,* 367, pp.31-71.

Ben-Yosef, E., Liss, B., Yagel, O.A., Tirosh, O., Najjar, M. and Levy, T.E., 2019. Ancient technology and punctuated change: Detecting the emergence of the Edomite Kingdom in the Southern Levant. *PLoS ONE,* 14(9), e0221967. https://doi.org/10.1371/journal.pone.0221967.

Beyth, M., Segev, A. and Ginat, H., 2013. Stratigraphy and Structure of the Timna Valley and Adjacent Ancient Mining Areas. *Ministry of Energy and Water Resources, Geological Survey of Israel, Report,* 15, pp.1-28.

Bode, M., Kiderlen, M., Mastrotheodoros, G.P., Filippaki, E. and Bassiakos, Y., 2020. Das Kupfer der griechischen spätgeometrischen Dreifußkessel (ca. 750–700 v. Chr.): eine Diskussion der chemischen und bleiisotopischen Analysen. In: H.G. Yalçın and O. Stegemeier, eds. 2020. *Metallurgica Anatolica. Festschrift für Ünsal Yalçın anlässlich seines 65. Geburtstags*. İstanbul: Ege Yayınları. pp.329-348.

Bourgarit, D., 2019. Mineralogy of slags: a key approach for our understanding of ancient copper smelting processes. In: G. Artioli and R. Orberti, eds. 2019. *The contribution of mineralogy to cultural heritage*, Mineralogical Society of Great Britain & Ireland, pp.203-231. https://doi.org/10.1180/EMU-notes.20.5.

Craddock, P.T. and Meeks, N.D., 1987. Iron in ancient copper. *Archaeometry,* 29(2), pp.187-204.

Degryse, P., El-Desouky, H., Bretschneider, J., Jans, G., Vanhaecke, F. and Muchez, P., 2012. Lead Isotopic Analysis of Copper Alloy Artifacts from Tell Tweini. Changing Ore Sources from the Early Bronze Age to the Iron Age? In: T. Boyi, J. Bretschneider, A. Goddeeir, H. Hameeuw, G. Jans, and J. Tavernier, eds. 2012. *The Ancient Near East, a Life! Festschrift Karel Van Lerberghe*. Leuven: Peeters. pp.131-142.

Egerton, R.F., 2005. *Physical principles of electron microscopy: an introduction to TEM, SEM and AEM*. New York: Springer.

Ehrlich, S., Harlavan, Y., Bar-Matthews, M. and Halicz, L., 2004. Lead and uranium isotopic behavior in diagenetic and epigenetic manganese nodules, Timna Basin, Israel, determined by MC-ICP-MS. *Applied Geochemistry,* 19, pp.1927-1936. https://doi.org/10.1016/j.apgeochem.2004.05.005.

Gale, N.H., Bachmann, H.G., Rothenberg, B. and Stos-Gale, Z.A., 1990. The adventitious Production of Iron in the Smelting of Copper in Timna, W. Arabah. In: B. Rothenberg, ed. 1990. *The Ancient Metallurgy of Copper*. IAMS, UCL London. pp.182-191.

Harlavan, Y., Bar-Matthews, M., Matthews, A., Asael, D. and Segal, I., 2017. Tracing the sources of sedimentary Cu and Mn ores in the Cambrian Timna Formation, Israel using Pb and Sr isotopes. *Journal of Geochemical Exploration,* 178, pp.67-82. https://doi.org/10.1016/j.gexplo.2017.03.016.

Hauptmann, A., 2000. *Zur frühen Metallurgie des Kupfers in Fenan/Jordanien*. Der Anschnitt, Beiheft, 11. Bochum: Deutsches Bergbau-Museum.

Hauptmann, A., 2007. *The Archaeometallurgy of Copper. Evidence from Faynan, Jordan*. Berlin Heidelberg, New York: Springer.

Hauptmann, A., Maddin, R. and Prange, M., 2002. On the Structure and Composition of Copper and Tin Ingots Excavated from the Shipwreck of Uluburun. *Bulletin of the American Schools of Oriental Research,* 328, pp.1-30.

Hauptmann, A., Begemann, F., Heitkemper, E., Pernicka, E. and Schmitt-Strecker, S., 1992. Early Copper Produced at Feinan, Wadi Araba, Jordan: The Composition of Ores and Copper. *Archaeomaterials,* 6(1), pp.1-33.

Hauptmann, A., Schmitt-Strecker, S., Levy, Th.E. and Begemann, F., 2015. On Early Bronze Age Copper Bar Ingots from the Southern Levant. *Bulletin of the American Schools of Oriental Research*, 373, pp.1-24.

Heinrich, K.F.J., 1991. Strategies of Electron Probe Data Reduction. In: K.F.J. Heinrich and D.E. Newbury, eds. 1991. *Electron Probe Quantitation*. Boston, MA: Springer. pp.9-18. https://doi.org/10.1007/978-1-4899-2617-3_2.

Jansen, M., 2011. *Möglichkeiten und Grenzen der Cu-Isotopie in der Archäometallurgie des Kupfers*. Masterthesis Ruhr-University Bochum.

Jansen, M., Hauptmann, A., Klein, S. and Seitz, H.M., 2017. The potential of stable Cu isotopes for the identification of Bronze Age ore mineral sources from Cyprus and Faynan: results from Uluburun and Khirbet Hamra Ifdan. *Archaeological and Anthropological Sciences,* 10(6), pp.1485-1502. https://doi.org/10.1007/s12520-017-0465-x.

Löffler, I., 2017. New thoughts about Iron Age metallurgy in Faynan: A discussion. In: P. Eisenach, Th. Stöllner and A. Windler, eds. 2017. *The RITaK Conferences 2013-2014. Der Anschnitt, Beiheft,* 34. Bochum: Deutsches Bergbau-Museum. pp.151-161.

Ketelaer, A. and Hauptmann, A., 2016. In the Shadow of Timna? The Mining Region of Wadi Amram. New Analytical and Archaeological Aspects. *Metalla,* 22(2), pp.169-183.

Kiderlen, M., Bode, M., Hauptmann, A. and Bassiakos, Y., 2016. Tripod cauldrons produced at Olympia give evidence for trade with copper from Faynan (Jordan) to South West Greece, c. 950-750 BCE. *Journal of Archaeological Science: Reports,* 8, pp.303-313. https://doi.org/10.1016/j.jasrep.2016.06.013.

Langford, B., Frumkin, A., Avner, U. and Ginat, H., 2018. Nahal 'Amram, Southern Arabah Valley: a survey of underground copper mines. In: E. Ben-Yosef, ed. 2018. *Mining for ancient copper. Essays in memory of Beno Rothenberg. Tel Aviv University, Sonia and Marco Nadler Institute for Archaeology Monograph Series*, 37. University Park, PA/ Tel Aviv: Eisenbrauns & Emery and Claire Yass Publications in Archaeology of the Institute of Archaeology, Tel Aviv University. pp.217-227.

Levy, T.E., Najjar, M. and Ben-Yosef, E. ed., 2014. *New Insights into the Iron Age Archaeology of Edom, Southern Jordan - Surveys, Excavations and Research from the Edom Lowlands Regional Archaeology Project (ELRAP).* Los Angeles: Cotsen Institute of Archaeology Press UCLA.

Liss, B., Howland M.D, Lorentzenc, B., Smitheram, C., Najjar, M. and Levy, T.E., 2020. Up the Wadi: Development of an Iron Age Industrial Landscape in Faynan, Jordan. *Journal of Field Archaeology,* 45(6), pp.413-427. https://doi.org/10.1080/00934690.2020.1747792.

Merkel, J., 1983. Summary of experimental results for Late Bronze Age copper smelting and refining. *Museum Applied Science Center Journal*, 2(6), pp.173-179.

Merkel, J., 1990. Experimental reconstruction of Bronze Age copper smelting based on archaeological evidence from Timna. In: B. Rothenberg, ed. 1990. *The ancient metallurgy of copper*. London: Institute of Archaeo-Metallurgical Studies. pp.78-122.

Moeller, K., Schoenberg, R., Pedersen, R.B., Weiss, D. and Dong, S., 2012. Calibration of the New Certified Reference Materials ERM-AE633 and ERM-AE647 for Copper and IRMM-3702 for Zinc Isotope Amount Ratio Determinations. *Geostandards and Geoanalytical ResearchVolume*, 36(2), pp.177-199. https://doi.org/10.1111/j.1751-908X.2011.00153.x.

Montero-Ruiz, I., 2018. Copper ingots from the Nuraghe Arrubiu at Orroli. In: A. Giumlia-Mair and F. Lo Schiavo, eds. 2018. *Bronze Age Metallurgy on Mediterranean Islands.* Drémil-Lafage: Editions Mergoil. pp.167-175.

Montero-Ruiz, I., 2023. A change of perspective: Lead isotopes in Nuragic metallurgy. In: M. Perra and F. Lo Schiavo, eds. 2023. *Contatti e Scambi fra la Sardegna, l'Italia continentale e l'Europa nord-occidentale nell' Età del Bronzo (XVIII-XI sec. a.C.): La «Via del Rame», la «Via dell' Ambra», la «Via dello Stagno». Atti del V Festival della Civiltà Nuragica (Orroli, Cagliari).* Arkadia Editore. pp.261-269.

Papadimitriou, G., 2001. Simulation Study of Ancient Bronzes: Their Mechanical and Metalworking Properties. In: Y. Bassiakos, E. Aloupi and Y. Facorellis, eds. 2001. *Archaeometric Issues in Greek Prehistory and Antiquity*. Athens: Hellenic Society for Archaeometry. pp.713-733.

Pernicka, E., 1999. Trace Element Fingerprinting of Ancient Copper: A Guide to Technology or Provenance? In: M.M. Suzanne, A. Young, M. Pollard, P. Budd, A. Robert and A. Ixer, eds.1999. *Metals in Antiquity. BAR International Series*, 792. Oxford. pp.163-171.

Pernicka, E., 2014. Provenance determination of Archaeological Metal Objects. In: B.W. Roberts and C.P. Thornton, eds. 2014. *Archaeometallurgy in Global Perspective: Methods and Syntheses.* Springer Science & Business Media. pp.239-268.

Philip, G., Clogg, P.W., Dungworth, D., and Stos, Z.A., 2003. Copper metallurgy in the Jordan Valley from the third to the first millennia BC: chemical, metallographic and lead isotope analyses of artefacts from Pella. *Levant*, 35(1), pp.71-100. https://doi.org/10.1179/lev.2003.35.1.71.

Rademakers, F.W., Rehren, Th. and Pernicka, E., 2017. Copper for the Pharaoh: Identifying multiple metal sources for Ramesses' workshops from bronze and crucible remains. *Journal of Archaeological Science*, 80, pp.50-73. https://doi.org/10.1016/j.jas.2017.01.017.

Renzi, M. and Rehren, Th., 2016. Iron Age metal production in the Arabian region and in the Levant: A comparative study. *The BFSA Bulletin* (British Foundation for the Study of Arabia), 21, pp.26-27.

Renzi, M., Intilia, A., Hausleiter, A. and Rehren, Th., 2016. Early Iron Age metal circulation in the Arabian Peninsula: the oasis of Taymā as part of a dynamic network (poster). *Proceedings of the Seminar for Arabian Studies,* 46, pp.237-246.

Rothenberg, B., 1988. *The Egyptian Mining Temple at Timna. Researches in the Arabah in 1959-1984*. London: Institute for Archaeo-Metallurgical Studies.

Rothenberg, B., 1990. Copper Smelting Furnaces, Tuyeres, Slags, Ingot-Moulds and Ingots in the Arabah: The Archaeological Data. In: B. Rothenberg, ed. 1990. *The Ancient Metallurgy of Copper: Researches in the Arabah 1959–1984,* Vol. 2. London: Institute for Archaeo-Metallurgical Studies. pp.1-77.

Rothenberg, B. and Glass, J., 1992. The beginnings and the development of early metallurgy and the settlement and chronology of the western Arabah, from the Chalcolithic Period to Early Bronze Age IV. *Levant*, 24(1), pp.141-157. https://doi.org/10.1179/007589192790220829.

Salje, G. and Feller-Kniepmeier, M., 1977. The diffusion and solubility of copper in iron. *Journal of Applied Physics*, 48(5), pp.1833-1839.

Scott, D.A., 1991. *Metallography and microstructure of ancient and historic metals*. The Getty Conservation Institute in association with Archetype Books.

Segal, I., Halicz, L. and Cohen, R., 1999. A Study of Ingots and Metallurgical Remains from ʿEin Ziq and Beʾer Resisim, Central Negev, Israel. In: S. Young, M. Pollard, P. Budd, and R.A. Ixer, eds. 1999. *Metals in Antiquity*. *BAR International Series*, 792. Oxford: Archaeopress, pp.179-186.

Segal, I., Roman, I., Cohen, R. and Brenner, I.B., 1996-1997. Chemical and metallurgical study of ʿEin Ziq and Be'er Resisim ingots. *Arx,* 2-3, pp.43-51.

Segal, I., Bar-Matthews, M., Matthews, A., Harlavan, Y. and Asael, D., 2015. Provenance of ancient metallurgical artifacts: implications of new lead isotope data from Timna ores. In: A. Hauptmann and D. Modaressi-Tehrani, eds. 2015. *Archaeometallurgy in Europe III. Proceedings of the 3rd International Conference. Deutsches Bergbau-Museum Bochum. June 29 – July 1, 2011*. Bochum: Deutsches Bergbau-Museum. pp.221-228.

Segev, A. and Sass, E., 1989. Copper-Enriched Syngenetic Dolostones as a Source for Epigenetic Copper Mineralization in Sandstones and Shales (Timna, Israel). In: R.W. Boyle, A.C. Brown, C.W. Jefferson, E.C. Jowett and R.V. Kirkham, eds. 1989. *Geological Association of Canada, Special Paper,* 36. pp.647-658.

Segev, A., Beyth, M. and Bar-Matthews, M., 1992. The Geology of the Timna Valley with Emphasis on Copper and Manganese Mineralization – Updating and Correlation with the Eastern Margins of the Dead Sea Rift. *Ministry of Energy and Water Resources, Geological Survey of Israel Reports,* 14, pp.1-31.

Shilstein, S. and Shalev, S., 2018. Preliminary study of copper slag in the Southern Arabah Valley. In: E. Ben-Yosef, ed. 2018. *Mining for ancient copper. Essays in memory of Beno Rothenberg*. Tel Aviv University, Sonia and Marco Nadler Institute for Archaeology Monograph Series, 37. University Park, PA/Tel Aviv: Eisenbrauns & Emery and Claire Yass Publications in Archaeology of the Institute of Archaeology, Tel Aviv University. pp.228-241.

Stacey, J.S. and Kramers, J.D., 1975. Approximation of terrestrial lead isotope evolution by a two-stage model. *Earth and Planetary Science Letters,* 26, pp.207-221.

Stos-Gale, Z.A., 2006. Provenance of metals from Tell Jatt based on their lead isotope analyses. In: M. Artzy, ed. 2006. *The Jatt metal Hoard in Northern Canaanite/Phoenician and Cypriot context. Cuadernos de Arquelogia Mediterranea*, Vol. 14. Publicaciones del Laboratorio de Arqueologia Universidad Pompeu Fabra de Barcelona. pp.115-120.

Stos-Gale, Z.A., 2015. Patterns of Trade in Cypriot Copper in the Bronze Age Eastern Mediterranean revealed using Data from Oxford Archaeological Lead Isotope Database (OXALID). In: K. Rosinska-Balik, A. Ochal-Czarnowicz, M. Czarnowicz and J. Debowska-Ludwin, eds. 2015. *Copper and Trade in the South-Eastern Mediterranean. BAR International Series*, 2753. Oxford. pp.111-122.

Stos-Gale, Z.A., 2023. Sardinia – a European metal trade junction in the 2nd millennium BC? In: M. Perra and F. Lo Schiavo, eds. 2023. *Contatti e Scambi fra la Sardegna, l'Italia continentale e l'Europa nord-occidentale nell' Età del Bronzo (XVIII-XI sec. a.C.): La «Via del Rame», la «Via dell' Ambra», la «Via dello Stagno». Atti del V Festival della Civiltà Nuragica (Orroli, Cagliari).* Arkadia Editore. pp.221-240.

Stos-Gale, Z.A., Gale, N.H. and Houghton, J. 1995. The origin of copper metal excavated in El Amarna. In: W.V. Davies and L. Schofield, eds. 1995. *Egypt, the Aegean and the Levant: Interconnections in the 2nd millennium BC.* London: British Museum Press. pp.127-135.

Vaelske, V. and Bode, M., 2018-2019. Early Iron Age Copper Trails: First Results of a Pilot-study at Sidon. In: *Archaeology and History in Lebanon,* 48-49, pp.130-133.

Vaelske, V., Bode, M. and Loeben, C.M., 2019. Early Iron Age Copper Trail between Wadi Arabah and Egypt during the 21st Dynasty: First results from Tanis, ca. 1000 BC. *Zeitschrift für Orient-Archäologie,* 12, pp.184-203.

Vaelske, V., Bode, M. and El Morr, Z., forthcoming. Early Iron Age Copper Trails: The case of Phoenicia. First results of a pilot-study. *Bulletin d'archéologie et d'architecture libanaises,* 19, pp.267-279.

Yagel, O., Ben-Yosef, E. and Craddock, P., 2016. Late Bronze Age Copper Production in Timna: New Evidence from Site 3. *Levant,* 48(1), pp.33-51. https://doi.org/10.1080/00758914.2016.1145943.

Yahalom-Mack, N. and Segal, I., 2018. The origin of copper used in Canaan during the Late Bronze /Iron Age transition. In: E. Ben-Yosef, ed. 2018. *Mining for ancient copper. Essays in memory of Beno Rothenberg*. Tel Aviv University, Sonia and Marco Nadler Institute for Archaeology Monograph Series, 37. University Park, PA/Tel Aviv: Eisenbrauns & Emery and Claire Yass Publications in Archaeology of the Institute of Archaeology, Tel Aviv University. pp.313-331.

Yahalom-Mack, N. and Segal, I., 2021. Chemical and Lead Isotope Analysis of Copper-Based and Lead Artifacts. In: A. Mazar and N. Panitz-Cohen, eds. 2021. *Tel Reḥov: a Bronze and Iron Age city in the Beth-Shean Valley*. Institute of Archaeology, Hebrew University of Jerusalem. pp.42-51.

Yahalom-Mack, N., Finn, D.M. and Erel, Y., 2023. Assessing the Circulation of Arabah Copper (Timna vs. Faynan) from the End of the Late Bronze and Iron Age in the Southern Levant by Combining Lead Isotopic Ratios with Lead Concentrations. In: E. Ben-Yosef and I.W.N. Jones, eds. 2023. *"And in Length of Days Understanding" (Job 12:12). Essays on Archaeology in the Eastern Mediterranean and Beyond in Honor of Thomas E. Levy*. Springer. pp.1181-1199.

Yahalom-Mack, N., Galili, E., Segal, I., Eliyahu-Behar, A., Boaretto, E., Shilstein, S. and Finkelstein, I., 2014. New insights into Levantine copper trade: analysis of ingots from the Bronze and Iron Ages in Israel. *Journal of Archaeological Science,* 45, pp.159-177. https://doi.org/10.1016/j.jas.2014.02.004.

Authors

Michael Bode (Corresponding author)
Deutsches Bergbau-Museum Bochum
Forschungsbereich Forschungsinfrastruktur
Herner Strasse 45
44787 Bochum, Germany
michael.Bode@bergbaumuseum.de
ORCID-number 0000-0001-5357-9931

Moritz Kiderlen
Humboldt-Universität zu Berlin
Institut für Archäologie
Unter den Linden 6 D
10099 Berlin, Germany
moritz.kiderlen@hu-berlin.de
ORCID-number 0000-0003-2325-2211

Giorgos Mastrotheodoros
West Attica University
Conservation of Antiquities and Works of Art
Department
Ag. Spyridonos Str.
12243 Egaleo, Greece
gmastrotheod@uniwa.gr
ORCID-number 0000-0002-0320-5867

Moritz Jansen
Deutsches Bergbau-Museum Bochum
Forschungsbereich Forschungsinfrastruktur
Herner Strasse 45
44787 Bochum, Germany
moritz.Jansen@bergbaumuseum.de
ORCID-number 0000-0002-3821-0666

Erez Ben-Yosef
Tel Aviv University
J. M. Alkow Department of Archaoelogy and Ancient
Near Eastern Cultures
6997801 Tel Aviv, Israel
ebenyose@tauex.tau.ac.il
ORCID-number 0000-0002-9483-3809

Omri Yagel
Tel Aviv University
J. M. Alkow Department of Archaoelogy and Ancient
Near Eastern Cultures
6997801 Tel Aviv, Israel
Omriyagel@gmail.com
ORCID-number 0000-0002-2889-5841

Martina Renzi
Diriyah Gate Development Authority Riyadh
8500 4000 Prince Sattam Ibn Abdulaziz
Al Khuzama, Diriyah
12572 Riyadh, Saudi-Arabia
martinarenzi@gmail.com
ORCID-number 0000-0001-6466-9385

Eleni Filippaki
Institute of Nanoscience and Nanotechnology, (I.N.N.)
National Centre for Scientific Research, (N.C.S.R.)
"Demokritos"
Lab of Palaeoenvironment and Ancient Metals Studies
Neapoleos 27 & Patriarchu Grigoriou E
Ag. Paraskevi 15341, Greece
e.filippaki@inn.demokritos.gr
ORCID-number 0000-0003-0881-3674

Yannis Bassiakos
Institute of Nanoscience and Nanotechnology, (I.N.N.)
National Centre for Scientific Research, (N.C.S.R.)
"Demokritos"
Lab of Palaeoenvironment and Ancient Metals Studies
Neapoleos 27 & Patriarchu Grigoriou E
Ag. Paraskevi 15341, Greece
y.bassiakos@inn.demokritos.gr
ORCID-number 0000-0002-5905-0120

Anno Hein
Institute of Nanoscience and Nanotechnology, (I.N.N.)
National Centre for Scientific Research, (N.C.S.R.)
"Demokritos"
Lab of Palaeoenvironment and Ancient Metals Studies
Neapoleos 27 & Patriarchu Grigoriou E
Ag. Paraskevi 15341, Greece
a.hein@inn.demokritos.gr
ORCID-number 0000-0002-1129-4820

Andreas Hauptmann
Deutsches Bergbau-Museum Bochum
Forschungsbereich Archäometallurgie
Am Bergbaumuseum 31
44791 Bochum, Germany
andreas.Hauptmann@bergbaumuseum.de
ORCID-number 0000-0003-1126-9390